ABSTRACT

Title of Document: SURFACE AND AEROSOL EFFECTS ON THE SOUTH ASIAN MONSOON HYDROCLIMATE.

Massimo Alberto Bollasina, Doctor of Philosophy, 2010

Directed By: Professor Sumant Nigam, Department of Atmospheric and Oceanic Science

This work targets important couplings in the South Asian monsoon system at interannual or longer time-scales and associated processes and mechanisms: aerosol-hydroclimate, atmosphere-ocean, and land-atmosphere.

Anomalous springtime absorbing aerosols loading over the Indo-Gangetic Plain (IGP) leads to large-scale variations of the monsoon: cloudiness reduction associated with increased aerosols is suggested to play an important role in triggering surface heating over India, which strengthens the monsoon. Indeed, a closer analysis with high resolution data depicts a complex interplay between aerosols, dynamics and precipitation. Interestingly, observations do not provide any evidence for the Elevated Heat Pump hypothesis, a mechanism proposed for the aerosol-monsoon link.

Current coupled climate models, which have been extensively used to study aerosol-monsoon interactions, are shown to have large, systematic, and coherent biases in precipitation, evaporation, sea-surface temperature (SST) over the Indian

Ocean during the monsoon. Models are also found to deficiently portray local and non-local air–sea interactions. For example, they tend to emphasize local oceanic forcing on precipitation or to poorly simulate the relationship between SST and evaporation. The Indian monsoon rainfall–SST link is also spuriously misrepresented, suggesting caution when interpreting model-based findings.

Both regional and remote forcings modulate the annual cycle of the heat-low over the desert areas (including the Thar Desert) between Pakistan and northwestern India, source of most of the dust loading over India. Land-surface heating has a limited role in the development of the low. Regional orography and monsoon summertime deep-convection over the Bay of Bengal, with its upstream descent to the west and related northerlies, contribute to the strengthening of the low, indicating a monsoon modulation on desert processes, including dust emission.

The Thar Desert is expanding westward and the potential impact of land-cover change (without consideration of the additional aerosol loading) on summer monsoon hydroclimate and circulation is found to be significant. Locally, the atmospheric water cycle weakens, air temperature cools and subsidence prevails. An anomalous northwesterly flow over the IGP weakens the monsoon circulation over eastern India, causing precipitation to decrease. Orographic enhanced precipitation occurs over the Eastern Himalayas and southern China.

SURFACE AND AEROSOL EFFECTS ON THE SOUTH ASIAN MONSOON HYDROCLIMATE

By

Massimo Alberto Bollasina

Dissertation submitted to the Faculty of the Graduate School of the
University of Maryland, College Park, in partial fulfillment
of the requirements for the degree of
Doctor of Philosophy
2010

Advisory Committee:
Professor Sumant Nigam, Chair
Research Professor Hugo Berbery
Professor Antonio Busalacchi
Professor James Carton
Professor Raghuram Murtugudde
Associate Professor James Farquhar

Preface

This work derives almost entirely from published (or submitted) research articles. As such, each Chapter (2-7) has its own Introduction, Methodology, Results, and Conclusion sections, as required by peer-reviewed publications. A certain amount of overlapping in the introductory sections of the first three Chapters is also inevitable, given that they investigate different aspects of the same problem. Two Chapters serve as leitmotif and connects the various topics: Chapter 1 provides a general introduction and motivation of the work in the framework of current monsoon research, and Chapter 8 gives an overall summary and concluding remarks.

Dedication

To the memory of my mom.

"Each true sorrow is written on slabs made of a mysterious substance compared to which granite is like butter. Eternity is not enough to wipe it off."

(Dino Buzzati, *The two drivers*, Milan, 1963)

"My mother […] if I was achieving something, if I was even only partly succeeding, was genuinely happy. On the contrary, if I was having a small pain, she was truly unhappy. This is the only kind of love – as far as I know – that completely realizes (without any imbalance) the extraordinary involvement of loving the others."

(Dino Buzzati, Milan, 1973)

Acknowledgements

I carry with me many memories of this five-year period.

Above all, I want to mention the precious closeness of my family. My grandma Stella, with her letters and daily phone calls, especially those received during the night. The countless conversations with my mom, my brother Roberto and my dad Mario, and the advices, support, help, and moments of laughs I had.

I am grateful to Sumant, my Advisor, for his valuable guidance and support, to my Dissertation Committee, and to the Faculty and Staff of the Department of Atmospheric and Oceanic Science, with whom I had a friendly relationship.

I have always been accompanied by the silent presence of my mountains, so dear to me.

Table of Contents

List of Tables

List of Figures

Chapter 1: Introduction

1.1 Background

The Asian (also called Asian-Australian) monsoon system extends from the western Arabian Sea through East Asia and North Australia and is a major dynamic component of the climate system. Changes in this convectively active region can result in severe drought or flood over large, densely populated regions (e.g., Webster et al. 1998). It is well known that the Asian summer monsoon is an extremely complex phenomenon that encompasses variability over a wide range of spatial (from a few kilometers to thousands of kilometers) and temporal (from days to decades) scales (e.g., Lau et al. 2000). Simulation and prediction of the monsoon is one of the major challenges of climate research (e.g., Kang and Shukla 2005; Sumi et al. 2005; Krishnamurti et al. 2006). A number of studies have pointed out the relevance of the Asian monsoon system as a major energy source in the global-scale circulation in middle and low latitudes (e.g., Trenberth et al. 2006). Monsoon precipitation is of vital importance for more than 60% of the world's population and their mainly agrarian societies which strongly rely on it.

The Asian monsoon is composed of two subsystems, the Indian (or South Asian) monsoon and the East Asian monsoon, roughly divided at 105°E. The South Asian encompasses the Indian Subcontinent, Indochina and the Indian Ocean. Although the South Asian monsoon as a whole is remarkably regular (for example,

over India the interannual standard deviation of precipitation is about only 10% of the long-term mean), even small perturbations (in time, such as an anticipated onset or a prolonged break, and/or in space, such a redistribution of rainfall) may result in natural disasters from floods or droughts (e.g., Goswami 2005). The monsoon accounts for 80% of the summer rainfall in India and its importance (scientific, societal, and economical) cannot be overemphasized.

Over the last few decades, a holistic view of the South Asian monsoon system (as well as of the greater Asian monsoon) has emerged as a result of more comprehensive observational and modeling studies (e.g., Webster et al. 2002; Webster 2006). In this perspective, the monsoon is seen as a strongly coupled phenomenon where ocean, atmosphere, and land are integral components of a grander self-regulating system.

A variety of processes, both internal to the monsoon and remote, act to regulate and vary the strength and duration of the South Asian monsoon (see for example the web site: http://www.clivar.org/organization/aamp/publications/pg2.htm). Although the monsoon have received fervent attention for nearly 250 years, starting with the early studies of the 18th century, it is not surprising that its complexity has hampered our understanding and that many issues are still largely debated in the scientific community (e.g., Sperber and Yasunari 2006; Wang 2006; Yasunari 2007).

1.2 Statement of the Problem and Significance

This work is aimed at investigating several relevant issues belonging to significant areas of current monsoon research at *interannual* or *longer* time-scales

(e.g., Lau et al. 2005). The topics studied in the following Chapters target the important couplings in the monsoon system: *aerosol-hydroclimate*, *atmosphere-ocean,* and *land-atmosphere interactions*. A short description of the framework, significance, and motivation for each issue follows hereafter. More comprehensive and specific background and context are provided at the beginning of each Chapter.

1.2.1 Aerosol Forcing

Observational studies have shown a recent increase of the aerosol loading over the Indian Subcontinent and its impact on monsoon clouds and precipitation, radiation balance and circulation has been considerably debated (e.g., Ramanathan et al. 2008; Lau et al. 2009). However, our knowledge of the pathways of aerosol-climate interaction is still very rudimentary (e.g., Denman et al. 2007). The understanding of the regional feedbacks between atmospheric dynamics, hydrological cycle and aerosols needs considerable improvement (e.g., CCSP 2009). In this respect, as models are still ill-equipped to deal with the complexities of aerosol-cloud interactions, particularly important during summertime, an observational approach – the one adopted here - may provide new insights.

1.2.2 Air-Sea Interactions over the Indian Ocean

Current coupled climate models, although providing valuable insights into monsoon mechanisms, are still unable to correctly reproduce some basic phenomena and processes (e.g., Randall et al. 2007). Air-sea feedbacks represent a source of large uncertainty in models (e.g., Lin 2007). Their realistic simulation is crucial given their important role in monsoon variability (e.g., Annamalai and Murtugudde 2004; Wu

and Kirtman 2005). The problem is certainly complicated since there is evidence that to a large extent regional sea-surface temperature (SST) in the Indian Ocean may vary independently from that in the tropical central-eastern Pacific (e.g., Lau and Wu 2001) and even be a passive response to atmospheric forcing. The investigation of model deficiencies in representing air-sea interactions in the Indian Ocean is fundamental for the understanding of present-day and future monsoon simulations.

1.2.3 Land-Atmosphere Processes over India

The Thar (or Great Indian) Desert is located between northwestern India and Pakistan. In summer the Thar Desert is the center of the most intense surface low-pressure system in the global tropics. Although the low is a distinctive element of the South Asian summer monsoon (e.g., Sikka 1997) and whose intensity is associated with subsequent monsoon rainfall, its structure, origin and evolution are still poorly characterized.

The Thar Desert region is also the most densely populated desert region in the world and vast areas are affected by rapid soil degradation and vegetation loss (e.g., Ravi and Huxman 2009). It has also been shown (e.g., Rodell et al. 2009) that, as a result of population growth and extensive agricultural practices, groundwater over northwestern India is progressively being depleted. The region is under the threat of future desertification (e.g., Goswami and Ramesh 2008). Land-use changes over northwestern India, by altering the surface water and energy budgets through changes in albedo, soil moisture, surface roughness, are expected to have significant impacts on monsoon hydroclimate, and not only regionally.

1.3 Objectives

In relation to the issues described above, the major goals of this work were to:

- Improve the understanding of the physical processes and mechanisms affecting the impact of *interannual* variations of absorbing aerosols over India on monsoon circulation and hydroclimate;
- Investigate biases and weaknesses of current global climate models in representing coupled air-sea interactions over the Indian Ocean;
- Advance the understanding of the origin and evolution of the desert heat-low over Pakistan and northwestern India and the mechanisms driving its annual cycle;
- Investigate the impact of land-cover change (i.e., expansion of the desert) over northwestern India on monsoon hydroclimate.

1.4 Thesis Outline

An observational analysis of the effects of interannual variations of absorbing aerosols over the Indo-Gangetic Plain on monsoon hydroclimate is presented in Chapter 2. The analysis is extended in Chapter 3, by using data at higher temporal resolution. Chapter 4 critically examines and discusses one of the mechanisms recently proposed to explain the aerosol impact on the monsoon. Coupled models simulations of the Indian monsoon and their representation of regional air-sea interactions are analyzed in Chapter 5. The origin and evolution of the heat-low over Pakistan/northwestern India is investigated in Chapter 6. Chapter 7 describes the

results of experiments of land-cover change over India. Finally, summary and concluding remarks follow in Chapter 8.

Chapter 2: Absorbing Aerosols and Summer Monsoon Evolution over South Asia: An Observational Portrayal[1]

2.1 Introduction

The aerosol influence on the Earth's radiation budget is better understood now than it was a few years ago, but it still remains the dominant uncertainty in climate change scenarios (IPCC 2007; Anderson et al. 2003). Several factors make identifying and quantifying aerosol effects on climate challenging (e.g., Menon 2004) and a substantial amount of literature on various aerosol effects now exists (see Menon 2004 for a review). Anthropogenic activities have been implicated in raising the aerosol concentration in the troposphere (e.g., Massie et al. 2004; Sarkar et al. 2006). Over polluted regions, the aerosol forcing at the surface and in the atmosphere can be an order of magnitude larger than those of anthropogenic greenhouse gases, as is the case for the Indo-Asian haze (Ramanathan et al. 2005).

One of the areas of the world with high aerosol concentration is South Asia, as a result of recent rapid urbanization and population growth. The Indian Ocean Experiment (INDOEX; Ramanathan et al. 2001) revealed that a 3 km thick brownish haze layer, composed of anthropogenic (up to 75% of the average Aerosol Optical Depth (AOD); Lelieveld et al. 2001) and natural aerosols, is spread over most of the tropical Indian Ocean toward the Himalayan region (Ramana et al. 2004), and extends

[1] This Chapter has been published as Bollasina, Nigam, and Lau (2008).

over Southeast Asia into the western Pacific (e.g., Rajeev et al. 2000). INDOEX documented the persistence of the brown cloud for several months from winter to spring, its large black carbon (BC) content (up to 10-14% of the total aerosol mass) and the large perturbation to the radiative energy budget of the region (up to -25 Wm^{-2} in the mean clear-sky radiation at the surface). During the last few years, observational studies have further characterized the aerosol composition and properties (e.g., Eck et al. 2001; Hsu et al. 2003; Ramanathan and Ramana 2005; Gautam et al. 2007).

In the same period, atmospheric and coupled ocean-atmosphere models have been used with quasi-realistic aerosol distributions to clarify the aerosol-monsoon linkage. The contribution of absorbing aerosols to the long-term changes of rainfall over India was investigated by Chung et al. (2002), Menon et al. (2002), Ramanathan et al. (2005), Lau et al. (2006), Chung and Ramanathan (2006) and, recently, by Meehl et al. (2008). Chung et al. (2002) used an atmospheric model with SSTs fixed to their climatological cycle and aerosol forcing imposed in terms of a radiative forcing perturbation (from October to May) over the Indian Ocean, derived from INDOEX measurements. The results (limited to winter and spring months) showed that the aerosols induced surface cooling by reducing solar radiation at the surface, but produced also warming of the lower troposphere by absorption. The dynamical response was large, from the enhancement of the meridional temperature gradient in the atmosphere and increased low-level convergence, which in turn led to stronger pre-monsoon rainfall. Menon et al. (2002) investigated the effects of absorbing aerosols (BC) on the summer monsoon using a similar modeling strategy, i.e., a

climate model with specified SSTs. The modeling analysis showed precipitation to decrease over the north equatorial Indian Ocean and northern China, and to increase over southern China and portions of India. The authors attributed this variation to the heating of the air and its effects on temperature profile, convection strength and induced large-scale ascending motion. Lau et al. (2006) have also ascertained the effects of absorbing aerosols on the summer monsoon with an atmospheric model forced by specified SSTs, and proposed an "Elevated Heat Pump" hypothesis (hereafter EHP): anomalous accumulation of absorbing aerosols (transported dust from the nearby deserts and BC from regional sources) against the southern slopes of the Himalayas induces a large-scale upper-level heating anomaly over the Tibetan Plateau in April and May which reinforces the meridional temperature gradient and intensifies the monsoon over India in June and July.

However, the impact of aerosols on monsoon rainfall in a coupled model was found to be different from that in uncoupled models with specified SSTs (the three papers described above) as a result of the response of SSTs themselves to aerosol forcing. Ramanathan et al. (2005) using a coupled ocean-atmosphere model, with aerosols over South Asia prescribed according to the ABC measurements, found that while aerosol absorption of solar radiation and consequent heating of the atmosphere leads to enhanced upward motion over India during winter, it also leads in summer to a weakening of the monsoon circulation and a reduction of rainfall over India. The latter effect was attributed to the aerosol-induced decrease of the meridional SST gradient in the Indian Ocean, with consequent cooler trend of SSTs in the northern Indian Ocean than in the southern part. Chung and Ramanathan (2006) sought to

estimate the two influences by running an atmospheric model with specified SSTs, imposing separately the SST trend in the Indian Ocean and the South Asian haze radiative forcing. Large-scale circulation changes arising from the modulation of the meridional SST gradient (simulating an interactive ocean) more than offset the rainfall increment resulting from increased ascending motions induced by aerosol heating of the low troposphere (keeping SSTs fixed), with an overall decrease of monsoon rainfall over India. Recently, Meehl et al. (2008) also used a coupled climate model but with a time-evolving global distribution of BC aerosols (with all the other natural and anthropogenic forcings fixed to their pre-industrial values) to investigate the effects on the Indian monsoon. A present-day distribution of BC was generated by assimilating satellite retrievals of optical depths and by using a chemistry-transport model. They found that BC aerosols lead to an increase of pre-monsoon rainfall over India but to a decrease in the monsoon season, with season-averaged break monsoon conditions associated with cooler SSTs in the Arabian Sea and the Bay of Bengal and warmer SSTs to the south (i.e., a weaker latitudinal SST gradient), confirming the findings of Ramanathan et al. (2005).

The aforementioned studies describe the potential effects of aerosols on monsoon rainfall over the Indian subcontinent, but with heavy reliance on models. The problem is challenging given the complexity of the radiative, cloud-microphysics, and hydro-meteorological processes involved, and their interaction with the large-scale circulation. Climate system models are a valuable tool for clarification of the underlying mechanisms but some caution is necessary as these models are known to have significant, and in many cases, unacceptable, biases in

quantities as basic and relevant as the monsoon rainfall distribution and onset (e.g., Annamalai et al. 2006). The biases often reflect inadequacies of the model physics in representing the ocean-atmosphere-ocean-land interactions in play during the monsoon.

Aerosol-monsoon interaction was recently studied using observations by Lau and Kim (2006; hereafter LK06), who found support for their elevated heat pump hypothesis primarily from analysis of precipitation and atmospheric circulation datasets.

The present study is complementary to most earlier ones because it focuses on the interannual variability of aerosol concentration and related monsoon rainfall variation, and because it is observationally rooted. The long-term aerosol trend is in fact removed from the record prior to analysis. An observational portrayal of aerosol-monsoon interactions is derived from rigorous analysis of remotely-sensed data sets and atmospheric reanalysis. While similar in some respects to LK06, the focus here is on the variations over the vast Indo-Gangetic Plain (IGP) and the distinction in the response over the eastern and western regions as opposed to the whole Indian sector in LK06. Another difference with respect to LK06 is the focus on land-surface in this paper, whose state, including contrast with adjoining bays and oceans, is fundamental to monsoon onset and evolution. The land-surface focus, however, is not one of choice, but dictated by the comprehensive analysis of aerosol-induced monsoon transitions between late spring and early summer, when aerosol concentration reaches a peak (in the annual and interannual variations). Examination of diabatic heating, outgoing longwave radiation, temperature and moisture profiles, surface air

temperature, surface radiative and heat fluxes, and cloudiness distributions not only complements the customary analysis of monsoon hydroclimate, but is essential in building a compelling picture of the aerosol-monsoon interactions.

Our results suggest that although anomalously high aerosols are associated with deficient precipitation over India in early spring, internal atmosphere–land-surface feedback actually strengthens the monsoon in subsequent summer months. Land-surface processes, once triggered by anomalous aerosol concentration, are important mediators in monsoon evolution.

The Chapter is organized as follows: Section 2.2 presents the data used in the analysis. Section 2.3 describes the variability of absorbing aerosols over India, and Section 2.4 shows the large-scale pattern of the aerosol-induced anomalies in atmospheric circulation and the land-surface state, and discusses a possible mechanism for the link. Discussion and conclusions follow in Section 2.5.

2.2 Data and Analysis

The distribution and variability of the aerosols is described in terms of the Aerosol Index (AI) derived from the Total Ozone Mapping Spectrometer (TOMS) measured radiances (Herman et al. 1997). The TOMS instrument has been operating aboard a series of satellites from 1978 to 2005. The AI is defined so that positive values correspond to UV-absorbing aerosols and negative values correspond to non-absorbing aerosols (Torres et al. 2002). A temporal gap of three years exists between 1993 and 1996, mainly because the data from the Meteor 3 satellite were not used in aerosol data processing due to its precessing orbit (Herman et al. 1997).

The TOMS project has produced the longest available global record of aerosol observations in terms of AI and a number of studies have demonstrated its feasibility and success (e.g., Torres et al. 1998; Chiappello et al. 1999; Hsu et al. 1999; Cakmur et al. 2001; Prospero et al. 2002; Duncan et al. 2003). Monthly data on a 1.25º x 1° grid are available at the TOMS web site (http://toms.gsfc.nasa.gov/aerosols/aerosols_v8.html).

A preliminary comparison of Nimbus 7 (1978-1993) and Earth Probe (1996-2005) AI data over the Indian Subcontinent and available documentation (e.g., Kiss et al. (2007), and the TOMS web site: http://toms.gsfc.nasa.gov/news/news.html) revealed significant differences in terms of mean annual cycle and time series of the area-averaged AI. A calibration drift was reported in 2000, instrumental problems were also noticed in 2001, and a warning to use caution in trend analysis with data after 2000 was also released in 2001 (see the web site: http://toms.gsfc.nasa.gov/news/news.html). Because of this, the study focused only on the period 1979-1992.

Atmospheric and surface variables are derived from the ECMWF Reanalysis (ERA-40; Uppala et al. 2005) monthly data on a 2.5° x 2.5° grid and at 23 vertical isobaric levels, and were obtained from the National Center for Atmospheric Research (NCAR). ERA-40 was produced by running the spectral model at T159 (roughly 125 km) horizontal resolution (and with 60 vertical hybrid levels). The diabatic heating was diagnosed as a residual of the thermodynamic equation (Nigam 1994; Hoskins et al. 1995; Chan and Nigam 2007).

Monthly precipitation data came from the Global Precipitation Climatology Project (GPCP) version 2 (Adler et al. 2003), the Climate Prediction Center (CPC) Merged Analysis of Precipitation (CMAP; Xie and Arkin 1997) and the Climate Research Unit (CRU) TS 2.1 dataset (Mitchell and Jones 2005). Both GPCP and CMAP precipitation are available on a 2.5° x 2.5° grid, while CRU precipitation is at 0.5° x 0.5° over land only. In the following analysis, the observation-only CMAP product was used, which does not include precipitation values from the National Centers for Environmental Prediction/NCAR reanalysis. It is worth remembering that land stations used in CRU are quite sparse over India north of about 20°N and over surrounding regions (e.g., New et al. 2000).

Surface shortwave and longwave radiation data were obtained from the Global Energy and Water Cycle Experiment (GEWEX) Surface Radiation Budget (SRB) Project (Gupta et al. 1999; see the web site: http://grp.giss.nasa.gov/gewexdsetsbrowse.html) and from the International Satellite Cloud Climatology Project (ISCCP) radiative flux dataset (FD, Zhang et al. 2004). Both datasets are available on a 2.5° x 2.5° grid from January 1984 onward at the web site: http://isccp.giss.nasa.gov/products/browsed2.html).

Outgoing Longwave Radiation (OLR) data was provided by the NOAA/Earth System Research Laboratory (Liebmann and Smith 1996) as monthly averages at 2.5° horizontal resolution (see the web site: http://www.cdc.noaa.gov/cdc/data.interp_OLR.html). Despite some limitations, the OLR is commonly used as a proxy for deep convection and rainfall in most tropical regions.

ISCCP D2-series (Rossow et al. 1996) monthly mean total and low/middle/high cloud amount data available from July 1983 on a 2.5° x 2.5° grid were also used (see the web site: http://isccp.giss.nasa.gov/products/browsed2.html).

The analysis used linearly detrended time series for all variables. Detrending the data minimizes the influence of trends on the strength and significance of the deduced correlations/regressions.

2.3 TOMS Aerosol Index Variability over the Indian Subcontinent

Several studies have documented that aerosol concentration over the South Asian region progressively builds up during the dry season (October to April; e.g., Rajeev and Ramanathan 2002). The October-May distribution of the AI over the Indian Subcontinent reveals that the IGP is one of the areas with high loading of aerosols, the others being the Arabian Peninsula and the Taklamakan desert. Observations show that the IGP experiences a very persistent and heavy aerosol burden (AOD greater then 0.4) with peak concentrations in May (e.g., Ramanathan and Ramana 2005), and composition in large part made up of absorbing aerosols (single-scattering albedo as low as 0.85; Ramanathan et al. 2001).

This study is focused on the effects of accumulated absorbing aerosols on the summer monsoon transition, from the pre-monsoon phase to the active regime. The aerosol loading will be represented by the May AI as widespread monsoon rainfall in June rapidly washes out the aerosols, except over northwestern India. Figure 2.1

displays the AI distribution over a 14-year period. Spatial average of the AI over the IGP – formally the area with May standard deviation greater than 0.48 – was used to monitor the interannual variability. While the choice of the threshold seems somewhat arbitrary, the analysis is not too sensitive to different selections.

Figure 2.1a clearly shows that aerosols are pushed against the Himalayan range, with a distinct maximum over the IGP. The area of highest loading is longitudinally extended toward northwestern India and Pakistan, where a secondary maximum is present. The continuance of the westerly flow in spring across Afghanistan and Pakistan contributes to the piling up of aerosols in May. Indeed, during the pre-monsoon season, air masses carry the dry dust particles from the Middle East and the western Thar Desert (where dust activity peaks in late spring to early summer; see, e.g., Prospero et al. 2002) to the IGP, where they accumulate and interact with the large flux of regional pollutants from fossil fuels (typically invariant through the season) and biomass burning (predominant in spring; e.g., Dey et al. 2004; Habib et al. 2006).

The IGP is also the region of highest AI standard deviation, with variability amplitude equaling ~30% of the mean (Fig. 2.1b). The standard deviation distribution shows a northwest to southeast structure, just as the climatology. During this 14-year period, the AI exhibits a positive trend (between +0.02 and +0.1 $year^{-1}$) in the months of March to June over a wide area enclosing India, the Arabian Sea and Saudi Arabia. In May, the trend has a pronounced core over the IGP, with values greater than 0.1 $year^{-1}$. Figure 2.1c displays the original time series of the AI for the IGP. The trend, explaining 34% of the variance, is 0.086 $year^{-1}$, which, using a two-tailed *t*-test, is

significant at the 95% confidence level. The aerosol variations exhibit considerable spatial coherence as seen from the May correlation structure of the IGP averaged AI (Fig. 2.1d). The variation footprint (e.g., defined by the region with correlations > 0.9) extends over much of eastern India in Fig. 2.1d.

The aerosol index over the IGP rapidly increases from February to May (about 4 times the mean winter values), and then rapidly decreases in June and July due to the onset of monsoon rains (Fig. 2.1e). A secondary peak is seen in October. The seasonal cycle in other regions can peak in different months: from March over northeastern India, where rainfall starts in April, to June over northwestern India, where dust transport from the nearby deserts is unabated until the onset of monsoon in June.

The aerosol anomalies over the IGP during May have a strong relationship with antecedent aerosol anomalies over the same region, as seen in the lead autocorrelations displayed in Fig. 2.1f (for completeness, correlations with April aerosol concentration are also shown). At a confidence level above 90%, the interannual variations of the aerosol burden in May are linked to variations during March (lead = −2), suggesting the strong persistence of aerosol anomalies of the same sign throughout the spring until the rainy season. With the onset of the monsoon, the correlations sensibly drop, especially in July when rainfall is widespread over the IGP.

As mentioned earlier, dust from the deserts west of India is a large contributor to aerosol loading over the IGP. Indeed Figure 2.2 shows the spatial correlations of the aerosol anomalies over the IGP during May with the aerosol pattern during

previous months (i.e., March and April) over the Indian subcontinent. The climatological low-level westerly flow clearly carries the dust eastward, providing a constant source of aerosols over the IGP. In late spring aerosols are then transported over eastern India and the Bay of Bengal, as seen from lagged correlations of the AI time series over the IGP (not shown).

In the following analysis, variability of the aerosols is represented by the detrended time series of May AI anomalies over the IGP (i.e., the dashed line in Fig. 2.1c).

2.4 Absorbing Aerosols and South Asian Summer Monsoon Evolution

2.4.1 AI and Precipitation

Figure 2.3 shows the regressed precipitation for May, June and July. To corroborate the analysis, four different datasets are compared. During May, higher aerosol loading over the IGP are associated with lower precipitation over most of India, except the Northeast. The negative precipitation anomaly is not directly centered over the IGP, but shows a slight northwest to southeast orientation. The amounts are, on average, 0.5–1.5 mm day^{-1}, i.e., comparable to the 1979-1992 climatological May precipitation (about 1-1.5 mm day^{-1}). Positive anomalies in the northeast are even greater than 3 mm day^{-1}, but so is the climatology there (5-10 mm day^{-1}).

The situation is reversed in June: Associated with the anomalously high May AI is a positive precipitation anomaly over most of India (except the Northwest) of magnitude greater than 1 mm day^{-1}, compared to the 3-5 mm day^{-1} June-mean values. More abundant precipitation is also found over the ocean, with intense regional maxima in the Bay of Bengal and off the Western Ghats in the Arabian Sea (about 4-7 mm day^{-1} compared to the 10-15 mm day^{-1} mean values). High May AI is also accompanied by reduced precipitation in the north equatorial Indian Ocean.

The July regressions on May AI tend to be weaker and more diffuse. Not unexpectedly, since aerosols can get washed out in the June rains. Even with weaker regressions, datasets agree on the sign of the anomaly over India, southern slopes of the Himalayas, and over the southern Bay of Bengal.

That local maxima are in different areas through the season (i.e., deficient precipitation in May does not necessarily correspond to abundant precipitation in June/July over the same region) is also noteworthy. Interestingly, June and July have anomalies of the same sign (positive) over most of India.

The above analysis indicates that an anomalously large aerosol loading over the IGP at the end of the dry season initially potentially reduces the already modest pre-monsoon precipitation over India.[2] However, as the season progresses, the anomaly changes sign and precipitation is actually increased in June and July[3], that is the monsoon becomes stronger, in agreement with LK06.

---

[2] Average (1979-1992) monthly precipitation over India from the CRU dataset is 1.3 mm day^{-1} in May, as opposed to larger values in the monsoon season: 4.4 mm day^{-1} in June, 7.4 mm day^{-1} in July, and 6.7 mm day^{-1} in August.

[3] The August precipitation anomalies associated with high May aerosol loading are positive over northern India eastward of 80°E, but negative over western, central, and southern India, and over most of the Arabian Sea and the Bay of Bengal. Considering the Indian monsoon region as a whole, August precipitation is reduced.

2.4.2 AI and Diabatic Heating

Diabatic heating regressed on the May AI time series is examined in Fig. 2.4 to gain insight into the origin of the AI–precipitation links. A display of partitioned heating components would be preferable, and more revealing, but these are not available on account of the residual diagnosis of heating. The three-dimensional heating structure (Fig. 2.4) can however still be insightful, as seen shortly. Heating is, of course, very influential on the large-scale circulation, especially, in monsoon regions where the constituent latent heating is large and deep.

The left panels target this component, showing the mid-tropospheric heating. As expected, there is a close correspondence between vertically integrated diabatic heating and precipitation, especially ERA40's (last row in Fig. 2.3). During May, negative anomalies (−30 to −60 W m^{-2}) are found over most of India, while a positive band extends from the Arabian Sea to the Bay of Bengal, and over to northeastern India. Heating anomalies in June (and July) switch sign, becoming positive over India, consistent with increased precipitation (cf. Fig. 2.3). The lower tropospheric (p>775 hPa) heating anomalies are similar to the upper ones, except in May, when there is a striking difference: Positive anomalies (5–20 W m^{-2}) over central and northern India (north of ~15°N; see the May vertical cross section in Fig. 2.3), with a core centered at (25°N, 75°E), are found underneath the negative mid-tropospheric heating anomalies. Note that while the positive low-level heating anomalies are associated with larger aerosol burden, their core is not coincident with the maximum in aerosol distribution. Further analysis, in fact, suggests that these heating anomalies are related to variations in land-surface heating (as seen later in Fig. 2.8).

The vertical structure of heating is displayed in the right columns of Fig. 2.4, the cross-section being through the core region of reduced May precipitation. The opposite-signed anomalies in the lower and upper troposphere during May, mentioned earlier, are now evident, especially northward of 15°N. Of particular interest are the positive anomalies extending from the surface up to 800 hPa in the northern foothills region, with maximum heating rates (~1-2 K day^{-1}) at the surface. Such surface-trapped vertical structure is characteristic of sensible heating, a point we return to later. In June, and later in July, precipitation moves northward and intensifies but the northward progression is far from uniform as it rains over the Himalayan foothills first (in June) before it does over the Gangetic Plains and central India (in July). The heating anomaly over the southern slopes of the Himalayas is remarkable for its vertical reach – the tropopause. The core magnitude is about +1.5 K day^{-1} in June (at 500 hPa) and +2.5 K day^{-1} in July (at 600 hPa).

OLR regressions in Fig. 2.5 corroborate the midtropospheric heating analysis. OLR is a widely used indicator of deep convection in the tropics/subtropics with negative anomalies indicating deeper convection (e.g., Liebmann and Hartmann 1982). OLR is strongly positive over central and northwestern India in May, consistent with reduced precipitation and negative heating anomalies there (cf. Figs. 2.3 and 2.4). The anomaly sign is reversed in June, as expected.

2.4.3 AI and Circulation

Figure 2.6 shows in the left column the 1000-500 hPa integrated moisture flux (stationary+transient) anomaly and its convergence obtained, as before, from regressions on the May IGP AI time series. Southward (and divergent) moisture flux

anomalies are seen over much of the Indian subcontinent in May, with flux-divergence structure in accord with the precipitation and heating distributions (cf. Figs. 2.3 and 2.4). Another notable feature in the May plot is the eastward moisture transport from the Arabian Sea which turns cyclonically and becomes northward over the Bay of Bengal, finally impinging on the eastern Himalayas (~90°E) and producing rain. In June, the eastward transport occurs in a more northerly belt where it encounters the Western Ghats, leading to upstream precipitation and a rain-shadow over peninsular India.

The vertical structure of the circulation over central India is shown in the right column of Fig. 2.6. Low-level ascent and mid-to-upper level descent is in evidence in May, consistent with the dipolar heating structure (cf. Fig. 2.4) and the dominant thermodynamic balance in the Tropics between diabatic heating and adiabatic cooling from vertical motion.[4] Interestingly, this vertical motion field – low-level ascent and upper-level descent – can effectively trap and spread the aerosols at the top of the planetary boundary layer, for vertical convergence ($-\partial\omega/\partial p$) equals horizontal divergence ($\vec{\nabla} \cdot \vec{V}_h$) from the continuity equation. Clearly, there is scope for positive feedback here, as increased and expansive aerosol loadings can generate stronger vertical motions from further precipitation (deep-heating) reduction and surface heating.

Temperature and specific humidity profiles over central India linked with the IGP AI variations are shown in Fig. 2.7. Increased aerosol loading is associated with

[4] This balance is generally in evidence well away from the surface (e.g., in the midtroposphere) since only there can vertical velocity be large enough for adiabatic cooling to offset diabatic heating. Nearer to the surface, horizontal thermal advection cannot be ignored even in the Tropics. In fact, May streamlines suggests some offsetting of low-level heating by advection from the north. The thermodynamic balance is being quantitatively assessed from ERA40 data.

positive (negative) temperature (specific humidity) anomalies with maximum amplitude near the ground and a relative minimum in the midtroposphere in both cases. The lower troposphere anomalies are quite significant, with correlation exceeding 0.8 (0.5) for temperature (specific humidity). The vertical structure is entirely consistent with the presence of a heat source at the lower boundary, a heated land surface in this case, reflected also in the surface-trapped diabatic heating structure (cf. Fig. 2.4). A drier lower troposphere is also understood as resulting from a drier land-surface, since in the pre-monsoon period there is no other moisture source. The heating and drying of the land-surface are, of course, related. The June (and July) profiles, on the other hand, are very different, reflecting a dramatic cooling and moistening of the lower troposphere stemming from enhanced precipitation (cf. Fig. 2.3) and resultant cooling and wetting of the underlying land-surface.

2.4.4 AI and Surface Heat and Radiation Fluxes

The impact of AI variations on near-surface air temperature, and sensible and latent heat flux is shown in Fig. 2.8. Immediately apparent is the strong positive anomaly in 2-m temperature over most of the subcontinent, with amplitude greater than 3K in the core region (30°N, 75°E). The temperature anomaly is broadly coincident with the region of reduced May precipitation (cf. Fig. 2.3). Cooler temperatures, on the other hand, are evident over eastern India, Bangladesh and Burma, consistent with increased May rainfall over these regions.

Positive sensible heat flux anomalies (i.e., to the atmosphere) are present over India in May, indicating that the lower troposphere is being heated from below, in

accord with diabatic heating and temperature distributions.[5] At the same time, latent heat flux anomalies are negative, indicating reduced evaporation which must be a consequence of diminished May rainfall. Examination of soil moisture anomalies (not shown) indicates depletion in all soil layers, consistent with reduced May evaporation.

The corresponding June anomalies (right panels) show that land cools down as a result of increased precipitation, inducing a negative sensible heat flux anomaly. The latent heat flux, on the other hand, is nearly neutral because some of the excessive rainfall goes into recharging the drier-than-average land-surface. Again, the soil moisture distribution is consistent: Slightly positive near-surface anomalies atop negative ones in the two deepest layers (below 28 cm).

The impact of IGP AI variations on downward surface shortwave (SW) radiation is depicted in Fig. 2.9. A positive anomaly exceeding 20 Wm^{-2} is seen over the subcontinent, with a core over central India (15°N, 80°E). The ERA40 pattern corresponds (with opposite sign) to the precipitation anomaly in the model (cf. Fig. 2.3). Independent observational estimates of the downward surface SW flux, also shown in Fig. 2.9, confirm the above characterization of the SW flux anomaly given the remarkable similarity of the May patterns over both land and ocean. Interestingly, model and observational estimates fall apart in June, especially over the continent and when precipitation is enhanced.

[5] If all the sensible heat flux (~10 W m^{-2}) went into heating the planetary boundary layer (say 2 Km thick), the average temperature tendency would be ~0.45 K day^{-1} (=10/(ρC_p2000), where ρ is the air-density and C_p the specific heat of air). In the absence of thermal advection and other compensations, a radiative damping time scale of a week, would yield a temperature perturbation of ~3K; an estimate, in line with the displayed values of the field (cf. Fig. 2.6).

The finding of more downward surface SW radiation during periods of increased absorbing-aerosol loadings is at some odds with the winter season analyses. This is in part due to cloudiness variations which are muted in winter, at least, over the IGP region.

The related net longwave (LW) flux anomalies are shown in Fig. 2.10. The anomalies are strongly positive, exceeding 30 Wm^{-2}, over the IGP region and northwestern India, especially in the observational estimates. There is thus indication of more LW cooling in May, consistent with the warmer underlying land-surface and less cloudiness (as shown in the next figure).

Having accumulated indirect evidence for reduced cloudiness in Mays with increased absorbing aerosol loading over the IGP region (including reduced precipitation, more OLR, more downward SW, increased surface air temperature and sensible heat flux), the observed low, middle, high cloud amount anomalies are examined in Fig. 2.11. Not surprisingly, cloud amount is found significantly reduced at all levels over central and northwestern India in May, with the pattern corresponding well to the shortwave radiation and precipitation anomaly patterns of that month. The negative anomaly of cloudiness is larger for low and middle clouds, with the highest significance (and spatial extension) in the middle levels. Excess precipitation off the western coast of India and over Bangladesh and eastern India is also consistent with the positive local anomalies of low and middle cloud amount.

2.5 Conclusions

The influence of aerosol variability on the South Asian summer monsoon is characterized by means of an observational analysis. Absorbing aerosols have been shown to be influential in the context of long-term changes (or trends) in summer monsoon rainfall (e.g., Ramanathan et al. 2005; Chung and Ramanathan 2006; Lau et al. 2006; Meehl et al. 2008), and also its interannual variability (LK06). The summer season is particularly challenging because extensive cloudiness at this time brings the aerosol indirect effects also into play in addition to the land and ocean surface-related feedbacks.

The present study focuses on the interannual variability, rather than trend, of absorbing aerosols over South Asia. It provides insight on how year-to-year variations of aerosols over the IGP in May impact the subsequent summer monsoon.

Our analysis suggests that the significant, large-scale aerosol influence on monsoon circulation and hydroclimate is mediated by the heating of the land-surface, pursuant to reduced cloudiness and precipitation in May. The finding of the significant role of the land-surface in the realization of the aerosol impact is somewhat novel, as best as we can tell, as only heating of the lower troposphere and solar dimming effects on both land and oceans have hitherto been emphasized, albeit in context of long-term trends.[6] More specifically, we found that:

- Excessive aerosol in May leads to reduced cloud amount and precipitation, increased surface shortwave radiation, and to land-surface warming. The impacts and their relationships are supported by the structure of related vertical

[6] LK06 argue for the importance of aerosol induced low-level heating even in context of interannual variability.

motion, diabatic heating and OLR anomalies. Our analysis suggests that the "aerosol indirect/semi-direct effects" more than offsets solar dimming (the direct effect of absorbing aerosol) over the subcontinent, in context of interannual variability.

- The June (and July) monsoon anomaly associated with excessive May aerosols is of opposite sign over much of the subcontinent (although with a different pattern). The monsoon strengthens.

Our analysis suggests the following physical picture: Absorbing aerosols are responsible in May for a decrease of cloudiness over India, which leads, above all, to reduced precipitation, increased shortwave radiation at the surface, and heating of the dry ground. These changes may be attributed to the evaporation of the cloud layer from the absorption of solar radiation by aerosols and subsequent heating of the air – also known as the "semi-direct" effect (e.g., Hansen et al. 1997; Ackerman et al. 2000; Kaufman and Koren et al. 2006). Indeed, the resulting decrease in cloud cover and albedo can lead to a warming of the surface whose magnitude can exceed the cooling from the direct effect (Ackerman et al. 2000).

As the season progresses, the monsoon intensifies and although we have not conducted a modeling analysis to connect the anomalous heating of the land-surface in May to increased monsoon rainfall in June and July over both local and remote regions, we argue that the enhancement of the monsoon results from the increased thermal contrast (originated in May) as in the basic monsoon mechanism.

Our finding on the aerosol-monsoon link in the month of May is based on contemporaneous correlations. As such, one could argue that deficient rainfall in May (from other causes) leads to less aerosol washout, and thus greater aerosol concentration in the same month. This possibility is however refuted based on additional correlation analysis (not reported) where the April AI over the IGP region is correlated with precipitation and circulation anomalies in May and June. The lagged patterns regressed on April AI are found to be similar to the ones described above using the May AI, with the aerosol signal leading the May-June heating and circulation anomalies, indicating causality and support for our hypothesis. Lagged regressions allow such inference only because the IGP aerosol anomalies are reasonably long lived within each season, as indicated by the modest 1-month drop in April and May AI autocorrelations (cf. Fig. 2.1f). Figure 2.2 moreover shows that IGP aerosols are fueled up during the pre-monsoon months not only by local sources but also by the dust advected in by the prevailing westerly low-level flow.

An important analyzed field is diabatic heating, which was residually diagnosed from the ERA40 reanalysis using the thermodynamic equation. The diagnosed heating should implicitly include the component induced by shortwave radiation absorption to the extent its influence is manifest in the synoptic scale circulation and temperature fields being assimilated. The residual method, of course, does not yield the partitioned heating components whose knowledge would be helpful in elucidating the mechanisms generating the aerosol effects. It is thus entirely possible that the heating induced by absorption of shortwave radiation is obliterated by the much larger latent heating anomalies in summer. The heating field is of great interest since

significant low-level heating anomalies in May, with a surface trapped structure, provided the first clue on how the low-level atmosphere is being heated.

As mentioned in Section 2.1, the present study has common elements with LK06 who also analyzed the impact of absorbing aerosols in late spring on the summer monsoon evolution[7]. While both analyses show the enhancement of the monsoon in June and July subsequent to enhanced aerosol loading in May, the processes hypothesized being responsible for this appear to be different. LK06 emphasizes the piling up of aerosols against the southern slopes of the Himalayas and the consequent elevated heating of the atmosphere. Our analysis (e.g., Figs. 2.3 to 2.6) suggests that the aerosol impact and operative processes over central and western India are quite different, if not opposite, to those over the eastern regions. These processes are not well captured by the broad longitudinal sector average (65°-95°E) and the use of bi-monthly averages in LK06. In the analysis presented here, there is positive vertical motion and orographic precipitation associated with northward flow against the Himalayas eastward of ~90°E in May (see, for example, Figs. 2.3 and 2.6), and, although spatially confined, this is the region that dominates the zonal averages in Figs. 2 and 3 of LK06, overwhelming the negative anomaly in the larger sector west of 90°E. Inspection of the May aerosol distribution (Figs. 2.1a-b) moreover shows rather low aerosol concentration in the northeastern region, suggesting that the precipitation anomalies there likely arise from the large-scale circulation response of the aerosol effects to the west. As far as Fig. 4 in LK06 is concerned, the present analysis also finds the atmosphere warmer over India, but in

[7] A more comprehensive discussion of LK06's results is the topic of Chapter 4.

May only. Indeed, our Fig. 2.7 shows that the vertical profile in May is very different from that in June.

One issue to be investigated in future analysis is the influence of aerosol-induced SST changes in the Indian Ocean on the South Asian monsoon, possibly through modulation of the meridional temperature gradient and moisture supply. As noted in the Introduction, modeling studies of Ramanathan et al. (2005), Chung and Ramanathan (2006), and Meehl et al. (2008) found the gradient modulation to be very influential on summer rainfall, trumping the direct effect of the haze-induced heating of the lower troposphere.

The possible remote impact of the absorbing aerosols also deserves attention. A preliminary analysis of regressions over the tropical region shows that higher aerosol loading over India in May is associated with significant (above the 90% level) negative anomalies in upper-troposphere diabatic heating and precipitation over the eastern and central equatorial Pacific, and positive anomalies over the western Pacific warm pool (resembling a La Niña-like response). Both anomalies persist through the season. Some linkage with the ENSO cycle is conceivable, since an above-normal Indian monsoon is linked, albeit weakly, with contemporaneous and lagged La Nina-like responses (e.g., Webster et al. 1998; Chung and Nigam 1999).

The time series of May AI show also a significant (above 90% confidence level) negative correlation with the North Atlantic Oscillation (NAO) (data available at the web site: http://www.cgd.ucar.edu/cas/jhurrell/indices.html) when NAO leads by 1-2 months. This relationship can be qualitatively explained in terms of springtime

surface anomalies over Eurasia induced by variations of the NAO (e.g., Dugam et al. 1997).

A deeper understanding of the causal relationships among the processes involved in the aerosol-monsoon interaction is expected from a higher temporal resolution analysis, such as a pentad analysis, which is discussed in the following Chapter 3. The robustness of our findings also needs to be ascertained by using longer records of data.

The analysis presented here, despite many limitations, may have important bearing on the understanding of current and future variations of the monsoon hydrological cycle which, directly or indirectly, affects more than 60% of the world population.

2.6 Figures

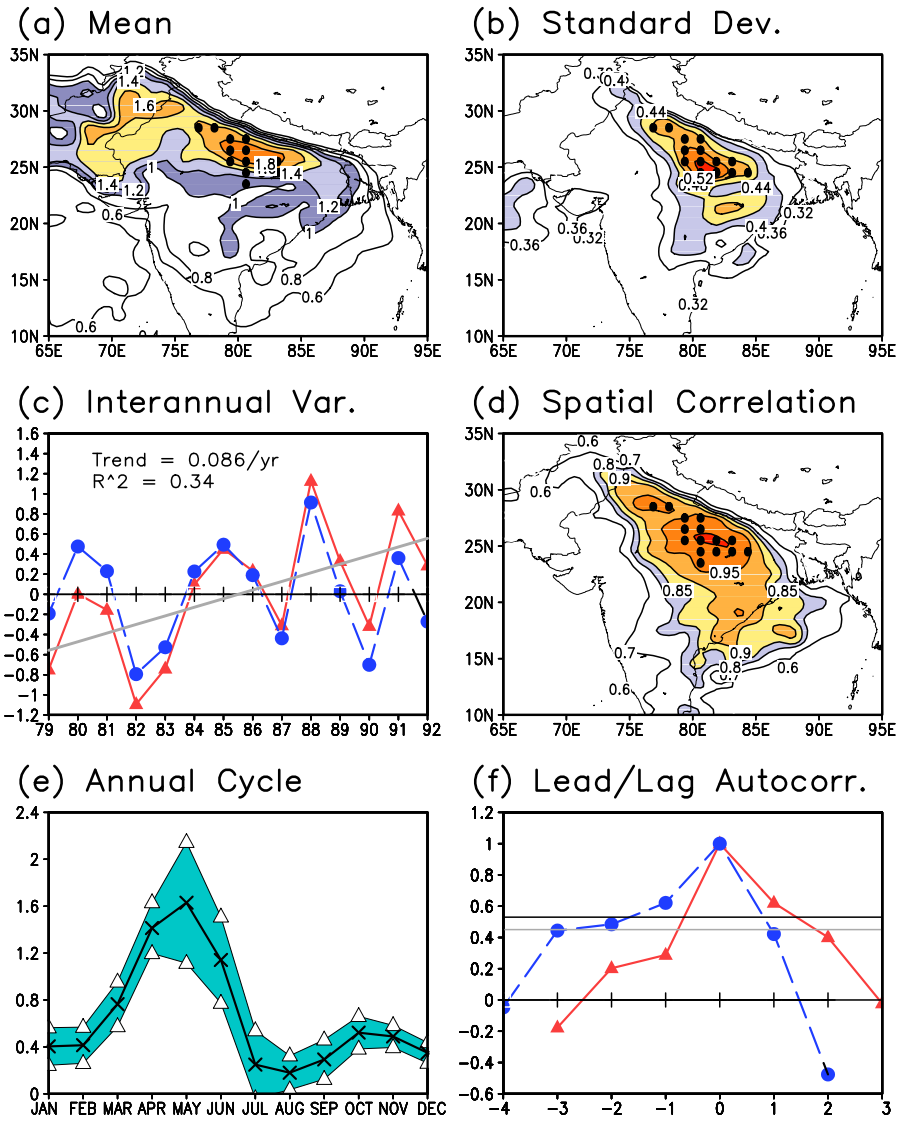

Figure 2.1: Climatological (1979-1992) characteristics of absorbing aerosols based on the TOMS AI (dimensionless) during May (except (e) and (f)): (a) its distribution; (b) standard deviation; (c) time series of anomalies averaged over the region marked with black points in (a), (b), and (d) (solid line with triangles: original data; dashed line with closed circles: original data after removing trend; continuous straight line: least square fit); (d) spatial correlation of the detrended time series in (c); (e) annual cycle (crossed line) with the range of plus/minus one standard deviation around the mean enclosed by the shaded area); (f) lead/lag autocorrelations of April (solid line with triangles) and May (dashed line with closed circles) time series of AI anomalies averaged over the same region as in (c) and (e), with the 90% and 95% confidence levels as straight lines (0.47 and 0.53, respectively). In (f), the x-axis represents the month of lead or lag (if negative or positive, respectively) with respect to the base time (contemporaneous correlations). All data (except the continuous line in (c)) were displayed after removing the trend. The trend (d) is 0.086 yr^{-1}, with $R^2 = 0.34$. The black dots in (a), (b), and (d) shows the points used in spatially averaging the AI and building the time series of anomalies, corresponding to locations with standard deviation greater than 0.48.

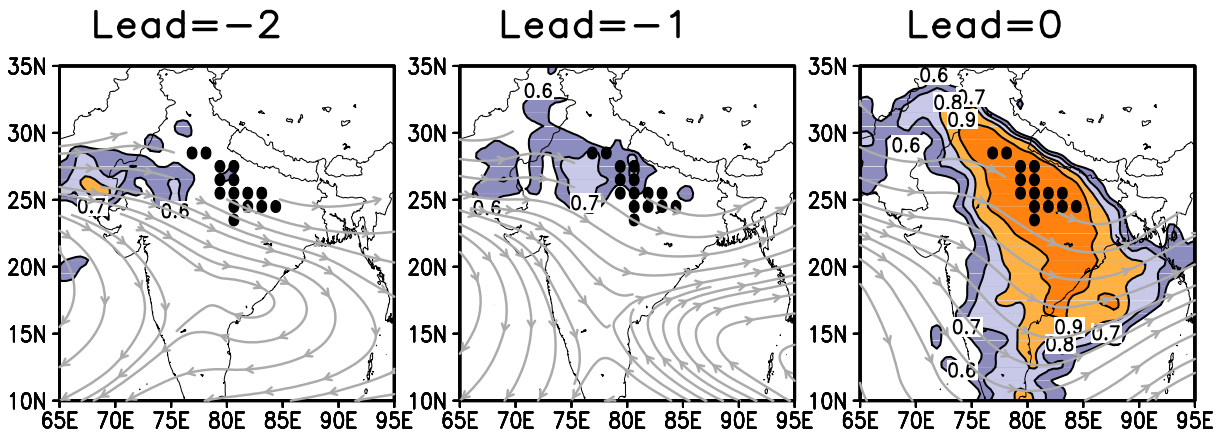

Figure 2.2: Correlations (shaded) between the time series of May AI anomalies (see Fig. 2.1) and the AI distribution in March (lead = -2; left), April (lead = -1; middle) and May (lead = 0; right, same as Fig. 2.1d), and the climatological (1979-1992) horizontal wind at 850 hPa represented as streamlines.

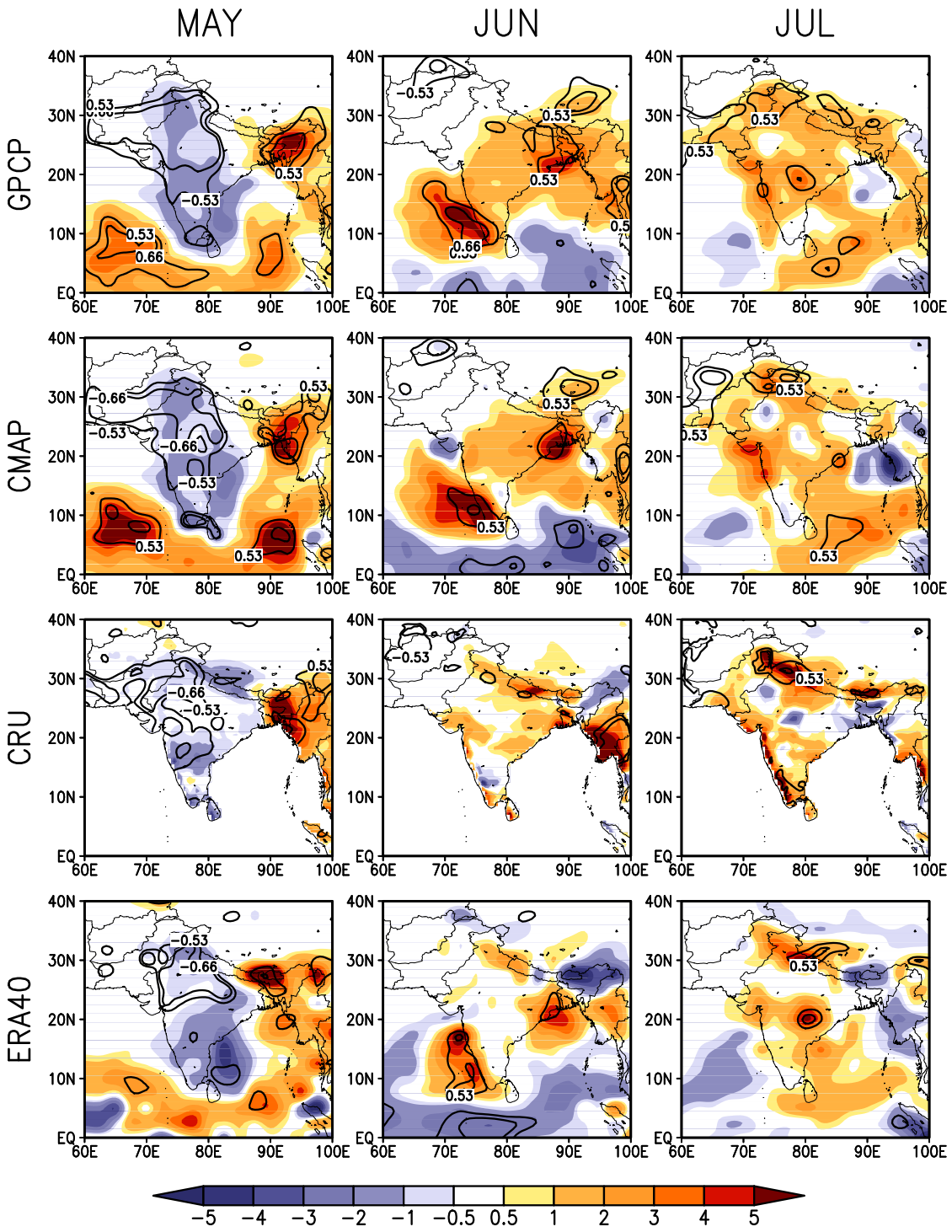

Figure 2.3: Precipitation (mm day^{-1}) regressed on the AI time series (see Fig. 2.1) for (left to right) May, June, and July, based on (top to bottom) GPCP, CMAP, CRU, and ERA40. The ±0.53 and ±0.66 contour lines show the 95% and 99% confidence levels, respectively.

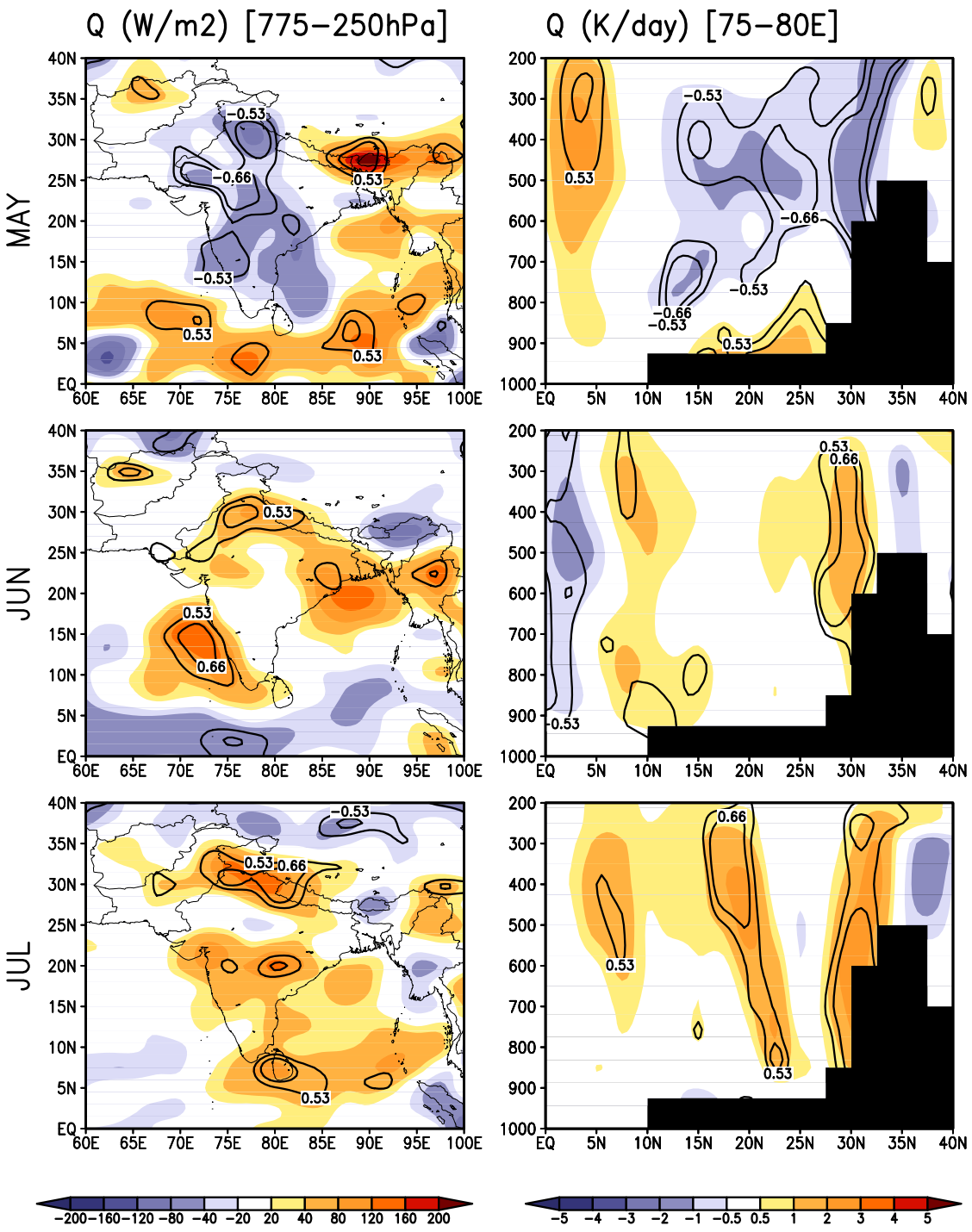

Figure 2.4: Diabatic heating regressed on the AI time series (see Fig. 2.1) for (top to bottom) May, June, and July. Left column: monthly mean distribution of the mass-weighted vertical integral between 775 and 250 hPa (W m^{-2}); right column: latitude-height cross-section (average between 75°-80°E; values in K day^{-1}), with topography in black. The ±0.53 and ±0.66 contour lines show the 95% and 99% confidence levels, respectively.

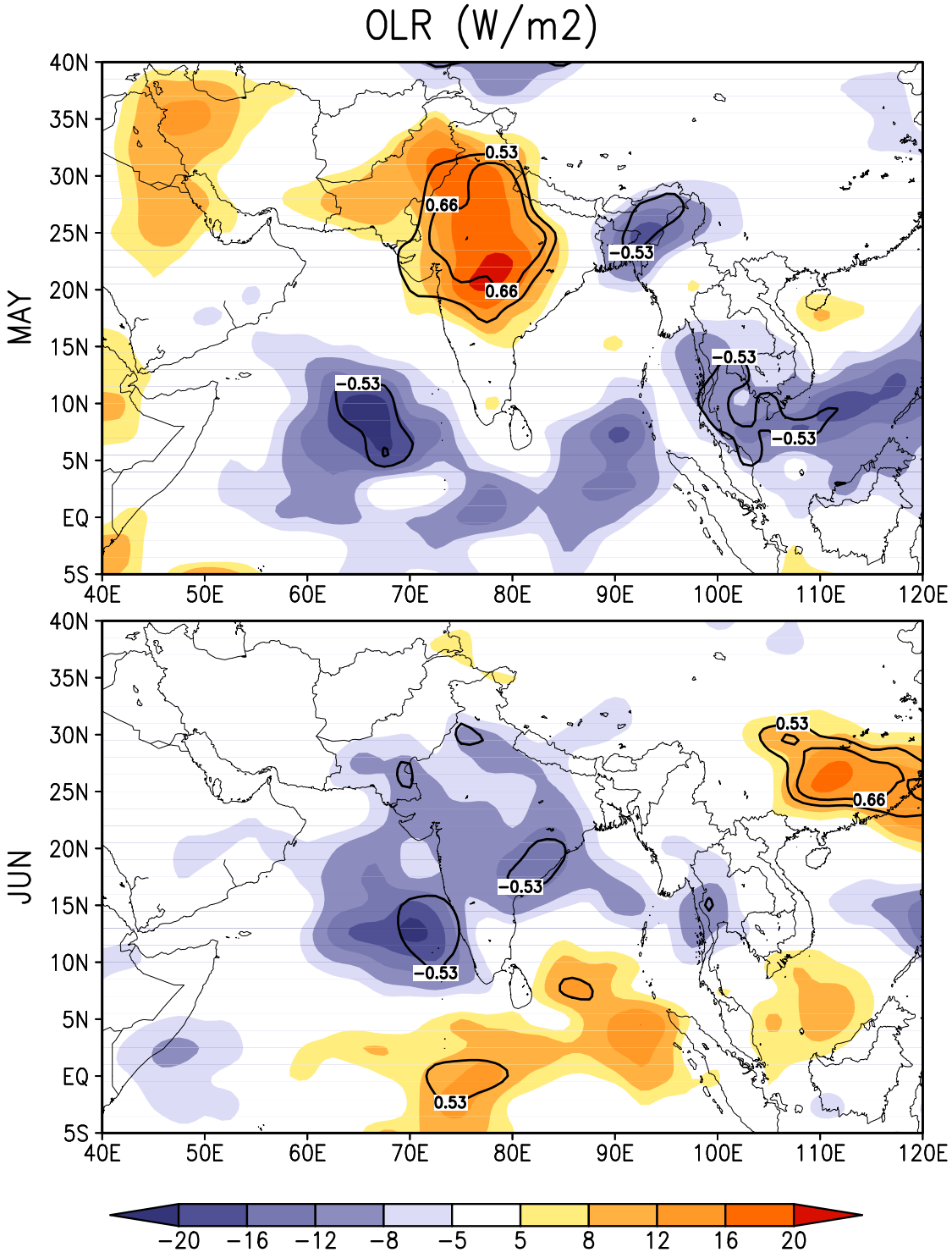

Figure 2.5: OLR (W m^{-2}) regressed on the AI time series (see Fig. 2.1) for May (top) and June (bottom). The ±0.53 and ±0.66 contour lines show the 95% and 99% confidence levels, respectively.

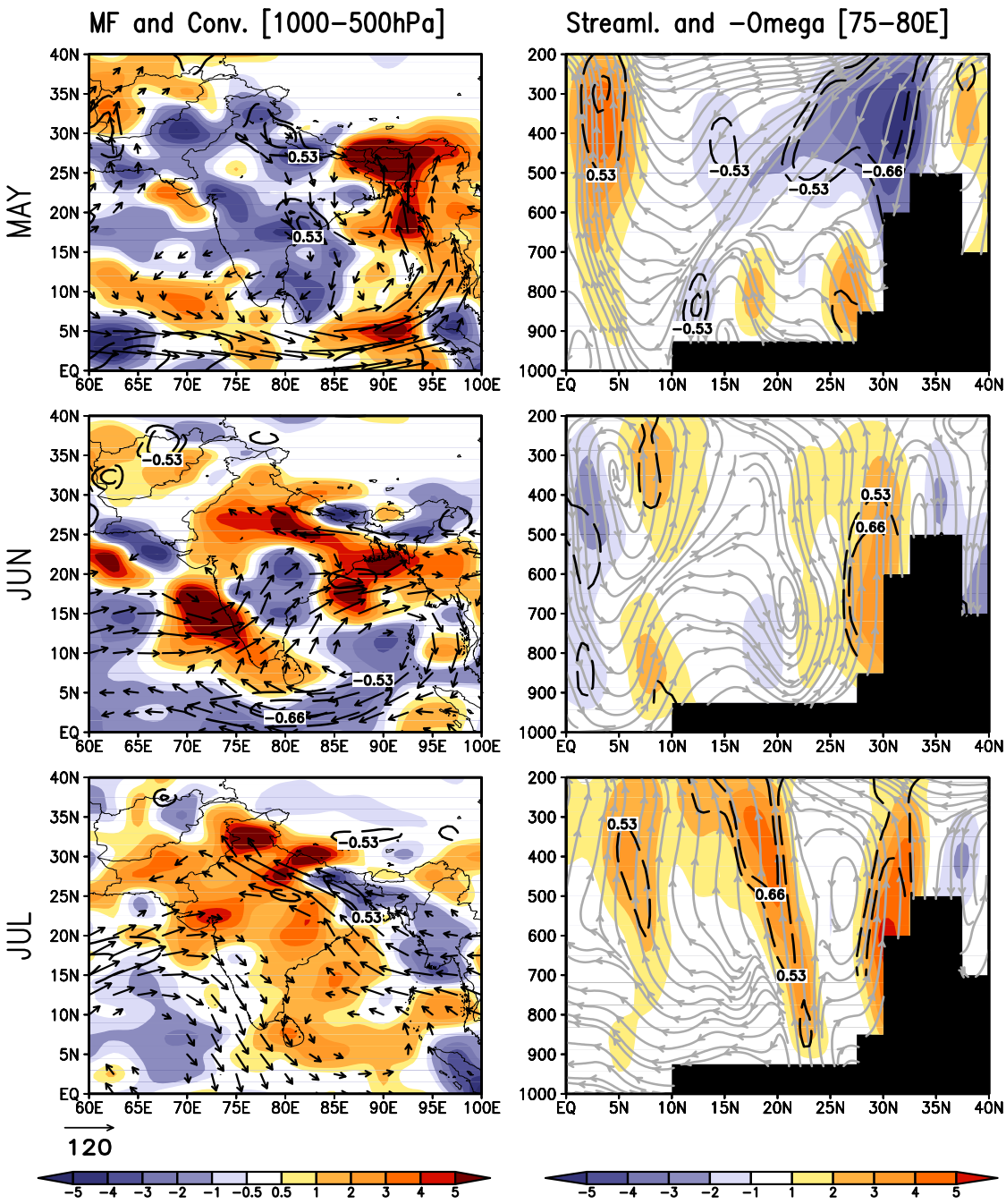

Figure 2.6: Left column: moisture flux (Kg m^{-1} s^{-1}; vectors, values below 20 Kg m^{-1} s^{-1} have been masked out) and its convergence (Kg m^{-2} s^{-1}; shaded, positive values representing convergence) mass-weighted vertically integrated between 1000 and 500 hPa and regressed on the AI time series (see Fig. 2.1) for (top to bottom) May, June and July. Right column: latitude-height cross-section (average between 75º-80ºE; topography in black) of streamlines (continuous gray lines) and – ω (shaded; in 10^2 Pa s^{-1}) regressed on the AI time series for (top to bottom) May, June and July. The ±0.53 and ±0.66 dashed lines show the 95% and 99% confidence levels, respectively, for the moisture flux (left column) and for the vertical velocity (right column).

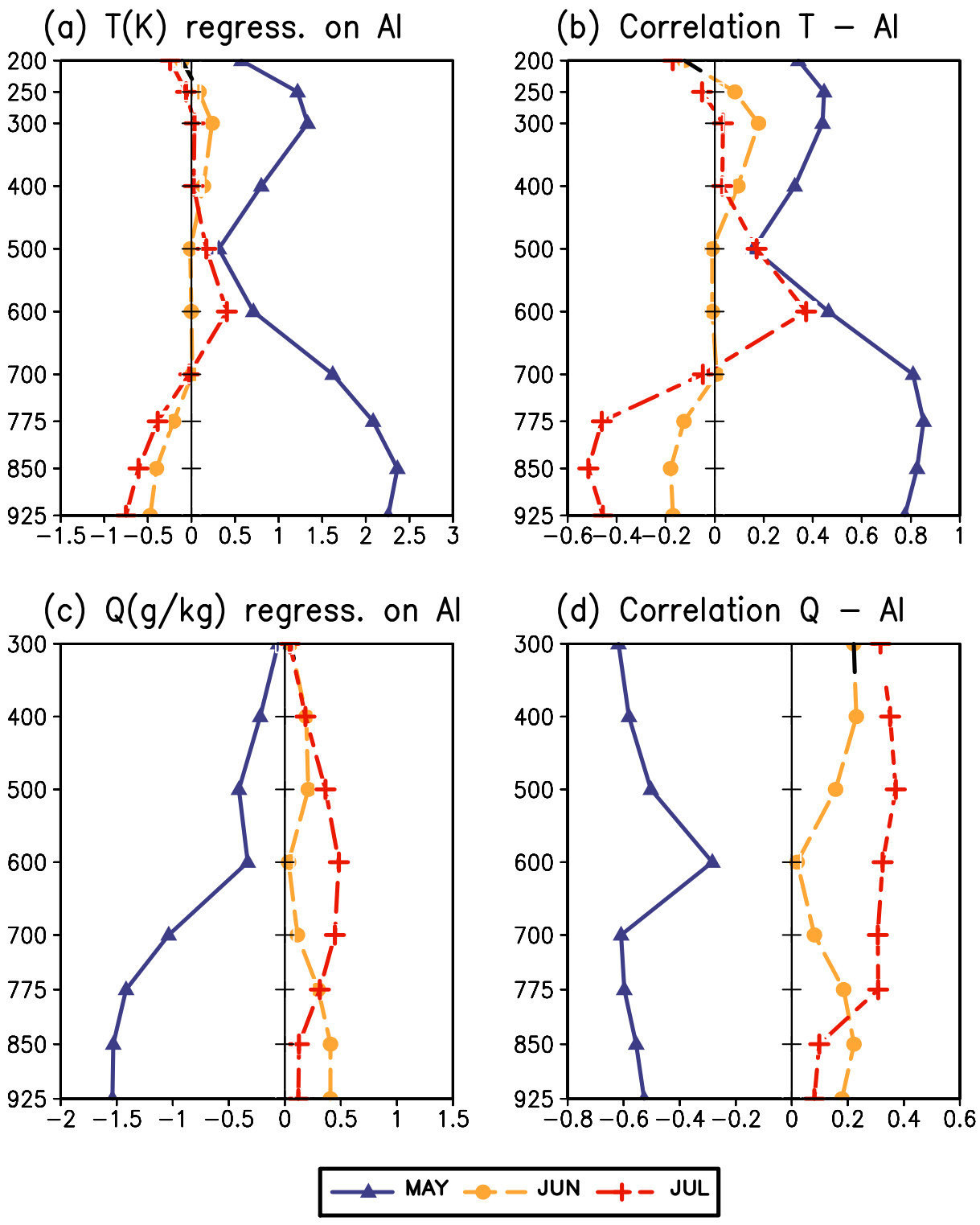

Figure 2.7: Vertical profiles (average over 20º-25ºN, 75º-80ºE) of temperature (K, top) and specific humidity (g Kg^{-1}, bottom) regressed on (correlated with) the AI time series (see Fig. 2.1) for May (solid line with triangle marks), June (dashed line with closed circle marks) and July (dashed line with plus marks). Regressions are shown in (a) and (c), correlations are shown in (b) and (d).

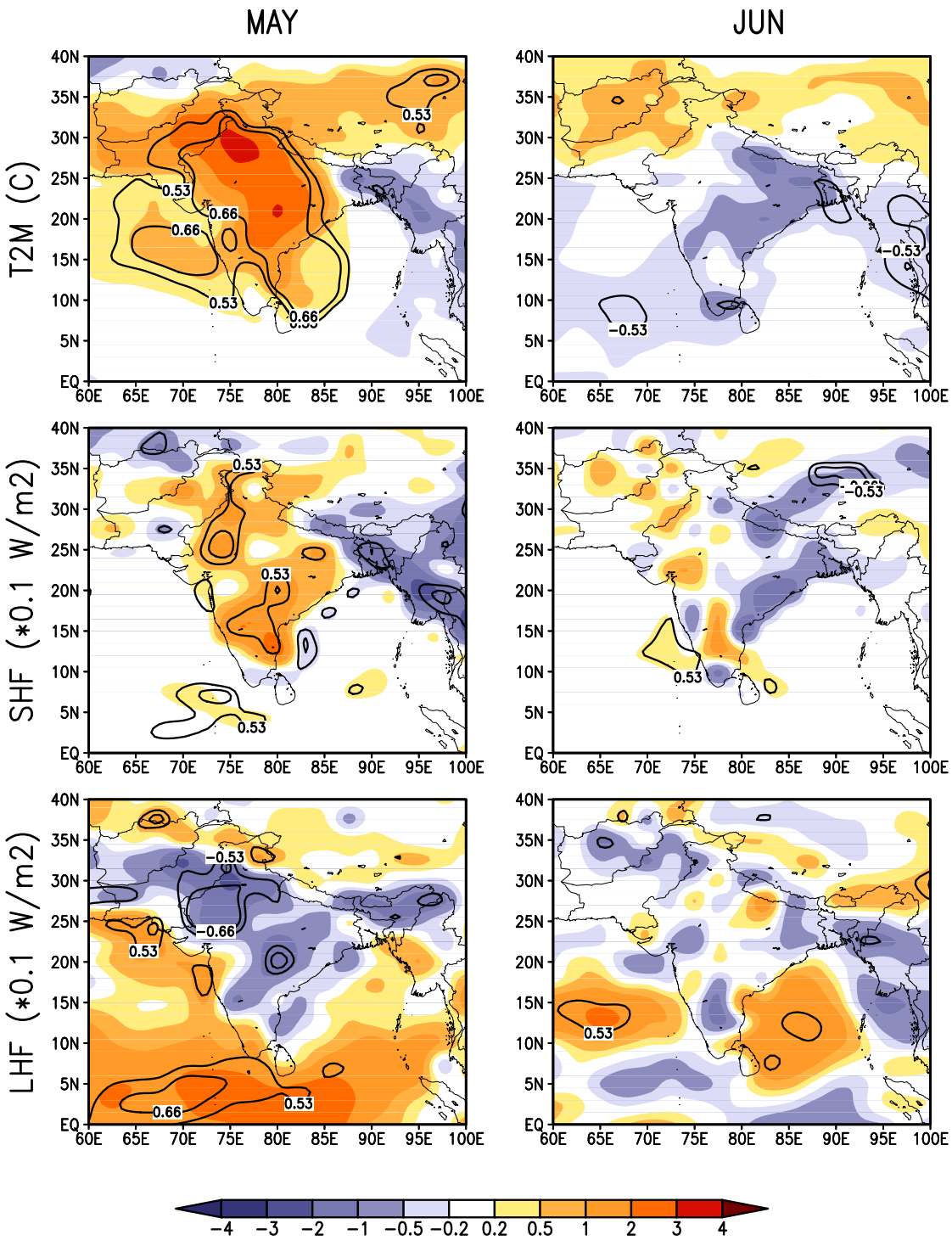

Figure 2.8: 2-m air temperature (C, top), sensible heat flux (W m^{-2}, middle), and latent heat flux (W m^{-2}, bottom) regressed on the AI time series (see Fig. 2.1) for May (left column) and June (right column). Positive fluxes are from the surface to the atmosphere. The ±0.53 and ±0.66 contour lines show the 95% and 99% confidence levels, respectively.

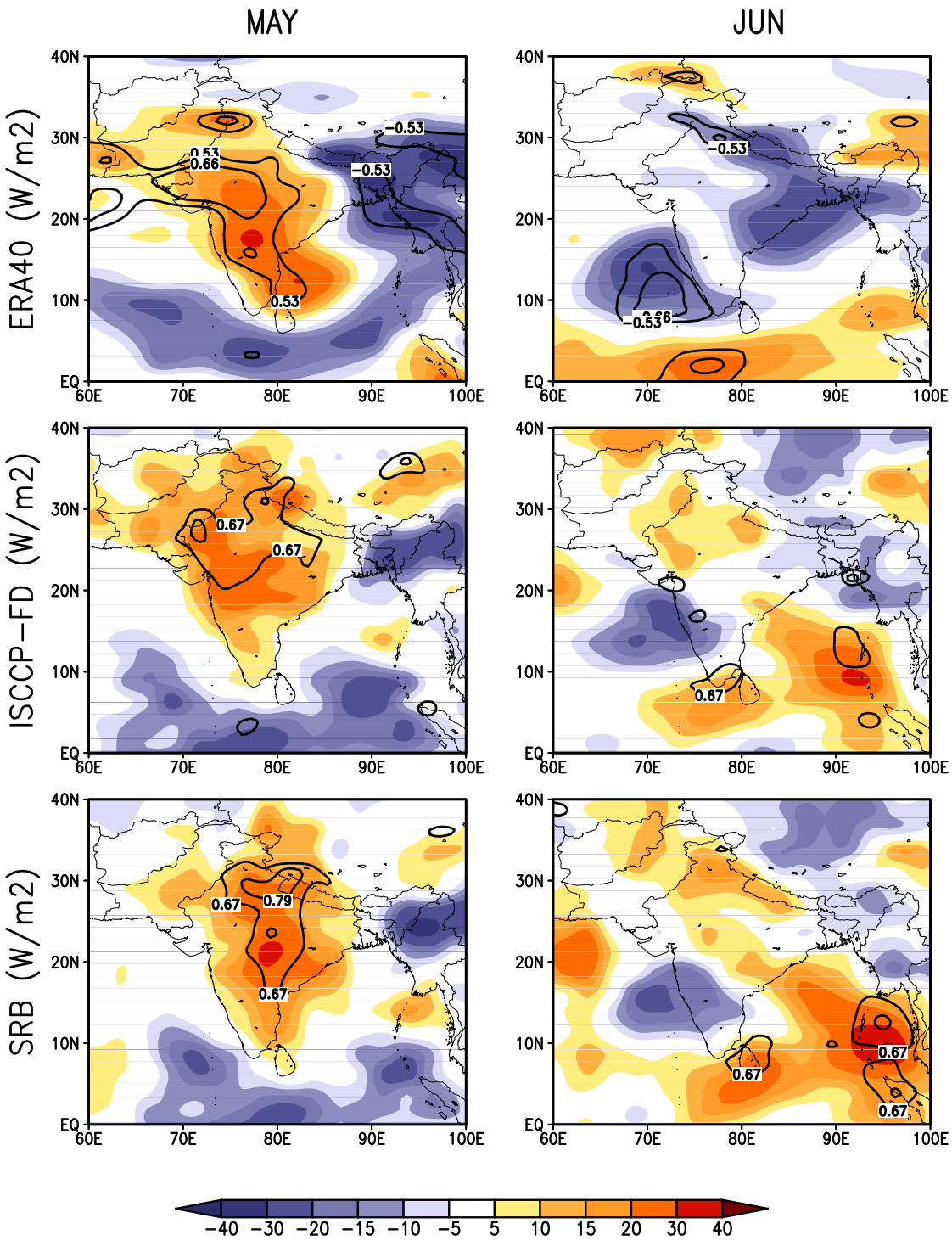

Figure 2.9: Downward shortwave radiation at the surface (W m^{-2}) regressed on the AI time series (see Fig. 2.1) for (left to right) May and June, based on (top to bottom) ERA40, ISCCP-FD, and GEWEX/SRB. For ERA40 data are for 1979-1992 (the ±0.53 and ±0.66 contour lines show the 95% and 99% confidence levels, respectively), for ISCCP-FD and GEWEX/SRB data cover 1984-1992 (the ±0.67 and ±0.79 contour lines show the 95% and 99% confidence levels, respectively).

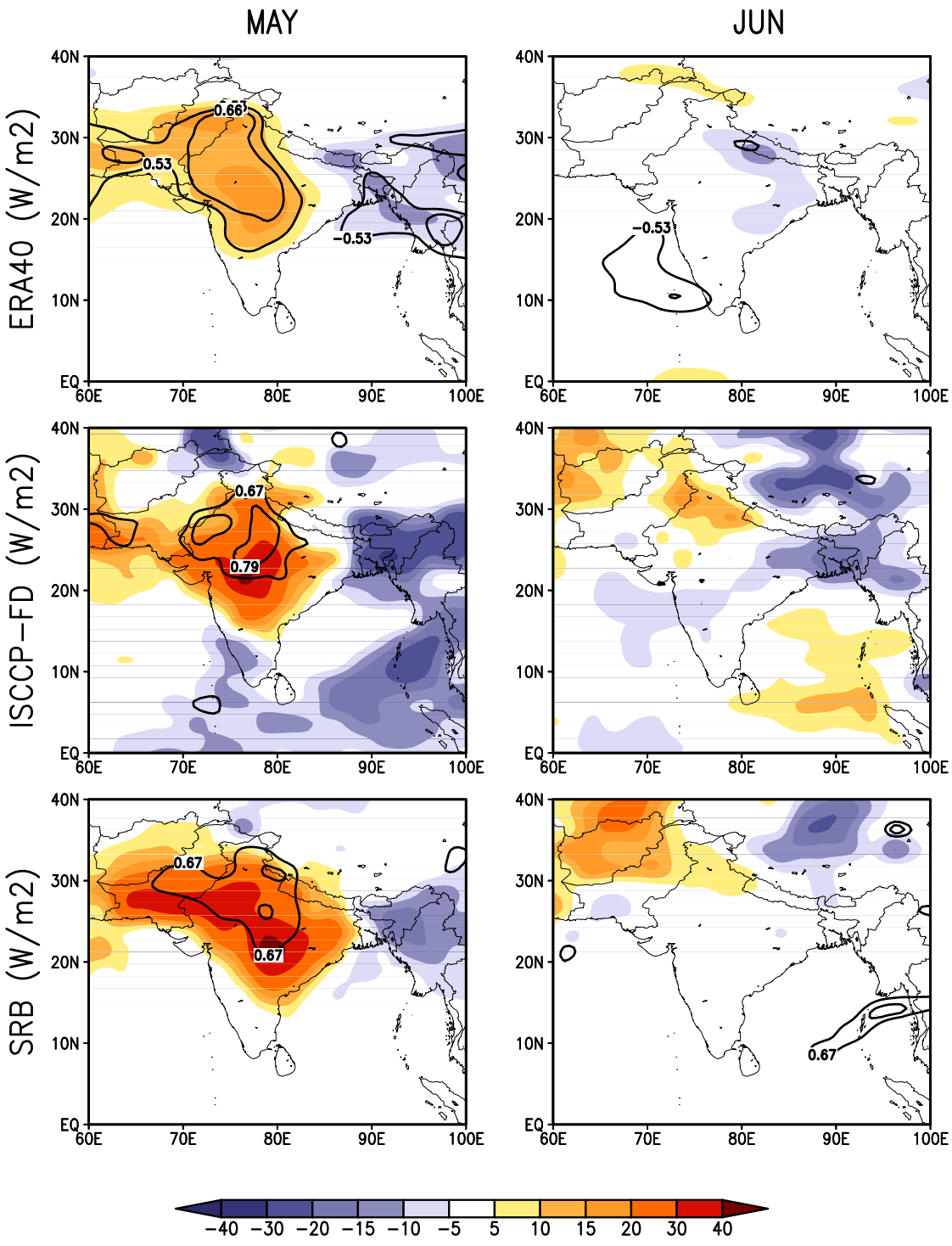

Figure 2.10: Net longwave radiation at the surface (W m^{-2}, upward flux is positive) regressed on the AI time series (see Fig. 2.1) for (left to right) May and June, based on (top to bottom) ERA40, ISCCP-FD, and GEWEX/SRB. For ERA40 data are for 1979-1992 (the ±0.53 and ±0.66 contour lines show the 95% and 99% confidence levels, respectively), for ISCCP-FD and GEWEX/SRB data cover 1984-1992 (the ±0.67 and ±0.79 contour lines show the 95% and 99% confidence levels, respectively).

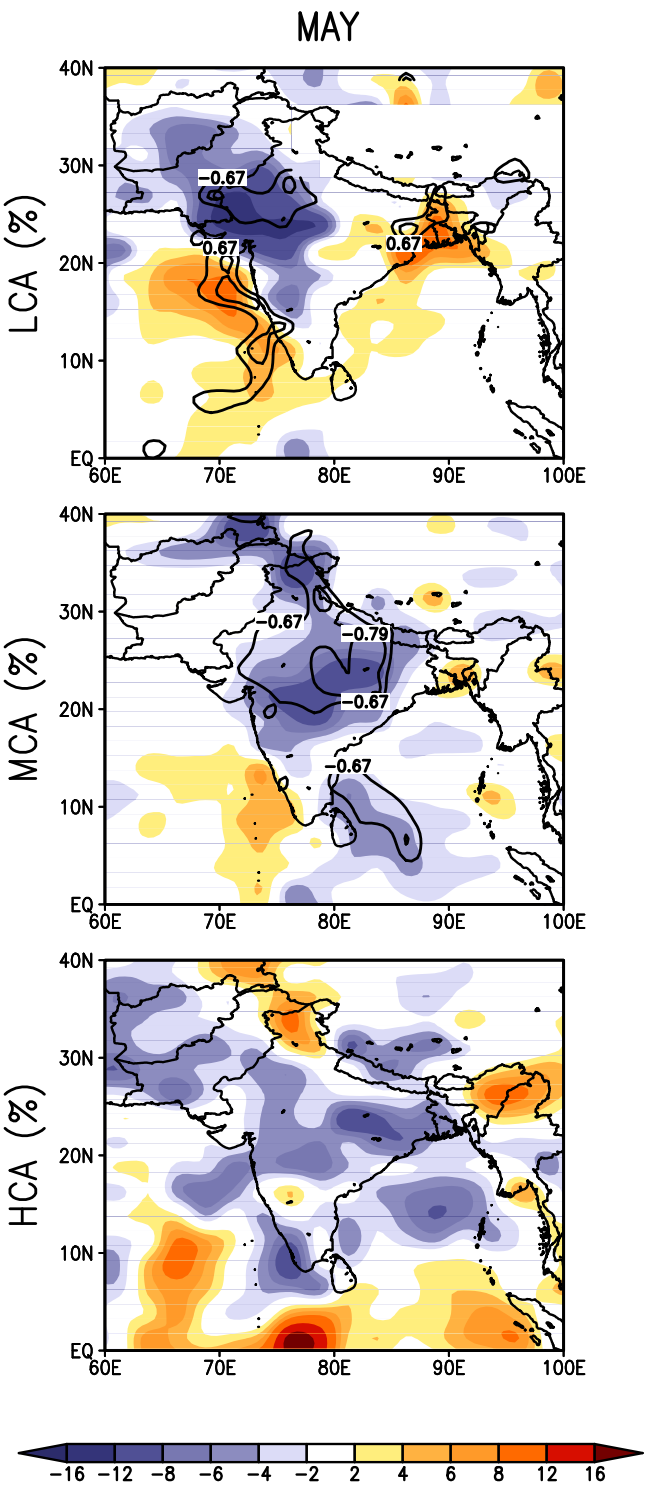

Figure 2.11: Low (LCA), middle (MCA), and high (HCA) cloud amount (%) regressed on the AI time series (see Fig. 2.1) during May based on ISCCP D2. Data are for 1984-1992 and the ±0.67 and ±0.79 contour lines show the 95% and 99% confidence levels, respectively.

Chapter 3: Absorbing Aerosols and Pre-Summer Monsoon Hydroclimate Variability over the Indian Subcontinent: The Challenge of Investigating Links[8]

3.1 Introduction

Over the past decade there has been substantial improvement in the knowledge of the amount, geographical distribution, physical and chemical properties of atmospheric aerosols. Intensive field experiments, new surface and remote-sensing observations, and improved representation of aerosol processes in models have shed new insights into the controlling mechanisms, radiative effects, and the influence of aerosols on climate.

The influence of anthropogenic aerosols on the Earth's radiation budget is however still considered the largest uncertainty in radiative forcing under climate change (IPCC 2007). The quantification of tropospheric aerosol effects is challenging because of their large spatial and temporal variability, diverse physical and chemical properties, and complex interactions of aerosols with radiation, microphysical processes and circulation (e.g., Ramanathan et al. 2001; Menon, 2004; Lohmann and Feichter 2005). The influence of large-scale circulation on both aerosol distribution and regional hydroclimate is an additional complicating factor in the analysis of aerosol effects – one emphasized in this study.

[8] This Chapter has been published as Bollasina and Nigam (2009).

A number of observational studies have characterized the South-Asian aerosol cloud (e.g., Eck et al. 2001; Hsu et al. 2003; Ramanathan and Ramana 2005; Dey and Tribathi 2007; Gautam et al. 2007; Prasad and Singh 2007; Ramachandran and Cherian, 2008), a 3-km thick brown layer persisting from October to May from the Himalayan foothills to the northern Indian Ocean, with a large contribution to aerosol optical depth from absorbing aerosols (e.g., dust (12%) and black carbon (11%); Ramanathan et al. 2001). This haze induces a large perturbation to the radiative energy budget of the region (up to -25 Wm^{-2} in the mean clear-sky surface radiation; Ramanathan et al. 2005) which has significant implications for the water budget, agriculture and health. Understanding the effects of aerosols on the distribution and duration of the South Asian monsoon rainfall (which accounts for nearly 75% of the yearly precipitation over many regions of the subcontinent) would be relevant for more than 60% of the world's population.

The large-scale impact of aerosols on the monsoon, mostly its climatological rainfall distribution, has been addressed by general circulation modeling studies (Menon et al. 2002; Ramanathan et al. 2005; Chung and Ramanathan 2006; Lau et al. 2006; Meehl et al. 2008; Randles and Ramaswamy 2008) and several mechanisms have been proposed (e.g., Ramanathan and Carmichael 2008). Despite the usefulness of climate models in highlighting the physical processes and mechanisms involved in aerosol-monsoon interaction, some caution is necessary in interpreting the results, as these models are known to have significant biases in the climatological distribution and evolution of monsoon precipitation (e.g., Dai, 2006; Bollasina and Nigam 2008, see Chapter 5). Furthermore, aerosol effects are only partially represented in many

models (e.g., Kiehl 2007), and large uncertainties are associated even with those effects currently included (e.g., Kinne et al. 2006).

Reanalysis and remote-sensed gridded observational datasets have been recently analyzed by LK06 and, somewhat more comprehensively, by Bollasina et al. (2008) (hereafter BNL08, see Chapter 2). In particular, BNL08 showed interannual variations of absorbing aerosols over the IGP in late spring to have a large-scale impact on the development of the ensuing summer monsoon through aerosol-induced anomalies of cloudiness (the "semi-direct" effect; Hansen et al. 1997) and the mediation of land-surface processes: reduced cloudiness (and rainfall) over the IGP in May associated with high aerosol loading leads to heating of the land surface and development of low-level cyclonic circulation that brought more rain to northeastern India in May, and to western peninsular India in June.

However, the coarse-resolution monthly data used in BNL08 did not allow a close temporal investigation of the development of aerosol anomalies and of the evolution of their linkages with atmospheric and surface anomalies. This motivated the present work.

This study analyzes observational data at higher temporal resolution (i.e., five-day averages (pentads) instead of monthly data) and focuses on the transition period prior to monsoon-onset. The goal was to describe the evolution of aerosol-related anomalies in radiative and hydrometeorological fields in order to better pinpoint aerosol effects. Indeed, the analysis showed IGP aerosols to lead large-scale anomalies over the Indian Subcontinent starting by the end of April and for several pentads. However, the identification of mechanisms at play and aerosol effects, per

se, is shown to be challenging given the dominant role played by the large-scale low-level horizontal advection and associated vertical circulation. In this view, caution is necessary in attributing causes and effects if one is not cognizant of the orchestrating role of the large-scale low-level circulation.

The Chapter is organized as follows: data and methods used in the analysis are described in Section 3.2. Section 3.3 examines the variability of absorbing aerosols over India and associated links with large-scale pre-monsoon conditions. Concluding remarks follow in Section 3.4.

3.2 Datasets

Several independent datasets were used in this study. The loading of absorbing aerosols was characterized by means of daily values of the TOMS AI, available on a 1.25º x 1° grid from November 1978 onwards (Torres et al. 2002). As in BNL08, several issues limited the length of the time series used in this analysis to the period 1979-1992.

ERA-40 (Uppala et al. 2005) provided 6-hourly atmospheric and surface data on a 2.5° x 2.5° grid. Observed precipitation came from the GPCP pentad dataset, available on a 2.5° x 2.5° grid from 1979 (Adler et al. 2003). Daily surface shortwave radiation and total cloud fraction data were obtained from the GEWEX SRB Project at 1° resolution from January 1984 onward (Gupta et al. 1999). The NOAA daily OLR data on a 2.5° x 2.5° grid (Liebmann and Smith 1996) were also used.

All data were averaged over pentad intervals (starting every year on January 1), and correlations/regressions were computed using linearly detrended time series of

anomalies (with respect to the 1979-1992 mean annual cycle) in order to minimize the influence of trends on the strength of the deduced relationships. Pentad averaging is effective in masking out the day-to-day fluctuations of weather while retaining sub-monthly variability arising from the super-synoptic time-scale processes in the atmosphere – the component of interest here.

3.3 Results

The fundamental characteristics of absorbing aerosols over the Indian Subcontinent are summarized in Fig. 3.1. The climatological distribution during 26 April-10 May – a three-pentad period corresponding to peak aerosol loading over most parts of India – is shown in Fig. 3.1a. The aerosol cloud is clearly piled up against the Himalayan foothills, and has a distinct maximum over the IGP with northwestward extension towards Pakistan. Climatologically, the lower-tropospheric subsidence over northwestern India associated with westerly flow across Afghanistan and Pakistan plays a major role in building up the aerosol layer during spring (e.g., Dey et al. 2004). Dust storms are common in the Middle East and the Thar Desert in late spring and early summer, and they are an effective dust source for the Indian subcontinent because of the prevailing westerlies. The IGP is one of the most densely populated basins in the world and the large emission of regional pollutants from fossil fuels (typically invariant through the season) and biomass burning (predominant in winter and spring) also contributes to the total aerosol loading (e.g., Habib et al. 2006).

The solid dots marked in Fig. 3.1a delineate the region used in defining the aerosol time series, consistently with BNL08 (see Fig. 2.1). The dots mark the locations of highest interannual variability of aerosols (standard deviation of TOMS AI greater than 0.5), and the resulting time series of areal averaged aerosol anomalies (referred to as the "IGP aerosol time series") is thus an efficient marker of the aerosol signal. Lead/lag regressions of the Sub continental atmospheric circulation on this regional aerosol time series are used to characterize the aerosol-related anomalies. The seasonal evolution of the detrended time series is displayed in Fig. 3.1b. The pentad data shows rapid buildup of aerosols in late spring and a precipitous drop in June due to monsoon onset – features not discernible in monthly data (cf. Fig. 2.1e). The aerosol loading peaks in the first pentad of May (i.e., 1-5 May). The envelope around the seasonal curve marks the range of variability at plus/minus one standard deviation. The interannual variability is evidently much larger in late spring and early summer (i.e., in the pre-monsoon onset period) than at other times.

The detrended record of the IGP aerosol anomalies averaged over three pentads (26 April-10 May) is shown in Fig. 3.1c, the linear trend in the 1979-1992 period being +0.042 yr^{-1}. The time series displayed in Fig. 3.1c is used in the following regression analysis.

Figure 3.2 displays the lead/lag regressions and correlations of the IGP aerosol anomalies with aerosols over central-eastern India (Fig. 3.2a), and of the IGP aerosol-tendency (computed as centered differences of the aerosol anomalies) with aerosols and precipitation of the same region (Figs. 3.2b and 3.2c, respectively). Central-eastern India, as defined here, includes the core of the Indian peninsula and, referring

to the homogeneous monsoon rainfall divisions of the Indian Institute of Tropical Meteorology, encloses the west central, central northeast (up to 85°E), and the peninsular (to 15°N) divisions. The IGP aerosol time series exhibits a certain amount of autocorrelation at all times (not shown) since aerosol loading is maintained by the eastward advection of dust and local emissions, resulting in a residence time of the order of one pentad. Figure 3.2a shows that IGP aerosols are strongly linked with aerosol loading over central-eastern India (a downstream region, see bottom panels in Fig. 3.3) from the end of April to mid-May, especially at +2-3 pentad lag (i.e., IGP aerosols leading by 2-3 pentads), indicating a role for large-scale advection in aerosol buildup over the latter region. The advection link is consistent with Fig. 3.2b, which shows the lead/lag relationship of the IGP aerosol-tendency. A positive tendency is linked with increased aerosol anomalies over central-eastern India 2-3 pentads later, but uncorrelated with antecedent anomalies of the same region.

The lead/lag links of the tendency of a quantity (as above) generally highlight the high-frequency response (Cayan 1992). These links are often more pertinent as the tendency, rather than the quantity itself, is part of the related prognostic equation. Figure 3.2c shows positive AI-tendency over the IGP region to be negatively linked with precipitation over central-eastern India in late April and early May. The negative correlations originate at lag 0 and persist for several (positive) lags. This pattern may indicate an influence of aerosols on the atmosphere. However, a similar delay in aerosol-increase and precipitation-decrease over central-eastern India suggests that either one pentad is a too long interval for discerning cause and effect or an orchestrating role for the large-scale circulation (shown later in Fig. 3.3).

The lead/lag links of aerosol-tendency, aerosols, and precipitation over the same region (e.g., central-eastern India) are similar to those depicted in Fig. 3.2, and thus not shown. The aerosol-tendency is anticipated to lead aerosols, but not precipitation, necessarily. For instance, aerosol-washout will manifest as negative contemporaneous correlation, in the absence of other influences. Negative correlations in Fig. 3.2c (and in a corresponding figure where all quantities are for central-eastern India, not shown) are however strongest at lag +2 pentads, suggesting that washout alone is not the major process, although it may well be important in conjunction with other processes (e.g., aerosol advection).

The relationship between regional aerosol variability (viz. the IGP aerosol tendency) and the larger-scale circulation and hydroclimate variability is shown in Fig. 3.3 with respect to the base period of 26 April – 10 May, when the IGP aerosols have pronounced delayed links. Mean spatial patterns during this three-pentad period are shown at various lead/lags, beginning with the distribution of absorbing aerosols themselves. Not surprisingly, the IGP AI-tendency is linked with aerosol buildup which is striking across the ±one-pentad lag/lead regressions. The buildup is not confined to the north central region (covered by solid dots in Fig. 3.1a) but is more expansive, covering much of the Subcontinent over a two-pentad period. The buildup evidently persists, at least for one more pentad (i.e., lag +2). The direction of the buildup (southeastward) and its delayed nature indicate a significant role of the large-scale circulation, especially advection.

The correlations between precipitation and AI-tendency show diminished precipitation, especially to the south of the core aerosol buildup. The lack of

collocation is noteworthy, and indicative of the significance of processes that generate a nonlocal hydroclimate response to aerosol loading, or of the role of circulation (advection and convergence) in modulating both aerosol loadings and precipitation. The next three variables – downward surface shortwave radiation, total cloudiness fraction, and 2-m air temperature – obtained from independent data sets, paint a coherent picture showing aerosol-buildup and diminished precipitation to be linked with reduced cloudiness, more surface shortwave radiation, and higher 2-m temperature (and reduced convection, as manifested in the OLR anomalies, not shown here). While a physically consistent scenario emerges, attribution remains challenging for reasons mentioned earlier. For instance, both diminished precipitation (from non-aerosol influence) and aerosol buildup can initiate the displayed sequences, the latter mechanism being envisioned through its semi-direct effect. Interestingly, both effects can be simultaneously generated by the large-scale flow, blowing from the dry and dusty desert regions to the west/northwest. Regardless of the instigating mechanism, this analysis indicates that aerosol buildup is accompanied by more surface shortwave radiation, suggesting that cloudiness fluctuations can easily overwhelm the surface radiation shortfall due to aerosol absorption.

The 850-hPa anomalous circulation (not plotted in the Himalayan foothills to avoid the use of fictitious, below-ground values), especially the northwesterly-to-westerly flow, argues for the importance of advection (and horizontal convergence) in aerosol buildup, which is also indicated by the rapidity of the buildup (cf. top panel). The advective contribution is further shaped by related vertical motions (not shown).

A comparison of 850 hPa convergence (Fig. 3.3, bottom panels) and aerosol distributions indicates that convergence can be influential (e.g., at lag +1).

3.4 Concluding Remarks

Sub-monthly evolution of the interannual variations of absorbing aerosols and related hydrometeorological conditions over South Asia in the pre-monsoon period is investigated using pentad-resolution observational datasets during the period 1979-1992. This study was motivated by the findings of BNL08 on the linkage between anomalous aerosol build-up in May and delayed rainfall onset, based on the analysis of monthly data. The delayed onset was attributed to the aerosol "semi-direct" effect and ensuing land-atmosphere interactions. The initial goal of this study was to uncover the process sequence underlying aerosol-climate interactions. However, the present analysis indicates the challenge of an observationally-based approach.

The pentad-resolution analysis portrays a complex picture of aerosol evolution over central-eastern India, in which circulation plays a significant role. The pervasive influence of advection precludes a robust analysis of the aerosol impact. Removal of the advective contribution is reasonably straightforward in case of aerosol loading, but not for many other meteorological parameters that interact with aerosols (e.g., cloudiness, precipitation).

The late-April to early-May variations are characterized by aerosol loadings in central-eastern India lagging the build-up in the northern plains. Anomalous aerosols are shown to be associated with significant anomalies of surface and atmospheric variables over the Indian Subcontinent. The precipitation evolution is nearly

synchronous but not collocated with the aerosol build-up core. Cloudiness, surface shortwave radiation, and 2-m air temperature evolve in concert, precluding attribution of the noted changes.

Extraction of the aerosol impact is very challenging, observationally, in large measure because of the significant influence of large-scale advection and horizontal divergence in shaping aerosol distribution as well as regional hydroclimate. For instance, the spatiotemporal evolution displayed in Fig. 3.3 – specifically, aerosol-increase, reduced cloudiness and precipitation, and increased downward shortwave radiation – can be reasonably interpreted as the manifestation of the aerosol "semi-direct" effect, or equally, of the influence of reduced precipitation (from non-aerosol causes), if one were not mindful of the concurrent circulation anomalies. Inspection of the low-level flow structure as well as its horizontal convergence however suggests that all the above effects can just as well arise, simultaneously, from the evolving synoptic scale flow and related hydrometeorology – pointing to the pitfalls of a columnar, circulation-blind analysis framework.

Regardless of the instigation mechanism, it is shown that aerosol buildup is accompanied by more surface shortwave radiation associated with cloudiness reduction, suggesting that cloudiness fluctuation can be as relevant as surface radiation shortfall due to aerosol absorption. This point is important for modeling studies of absorbing aerosol effects on climate, especially considering model deficiencies in realistically simulating cloud changes and feedbacks (e.g., Randall et al. 2007).

This pentad resolution analysis of anomalous aerosol evolution in the pre-monsoon-onset period indicates a prominent role for low-level circulation advection (and related vertical motions) in modulating aerosol loadings, both mechanistically and through related meteorology. The role of large-scale circulation in modulating aerosol loading (and related impacts) may be appreciable even in context of decadal variability and longer-term trends in regional hydroclimate.

3.5 Figures

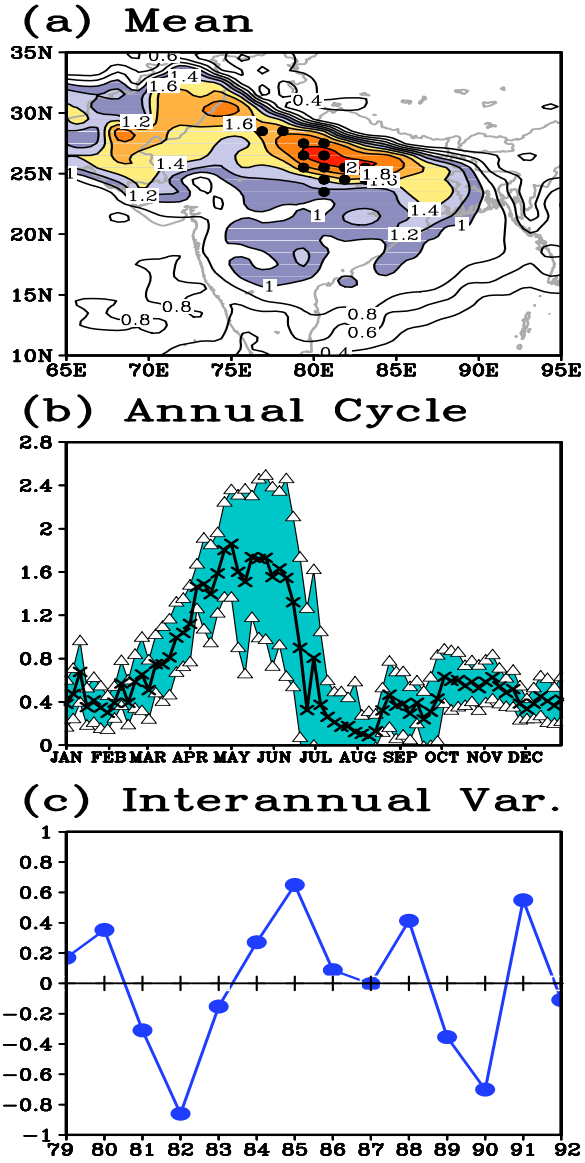

Figure 3.1: Characteristics of the absorbing aerosol layer based on the TOMS AI (dimensionless) during the period 1979-1992: (a) the mean spatial distribution for the three-pentad period 26 April – 10 May; (b) climatological annual cycle (crossed line), with the range of plus/minus one standard deviation around the mean enclosed by the shaded area, averaged over region marked with black points in (a); (c) time series of anomalies (averaged between 26 April – 10 May and after removing the linear trend, which is 0.042 yr^{-1}) averaged over the same region of (b). The points marked in (a) are consistent with BNL08 (see Fig. 2.1) and correspond to locations of highest interannual variability (standard deviation greater then 0.5).

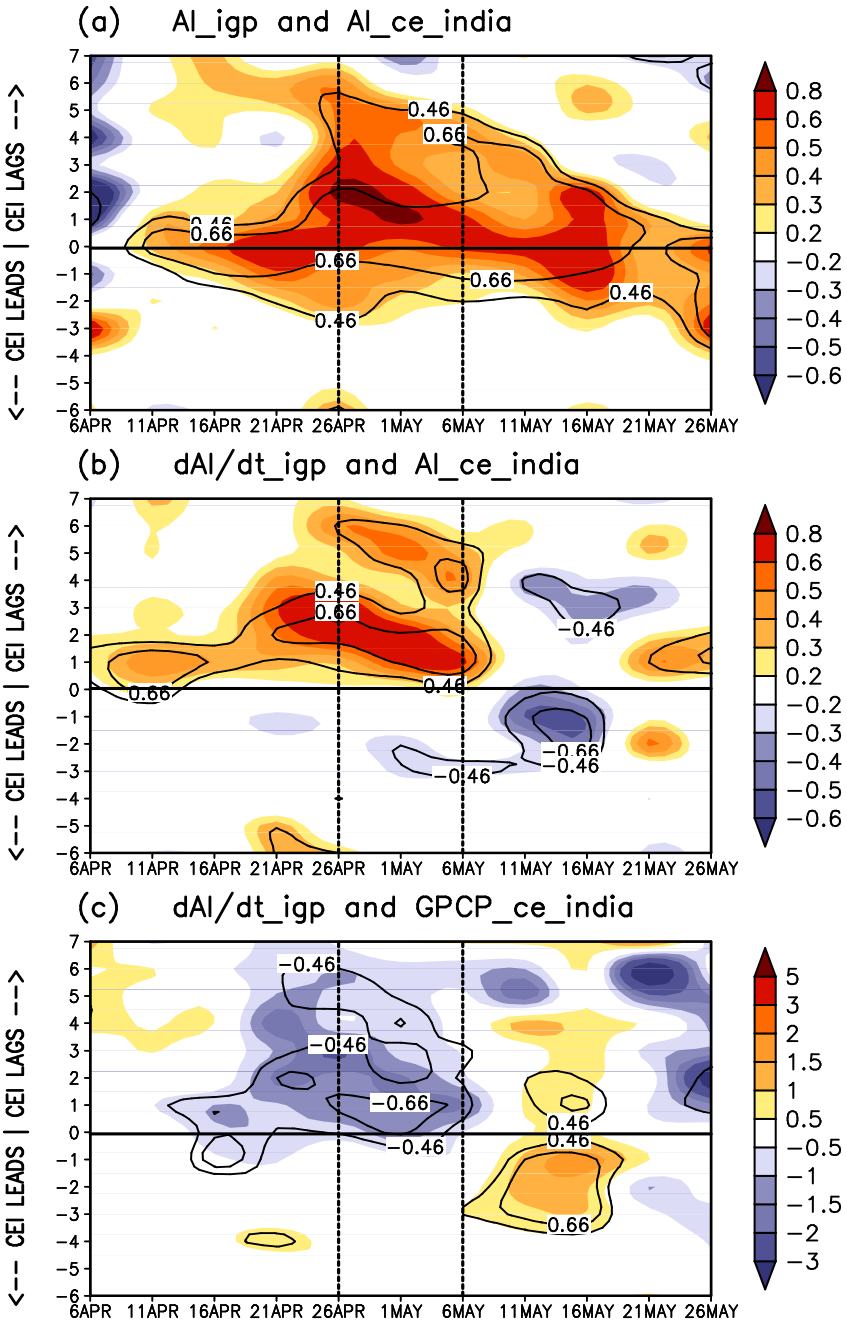

Figure 3.2: Time evolution of central-eastern India (CEI) anomalies (shaded) of aerosols ((a) and (b); dimensionless) and precipitation ((c); mm day^{-1}) lead/lag regressed on (a) the aerosol time series and (b) and (c) the aerosol tendency time series over the IGP (defined in Fig. 3.1). The ±0.46 and ±0.66 contour lines show the 90% and 99% confidence levels, respectively. The x-axis is the reference pentad of IGP anomalies, the y-axis is the lead/lag (negative/positive) of CEI anomalies with respect to IGP anomalies in terms of number of pentads. The horizontal line denotes the zero-lag axis, while the dotted vertical lines highlight the period 26 April – 6 May.

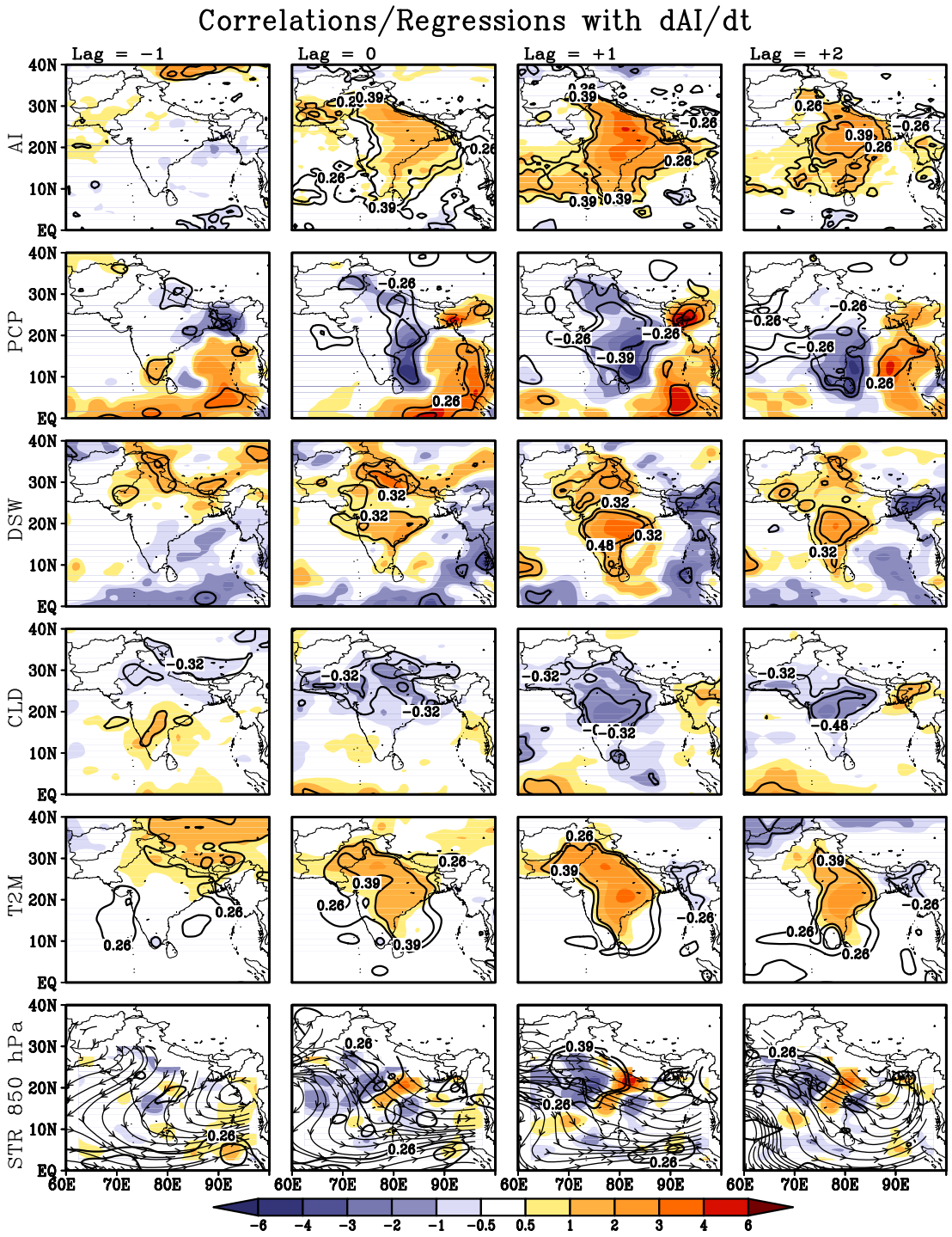

Figure 3.3: Aerosols (AI, dimensionless), precipitation (PCP, mm day^{-1}), downward shortwave radiation (DSW, W m^{-2}), total cloudiness (CLD, fraction), 2-m air temperature (T2M, ºC), 850-hPa streamlines (STR) and convergence (s^{-1}, shaded) regressed on the aerosol tendency time series over the IGP at different lead/lags during 1979-1992 (1984-1992 for cloudiness and radiation). The base period (lag 0) is the three-pentad period 26 April – 10 May. The ±0.26 (±0.32) and ±0.39 (±0.48) contour lines show the 90% and 99% confidence levels, respectively.

Chapter 4: The 'Elevated Heat Pump' Hypothesis for the Aerosol–Monsoon Hydroclimate Link: "Grounded" in Observations?[9]

4.1 Introduction

One of the areas of the world with high aerosol concentration is South Asia. The contribution of absorbing aerosols to the long-term change in summertime rainfall over the Indian subcontinent has been investigated by Chung et al. (2002), Menon et al. (2002), Ramanathan et al. (2005), Chung and Ramanathan (2006), Lau et al. (2006), Meehl et al. (2008), Randles and Ramaswamy (2008), Collier and Zhang (2009), and Sud et al. (2009). The interannual variability of aerosol concentration and related summer monsoon rainfall variations has also been analyzed (e.g., LK06; BNL08, see Chapter 2).

Atmospheric general circulation models and observational analyses have both been deployed to understand aerosol-monsoon interaction. Modeling studies are insightful because of their ability to associate cause and effect in context of modeling experiments, but some caution is necessary as model simulations are known to have significant biases in the climatological distribution and evolution of monsoon precipitation (e.g., Dai 2006; Bollasina and Nigam 2008, see Chapter 5).

[9] This Chapter has been accepted for publication in *J. Geophys. Res.* as Nigam and Bollasina (2010).

Furthermore, aerosol effects are only partially represented in many models (e.g., Kiehl 2007), often with large uncertainties (e.g., Kinne et al. 2006). It is expected that aerosols-clouds-precipitation processes and interactions will be greatly improved in the next generation of climate models (e.g., Ghan and Schwartz 2007). Observational studies, on the other hand, analyze a realistic system, but characterization of the pertinent process sequence remains challenging on account of the myriad of feedbacks in the climate system. The influence of large-scale circulation on both aerosol distribution and regional hydroclimate also confounds efforts to elucidate the aerosol impact mechanisms (Bollasina and Nigam 2009, see Chapter 3).

Several pathways have nonetheless been proposed for aerosol's influence on monsoon hydroclimate:

- Anomalous heating of air due to shortwave absorption by black carbon aerosols, which enhances regional ascending motions and thus precipitation in atmospheric general circulation models (Menon et al. 2002; Randles and Ramawamy 2008).
- Modulation of the summertime meridional SST gradient in the Indian Ocean from reduced incidence of downward shortwave radiation in the northern basin in the preceding winter/spring. Ramanathan et al. (2005) and Chung and Ramanathan (2006) showed that aerosol-induced weakening of the SST gradient (leading to weaker summer monsoon rainfall) more than offsets the increase in summertime rainfall resulting from the "heating of air" effect in a coupled ocean-atmosphere model, leading to a net decrease in summer

monsoon rainfall in the latter half of the 20th century. The study of Meehl et al. (2008), also with a coupled model but with a more comprehensive treatment of aerosol-radiation interaction, supports Ramanathan et al.'s findings on the effect of black carbon aerosols on the Indian summer monsoon rainfall.

- Modulation of the meridional tropospheric temperature gradient from anomalous accumulation of absorbing aerosols against the southern slopes of the Himalayas in the pre-monsoon period. The elevated diabatic heating anomaly from aerosol absorption of shortwave radiation (EHP; Lau et al., 2006; LK06) over the southern slopes of the Tibetan plateau in April-May reinforces the climatological meridional temperature gradient and leads to monsoon intensification in June-July in this scheme.
- Anomalous heating of the land-surface by aerosol-induced reduction in cloudiness (the "semi-direct" effect) and the attendant increase in downward surface shortwave radiation. Stronger heating of the land-surface in May generates greater ocean-atmosphere contrast and thus more monsoon rainfall in June in this posited mechanism (BNL08). The importance and potential impacts of aerosol-land–atmosphere interactions on the Indian monsoon have been summarized by Niyogi et al. (2007) and Pielke et al. (2007).

It is interesting that none of the mechanisms except the last one consider aerosol effects on cloudiness (other than those due to attendant heating and circulation changes). The first three pathways are primarily rooted in the aerosol's direct effect on shortwave radiation: tropospheric absorption and surface dimming

over both land and ocean. The impact on cloudiness can, perhaps, be neglected in winter when the central and northern Indian subcontinent is relatively cloud-free, but not in late spring and summer when cloudiness tracks monsoon development. Climate models are still ill-equipped to deal with the complexities of aerosol-cloud interaction (reckoned important in summer) and can thus provide limited insight on the net effect of aerosols on summer monsoon hydroclimate and the related impact mechanisms. The indirect effect is not well understood and thus inadequately represented. As for the semi-direct effect, it is likely underrepresented due to uncertainties in aerosol distribution and optical properties, and potential misrepresentation of related cloud responses.

A key objective of the present study is to examine the viability of the interesting EHP mechanism. LK06 investigated the link between absorbing aerosols and summer monsoon rainfall and circulation in an observational analysis, targeting the effects of the pre-monsoon aerosol loading over the Indo-Gangetic Basin (IGB). Using composite and regression analysis keyed to the TOMS AI averaged over the IGB, the authors posit that piling up of absorbing aerosols (i.e., dust and black-carbon) along the Himalayan foothills and southern slopes of the Tibetan Plateau during April-May leads to diabatic heating of the lower-to-mid troposphere from aerosol absorption of solar radiation. The heated air over the southern slopes of the Tibetan Plateau rises, drawing warm and moist low-level inflow from the northern Indian Ocean. Aerosol extinction (due to absorption and scattering) of solar radiation – the "solar dimming" effect – is moreover reckoned to produce surface cooling over central India, with the resulting increased stability leading to rainfall suppression

there. A large-scale response, including a regional meridional overturning circulation with rising motion (and increased rainfall) in the Himalayan foothills and northern India and sinking motion over the northern Indian Ocean, is then envisioned (see Section 2 in LK06 for more discussion). The EHP hypothesis has recently motivated a NASA field campaign involving ground and remote observations in the IGB and Himalayan-Tibetan regions.

A careful review of LK06 and other analyses since then (BNL08; Gautam et al., 2009) however reveals that the EHP hypothesis is not grounded in observations. The study of BNL08, observationally based and similar to LK06 in many respects, indicates in particular that the EHP mechanism is rooted in the expansive zonal averaging employed in LK06. Such overly-wide averaging is without basis since the western and eastern sectors of the averaged region have oppositely signed hydroclimate signals, leading to spurious collocation of aerosol loading (concentrated in the western sector) and the dominating hydroclimate signal (of the eastern sector). The EHP hypothesis has other difficulties as well, all discussed below.

Another objective of this study is to extend BNL08's analysis of aerosol-monsoon links which emphasized the aerosol semi-direct effect and attendant heating of the land surface. The EHP hypothesis, in contrast, highlights the direct effect of aerosols and related cooling (heating) of the land surface (atmosphere). BNL08's contemporaneous analysis for late-spring is complemented here by displaying the aerosol-monsoon links with aerosol leading, which provide further insights into cause and effect, albeit cursorily in view of the monthly analysis resolution.

The Chapter is organized as follows: Section 4.2 articulates the perceived difficulties with the EHP hypothesis vis-à-vis observations, while Section 4.3 presents key results from the analysis of aerosol-monsoon links. Concluding remarks follow in Section 4.4.

4.2 Difficulties with the EHP hypothesis

To critique the observational basis for the EHP hypothesis, we first reproduced LK06 analysis before assessing its sensitivity to some attributes. The EHP hypothesis lacks observational support in our opinion for the following reasons:

- LK06, unfortunately, did not show the IGB AI-related precipitation footprint in May when aerosol concentration is at its peak. The lack of appreciation of the precipitation distribution – primarily zonal, with decreased rainfall over western-central India (where aerosol is concentrated) and increased rainfall over northern Burma and the far eastern Indian state of Assam (Fig. 4.1a)[10] – must have allowed LK06 to entertain EHP-type notions, we surmise. Had the authors realized that the IGB AI rainfall regressions in the aerosol-loading region which includes Himalayan foothills (Box-I in LK06's Fig. 1b; green-sided rectangle in Fig. 4.1a here) are weak and that too of opposite sign (i.e., rainfall reduction) in May, they may have shied away from proposing the EHP

[10] Figure 4.1 shows the May regressions /correlations on the May IGB AI. The May index was chosen for consistency with BNL08 but one could have as well chosen the April-May average IGB AI to be fully consistent with LK06. The May precipitation regressions on the latter are indistinguishable from those in Fig. 4.1a.

hypothesis[11]. The May rainfall signal of a more geographically focused AI time series (defined by solid dots in Fig. 2.1) is also very weak in the Himalayan foothills and northeastern India, with rainfall suppression again indicated (Fig. 2.3).

- A figure that plays a key role in the formulation of the EHP hypothesis is Fig. 2 in LK06: Panels 2a and 2b depict the monthly evolution of sector-averaged aerosol and precipitation anomalies as a function of latitude. The anomalies are from composites keyed to the IGB AI. Based on this figure – misleading for reasons discussed next – LK06 (Section 3.2) conclude that "*At the time of the maximum build up of aerosol in May, rainfall is increased over northern India (20°–28°N) but reduced over central India (15°–20°N). The rainfall pattern indicates an advance of rainy season over northern India starting in May, followed by increased rainfall over all-India from June to July, and decreased rainfall in August.*" This incorrectly drawn conclusion is the backbone of the EHP hypothesis. Panel 2b, in particular, is misleading in the context of this hypothesis because an overly-wide longitudinal sector average (65°-95°E) is displayed (the sector is marked in yellow in Fig. 4.1a). Such extensive averaging is misleading as it suggests spatial collocation of aerosol loading and enhanced precipitation, when, in fact, there is little overlap among them: Precipitation is enhanced in the very narrow sector to the far East (90°-95°E), and not at all in region I (70°-90°E); see Fig. 4.1a. A similar reasoning can be applied to Fig. 3a in LK06: Enhanced meridional motion and subsequent

[11] The EHP signal should be manifest in the monthly average as the contributing processes operate on shorter time scales.

upward velocity are actually observed only eastward of 90°E (Fig. 4.1f of the present work), which is a very narrow band compared to the range of longitudes included in the average. Figures 2b and 3a in LK06 thus do not provide observational evidence for the EHP hypothesis, contrary to the claims. Examination of the IGB AI-related May precipitation anomaly (Fig. 4.1a) shows clearly that rainfall does not increase over Northern India (where aerosol loadings are largest); it is, in fact, suppressed. LK06 obtain a precipitation increase only because their overly-wide averaging masks the suppressed precipitation over North India favoring the large precipitation increase farther to the east.

- The EHP hypothesis is predicated on the piling up of absorbing aerosols against the southern slopes of the Himalayas and over southern Tibetan plateau. The core of the May aerosol standard deviation is however located not over elevated terrain but well south of the Himalayan range (Fig. 2.1 and Fig. 1b in LK06).
- An important element of the EHP hypothesis is the diabatic heating of the troposphere above elevated terrain. Citing Gautam et al. (2009), *"According to the EHP hypothesis, aerosol forcing resulting from absorption of solar radiation due to enhanced build-up of dust aerosols in May, mixed with soot from industrial/urban pollution over the IGP, may cause strong convection and updrafts in the middle-upper troposphere resulting in positive tropospheric temperature anomalies northward, most pronounced over the southern slopes of the TP and the Himalayas [Lau et al., 2006; Lau and Kim, 2006]."* The AI-related tropospheric (1000-300 hPa layer-average) warming (Fig. 4a in LK06)

is, of course, not evidence of this (although it is taken as such in Gautam et al. 2009) as the displayed warming signal lags AI by one month in the LK06 figure. The IGB-AI related contemporaneous (May) warming in the lower (surface-700 hPa) and upper troposphere (700-300 hPa) is shown in Figs. 4.1b-c, respectively. Correlation analysis shows only the former to be significant. In neither case, however, positive temperature anomalies are found northward of the core aerosol loading region, and certainly not above the 700 hPa level. As discussed later, the lower tropospheric warming arises from the warming of the land-surface, as evident from the vertical structure of the AI-related temperature signal (Fig. 2.7).

- The EHP hypothesis posits that rainfall enhancement is confined to the foothill region because aerosol induced "solar dimming" leads to the cooling of the IGP, limiting convective instability. There is no evidence for this in observations. To the contrary, the AI-related downward shortwave radiation anomaly (Fig. 4.1d)[12] is positive over much of the subcontinent, leading to a warmer land-surface. Other factors, e.g., advection may contribute as well. The associated 2-m temperature anomaly (Fig. 4.1e) reflects the modulation of insolation. The "solar dimming" feature of the EHP hypothesis was perplexing to begin with, as detection of "solar dimming" is far more challenging in late spring and early summer when cloudiness variations can be confounding.

[12] The downward surface shortwave radiation is from the International Satellite Cloud Climatology Project (ISCCP) FD SRF data set (Zhang et al. 2004). The field is generated by NASA's Goddard Institute of Space Studies (GISS) general circulation model using ISCCP cloud fields and the GISS aerosol climatology. As shown in Fig. 9 in BNL08, this analysis of surface shortwave radiation compares favorably with the Global Energy and Water Cycle Experiment's (GEWEX) SRB diagnosis (Gupta et al. 1999).

Observational evidence shows an unambiguous warming of the land surface in May when aerosol loading is anomalously high, attesting to the dominance of the aerosol semi-direct effect (or decreased cloud cover) over any "solar dimming" due to aerosol extinction.

- Recently, Gautam et al. (2009) have correlated the lower and upper tropospheric temperature anomalies over Northern India in March-May with the concurrent AI over the region (their Fig. 3), finding significant correlations (~0.65). This correspondence however cannot be considered evidence for the EHP hypothesis any more than it can for the aerosol semi-direct effect. As discussed above (and in Fig. 2.9), the AI-related signal in downward surface shortwave radiation is positive over the subcontinent, leading to surface (and lower tropospheric) warming, providing forceful evidence for the dominance of the semi-direct effect.
- The non-collocation of the aerosol loading and rainfall enhancement regions in May is concerning in context of the EHP hypothesis, as noted above. A more reasonable and straightforward explanation for increased rainfall over northeastern India is orographic uplift of the moisture laden air from the Bay of Bengal. The southerly flow is generated as part of the anomalous low-level cyclonic circulation (Fig. 4.1f), anchored by land-surface heating (Figs. 4.1e, 4.1b) and resulting low pressure over the subcontinent. [More generally, the aerosol loading and rainfall enhancement/suppression regions need not be collocated as the aerosol impact is often generated from induced regional circulation anomalies.]

The EHP hypothesis is not without conceptual difficulties as well: For instance, if aerosol-induced rising motions were to lead to *local* rainfall enhancement in the foothill region, aerosol washout would rapidly occur. The EHP would then serve as an *aerosol self-limiting mechanism* in the Himalayan foothills, limiting its efficacy in impacting summer monsoon evolution over the larger subcontinent.

4.3 Aerosol-leading Hydroclimate Links

The contemporaneous analysis of aerosol-monsoon hydroclimate links for May reported in BNL08 precludes attribution of cause and effect. One interpretation of the findings, as discussed in section 5 of that paper, could have been that aerosol loading responds to concurrent rainfall variations due to washout effect, which is not an unreasonable proposition. This possibility was however ruled out in BNL08 by additional analysis in which the April AI over the IGP was regressed on May and June's precipitation and circulation. Although discussed to some extent, the lagged regression patterns were not displayed in BNL08, leading to some lingering concerns on causality.

Monthly lagged regressions on the IGP aerosol index (defined as in BNL08) can be insightful provided that the AI itself is autocorrelated on time scales longer than a month. Figure 2.1f shows the autocorrelation structure of both April and May indices. The indices are significantly correlated (~0.6), indicating anomaly persistence longer than one month. Figure 2.2 provides context for the multi-month timescale by showing how 'aerosol events' over the IGP can be generated in the pre-

monsoon period from advection of dust and pollutants by the prevailing low-level westerlies, i.e., by a process other than local precipitation which operates on much shorter time scales.

The contemporaneous and lagged precipitation regressions on the April IGP AI are shown in Fig. 4.2 (a-c). Close comparison with Fig. 2.3 (top row; contouring and shading intervals are identical) indicates striking similarity between the contemporaneous and one-month aerosol-leading regressions of May precipitation [Fig. 2.3 (top-left panel) and Fig. 4.2b, respectively]. The east-west asymmetry, in particular, is well captured in the aerosol-leading regressions. The similarity extends to the June precipitation patterns: the 2-month lagged regressions on the April AI and the 1-month lagged regressions on the May AI. The April and May IGP AI regressions of the May 2-m air temperature also exhibit notable similarity [Fig. 4.2d-e and Fig. 2.8 (top-left), respectively], indicating coherent development of surface warming and the dominance of the aerosol semi-direct effect over the direct one.

The extensive similarity between the aerosol-leading and contemporaneous regressions of precipitation along with evidence for the multi-month duration of aerosol episodes in the pre-monsoon onset period should address the causality issue. The findings of BNL08 obtained from contemporaneous analysis thus represent the impact of aerosols on precipitation, not vice-versa.

4.4 Concluding Remarks

The study seeks to ascertain the viability of the EHP hypothesis – a mechanism proposed by LK06 for absorbing aerosols' impact on South Asian summer monsoon

hydroclimate. A careful review of LK06's analysis and others since then (BNL08; Gautam et al. 2009) reveals that the EHP hypothesis is not grounded in observations. A lack of appreciation of the spatial distribution of the aerosol-related May precipitation signal over the Indian subcontinent – its east-west asymmetric structure, in particular – as reflected in gross zonal-averaging (65°-95°E) of the signal in LK06 (Fig. 2b) led to this hypothesis.

We show that key elements of the EHP hypothesis have no basis in observations and the hypothesis is thus deemed untenable:

- The core of the May aerosol standard deviation is located not over the southern Himalayan slopes or elevated terrain but southward over the northern IGP.
- Aerosol-related downward surface shortwave radiation and 2-m air temperature signals are positive over the core region and the northern subcontinent, i.e., increased loadings are associated with more surface insolation and a warmer land surface (not a colder one, as per EHP hypothesis). This indicates the dominance of the aerosol semi-direct effect over the direct one (solar dimming).
- More importantly, the concurrent local precipitation signal over the core aerosol region in May is negative, i.e., increased loadings are linked with suppressed precipitation (not enhanced precipitation, as claimed by the EHP hypothesis).
- Aerosol-related tropospheric warming is confined to the lower troposphere. Sensible heating from the land-surface is, perhaps, most important (see Fig. 2.8).
- The EHP hypothesis has a self-limiting element: If aerosol-induced rising motions were to lead to local rainfall enhancement in the foothill regions, as

claimed, aerosol washout would occur, limiting its intensity and large-scale influence.

- The EHP hypothesis can perhaps be mimicked by atmospheric models but this cannot be an indication of its relevance in nature as the representation of aerosol indirect and semi-direct effects in models mentioned above is primitive. Observational analysis is, of course, not without its own uncertainties.

Finally, we extend the analysis of contemporaneous aerosol-monsoon links reported in BNL08 by examining the structure of the one- and two-month aerosol-leading regressions on hydroclimate. The extension is motivated by the need to address causality. The extensive similarity between the aerosol-leading and contemporaneous regressions on precipitation along with evidence for the multi-month duration of aerosol episodes in the pre-monsoon period suggest that the BNL08 findings obtained from contemporaneous analysis represent the impact of aerosols on precipitation, not vice-versa.

The possibility that both aerosol and precipitation anomalies, in turn, are shaped by a slowly evolving, large-scale circulation pattern cannot presently be ruled out, in part because current atmospheric models and observational analyses are unable to tease apart regional feedbacks from the large-scale influence. Some caution is thus warranted in the interpretation of aerosol mechanisms, as further discussed in Bollasina and Nigam (2009) and presented in Chapter 3.

4.5 Figures

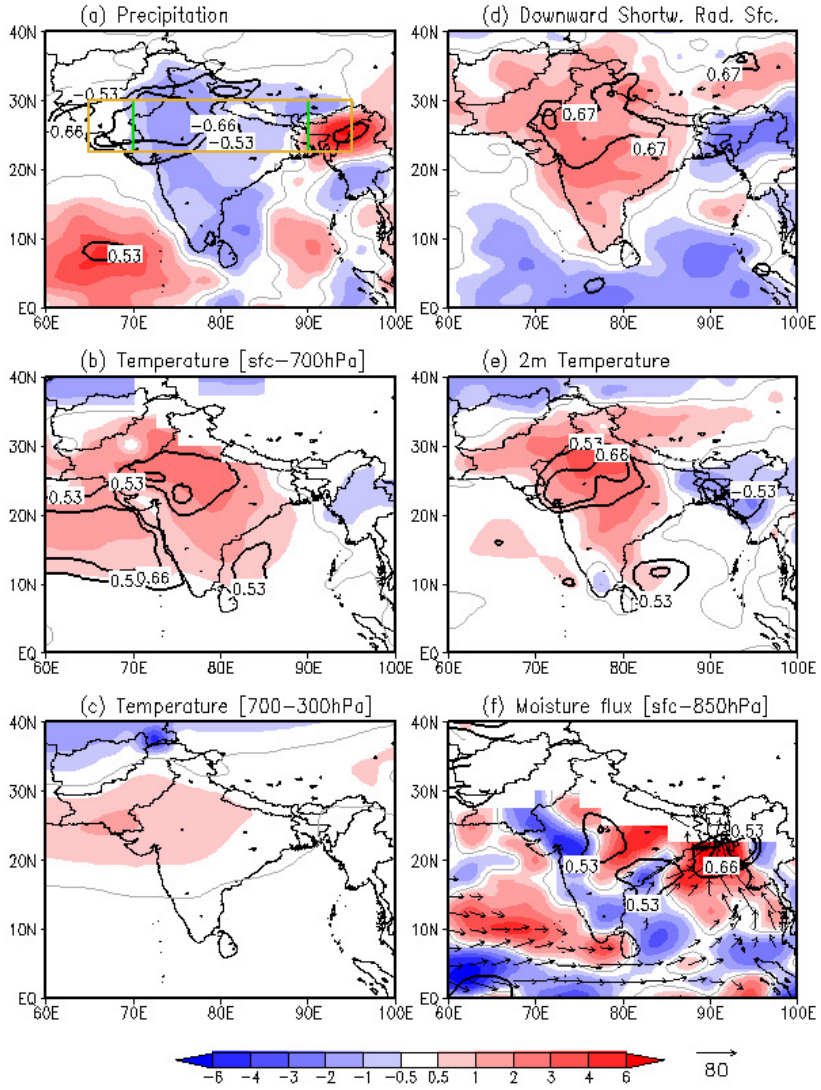

Figure 4.1. May contemporaneous regressions (shaded, with the grey line indicating the zero contour) and correlations (black contours) on the TOMS AI time series averaged over the area (70°-90°E, 22.5°-30°N, green rectangle in (a); the Box-I domain in LK06) of: (a) precipitation (mm day^{-1}, from the Global Precipitation Climatology Project, GPCP); (b) surface-700 hPa average temperature (°C, from the ECMWF Reanalysis, ERA-40); (c) 700-300 hPa average temperature (°C, from ERA-40); (d) downward shortwave radiation at the surface (0.1×W m^{-2}, from the ISCCP FD dataset), (e) 2-m air temperature (°C, from ERA-40), (f) moisture flux (Kg m^{-1} s^{-1}; vectors, values below 20 Kg m^{-1} s^{-1} have been masked out) and its convergence (Kg m^{-2} s^{-1}; shaded, positive values representing convergence) mass-weighted and vertically integrated between the surface and 850 hPa. The time series were not detrended before computing the correlations, to closely compare with maps in LK06. Data are for the period 1979-1992, except radiation which is only available from 1984. Correlations are only shown in terms of the 95% and 99% significance levels (±0.53 (±0.67) and ±0.66 (±0.79), respectively). Inconsistency in the AI time series after 1992 restricted the correlations to the 14-year period considered here. Green and yellow rectangles in Fig. 4.1a denote the regions (70°-90°E, 22.5°-30°N and 65°-95°E, 22.5°-30°N, respectively) used by LK06 to define the AI time series (their Fig. 1c) and for displaying cross-sections of composite anomalies (their Figs. 2b and 3), respectively.

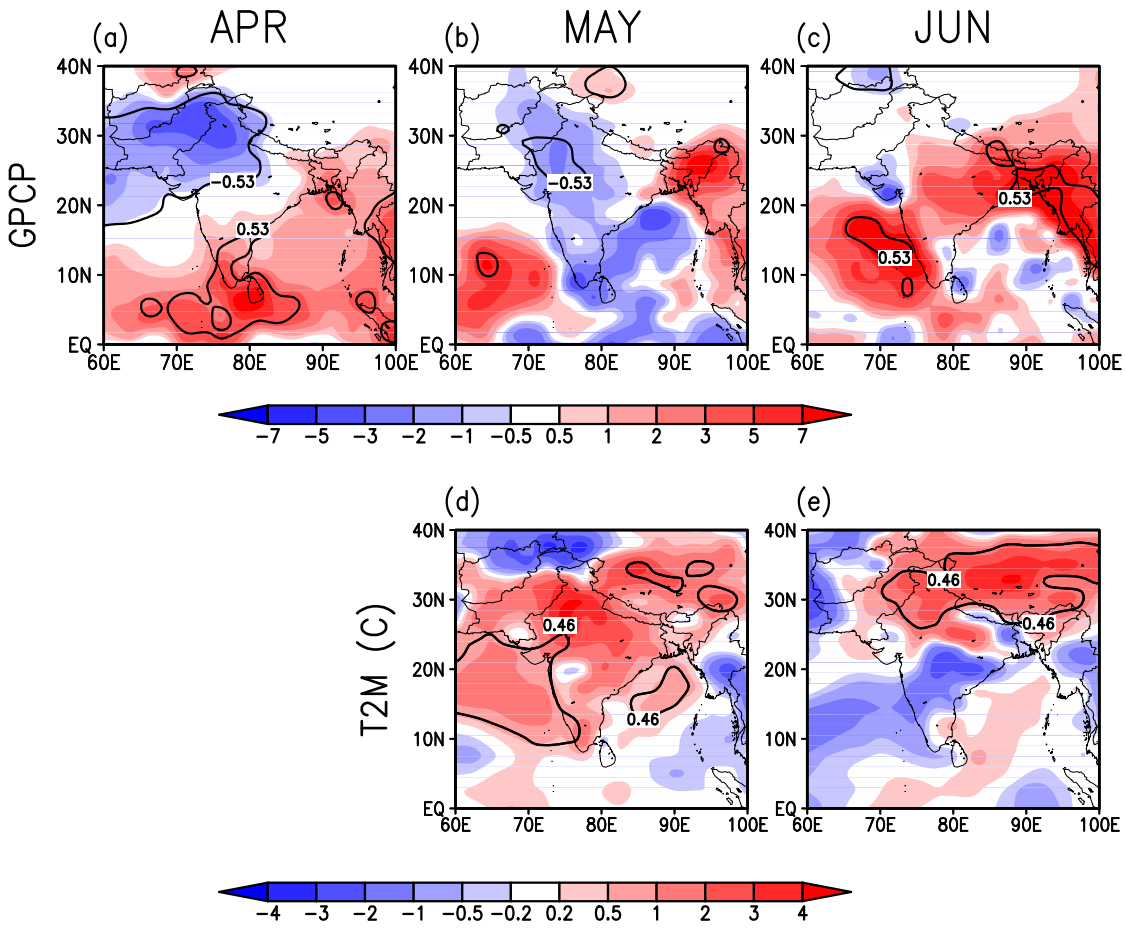

Figure 4.2. *Top panels:* GPCP precipitation (mm day^{-1}) regressed on the TOMS April AI time series (averaged over the same points highlighted in Fig. 1a of BNL08) for (a) April, (b) May, and (c) June. The ±0.53 contour line shows the 95% confidence level. *Bottom panels:* 2-m air temperature (T2M, °C; data from ERA-40) regressed on the April AI time series for (d) May and (e) June (the ±0.46 contour line show the 90% confidence level). Data are for the period 1979-1992. Both data were detrended before computing the regressions.

Chapter 5: Indian Ocean SST, Evaporation, and Precipitation during the South Asian Summer Monsoon in IPCC-AR4 Coupled Simulations[13]

5.1 Introduction

Although general circulation models (GCMs) are improving in simulating the mean global climate (e.g., Randall et al. 2007), their performance at regional scale still remains challenging. This is the case for the Asian summer monsoon. The skill of atmospheric GCMs (AGCMs) forced with observed SSTs in simulating the Asian summer monsoon has only slightly improved in the last two decades (e.g., Kang et al. 2004; Wang et al. 2004), with large systematic biases still evident in the simulations (e.g., Kang et al. 2002).

Coupled atmosphere-ocean GCMs (CGCMs), too, show remarkable intra-model variability and discrepancies compared to observations (e.g., Covey et al. 2003; Meehl et al. 2005). Systematic deficiencies include a cold bias in the Pacific cold tongue and warm pool regions, a double-intertropical convergence zone (ITCZ), and a westward shift of El Niño Southern Oscillation (ENSO) variability (e.g., Covey et al. 2000; AchutaRao and Sperber 2006; Joseph and Nigam 2006).

An assessment of monsoon precipitation from the Intergovernmental Panel on Climate Change (IPCC)-participating CGCMs (Dai 2006; Annamalai et al. 2007;

[13] This Chapter has been published as Bollasina and Nigam (2008).

Kripalani et al. 2007; Lin 2007; Waliser et al. 2007) reveals the continuing challenge of simulating the seasonal and interannual variability of the Asian summer monsoon. Current models also exhibit discrepancies with respect to observed regional air-sea feedbacks (e.g., Wu et al. 2006; Lin 2007; Wu and Kirtman 2007; Wu et al. 2007). For example, interactions in the tropical Indian Ocean (IO) have varied representation in the models. This is not altogether surprising, for, despite a long investigative history, the role of the IO in regional monsoon variability remains controversial (Annamalai and Murtugudde 2004).

The impact of IO SSTs on the interannual variability of South Asian monsoon precipitation has been ascertained from both diagnostic (e.g., Rao and Goswami 1988; Harzallah and Sadourny 1997; Clark et al. 2000) and modeling (e.g., Zhu and Houghton 1996; Chandrasekhar and Kitoh 1998) studies. Overall, the relationship between IO SST and monsoon rainfall still remains poorly characterized.

Given the previous considerations, this study aims at addressing the following questions: are coupled models able to simulate the local observed atmosphere-ocean interactions in the IO during the summer monsoon? Do antecedent SSTs in the IO realistically affect summer precipitation over India in coupled models?

Systematic model biases in precipitation, evaporation, SST and near-surface winds are first analyzed since they also affect the correct representation of air-sea interactions. Secondly, local and non-local air-sea relationships are documented by computing lead-lag correlations.

This Chapter is organized as follows: after describing the data used in Section 5.2, Section 5.3 describes the model biases over the Indian Subcontinent. Section 5.4

discusses air-sea interactions, and Section 5.5 analyses the relationship between Indian precipitation and surrounding SSTs. Summary and conclusions follow in Section 5.6.

5.2 Model Data and Observations

Model data for the 20th Century climate integrations were collected from the World Climate Research Programme (WCRP) Coupled Model Intercomparison Project phase 3 (CMIP3). Only five representative models (all without any form of "flux adjustment") were analyzed in this study (see Table 5.1) given the limited computational resources available and to avoid some redundancy of the results. Precipitation data came from the Climate Prediction Center (CPC) Merged Analysis of Precipitation (CMAP; Xie and Arkin 1997), available on a 2.5° x 2.5° grid from January 1979 onward.

The All-India rainfall time series (AIR; Parthasarathy et al. 1995), a combination of 306 almost uniformly-distributed station measurements, was also used. Updated time series were downloaded from the website of the Indian Institute of Tropical Meteorology (http://www.tropmet.res.in).

SSTs were taken from the Hadley Centre Sea Ice and Sea Surface Temperature dataset (HadISST), which is a unique combination of global SST and sea ice concentration on a 1° x 1° grid from 1870 to date.

Evaporation data were obtained from the Woods Hole Oceanographic Institution (WHOI) Objectively Analyzed air-sea Heat Fluxes (OAFlux) dataset, an

optimal blending of multi-platform satellite retrievals and numerical weather prediction reanalyses (Yu et al. 2008) available from 1958 onward on a 1° x 1° grid. The ECMWF Reanalysis (ERA-40; Uppala et al. 2005) provided atmospheric variables on a 2.5° x 2.5° grid.

This analysis is based on 22 years (1979-1999) of monthly data, referred to also as the "climatology".

5.3 Seasonal Precipitation, SST, and Evaporation

5.3.1 Seasonal Precipitation and 850-hPa Circulation

Summertime (June-September, JJAS) precipitation and 850-hPa winds in observations and the departure of each model from observations are shown in Fig. 5.1. Significant large-scale biases are evident in all models: excessive precipitation over the western-central north equatorial IO and the Maritime Continent, and precipitation deficit in the south-central equatorial IO with extension into the Bay of Bengal. The meridional dipole structure of the bias suggests that the ITCZ is shifted northwestward in these models. Other notable precipitation biases include reduced rainfall along the western coast of India and excessive rain over peninsular India. The simulated 850-hPa circulation shows anomalous easterly/southeasterly winds over the western IO, consistent with excessive rainfall there. This circulation bias attenuates the prevailing cross-equatorial southwesterly flow that carries moisture to the Subcontinent.

5.3.2 Monsoon Evolution

The evolution of South Asian monsoon precipitation is examined in Fig. 5.2 by displaying the time-latitude cross-section over the Indian sector (60º-100ºE). In observations, the rain belt moves significantly northward from ~5ºS in winter to ~15ºN in summer. An additional convergence zone exists over the eastern equatorial IO (~5ºS): it is a bit weakened during the Asian monsoon onset, but it recovers with monsoon's waning, indicating a competition between oceanic and continental convection zones.

This competition during boreal summer is largely absent in the coupled simulations, except, perhaps, in the GFDL (and ECHAM) models. The oceanic convection zone (10ºS-Equator) is not evident in the other simulations, consistent with summer precipitation underestimation in this region (cf. Fig. 5.1). There are other discrepancies between observations and coupled simulations as well, relating to interrupted northward progression of the monsoon (e.g., MIROC) and delayed onset (e.g., HadCM3), for example. The monsoon evolution in the GFDL model seems reasonable but for the skewed amplitudes of the convection zones.

5.3.3 Rainfall over the Indian Subcontinent and the Southern Equatorial Indian Ocean

The distribution of monsoon precipitation over the South Asian continent and the IO is examined in Fig. 5.3a, which displays the spatial correlation between simulated and observed precipitation. Not surprisingly, correlations are highest in winter, when precipitation is confined to smaller regions. The correlations decrease

with the arrival of monsoon rains, principally from differences in the distribution over the IO. MIROC and CCSM3 stand out as particularly deficient, using this metric.

The annual cycle of precipitation averaged over two key monsoon regions (India and the southern IO) is depicted in Figs. 5.3b and 5.3c, respectively. Only land point values were included in the average over India, given our intent to compare simulations against station-based rainfall climatology (AIR) as well. Oceanic precipitation was averaged over the region exhibiting strong negative bias in Fig. 5.1. That CMAP and AIR estimates are indistinguishable in Fig. 5.3a is reassuring. The average rainfall over the Subcontinent is simulated quite reasonably, although differences in the timing of the peak and duration of the rainy season are recognizable (e.g., a delayed monsoon onset in HadCM3, a too gradual and anticipated onset in CCSM3, a weaker peak rainfall and prolonged rainy season in GFDL). In contrast, modeled rainfall over the south-central IO shows great variance with respect to observations, and even among simulations. As noted earlier, only the GFDL model produces realistic seasonal variation of rainfall in this region.

5.3.4 Seasonal SST Variability in the Coupled Simulations

The seasonal variability of SST in the coupled simulations is examined in Fig. 5.4, which shows the amplitude and phase of the annual cycle using vectors. The annual-mean SSTs are contoured for reference. The warmest SSTs are observed in boreal spring when the 29ºC contour encloses the area from 10ºS to 15ºN. The monsoon onset leads to cooling of SSTs in the northern IO, especially along the Somali coast. In the northern Arabian Sea and the Bay of Bengal, SSTs are warmest a few months later, in mid summer.

The CGCMs can generate fairly realistic annual-mean SST distributions, as seen in Fig. 5.4. HadCM3 produces the warmest SSTs, especially in the 5ºS-5ºN belt, with the western IO warmer by ~1.5ºC. The GFDL and MIROC models, on the other hand, produce a slightly cold equatorial region. The SST annual cycle in the southern Tropics is realistically captured in all simulations, but the corresponding variability in the western and northern IO is challenging for the models, especially CCSM3 and HadCM3. CCSM3, HadCM3, and MIROC have also a weak seasonality along the Equator.

5.3.5 Monsoon Season SST and Near-surface Winds

SSTs and near-surface winds in the monsoon season are displayed in Fig. 5.5. Model departures from observations are shown, as in Fig. 5.1. The simulation of SST is apparently challenging, especially along the Somali Coast and the south-central IO, i.e., in the regions of notable precipitation error (cf. Fig. 5.1). A cold bias also surrounds the Indian peninsula in many simulations. The SST bias defies further characterization. The near-surface winds have a southeasterly component across much of the IO. The bias is similar to that of the 850-hPa wind (cf. Fig. 5.1), but not in all simulations (e.g., MIROC). The biased wind is often directed from the cold SST-bias regions into the warm ones.

As a result, the speed of the trade winds in the Southern Hemisphere (SH; see also Fig. 5.6) is increased but the Somali Jet is damped, affecting local SSTs (through increased ventilation and reduced coastal upwelling, respectively). The southeasterly bias also opposes the monsoon westerlies north of the equator, leading to reduced wind speed and evaporation there, which are reflected in the region's warm SST bias.

5.3.6 Evaporation Biases in Coupled Simulations

The potential of coupled GCMs in simulating summertime evaporation over the IO is examined in Fig. 5.6, where evaporation biases are superposed on wind-speed biases. As before, the observed full fields are shown in the top-left panel. In nature, evaporation is largest near the Tropic of Capricorn, both from wind speed effects but even more because of humidity differences arising from the fluxing of dry air off the northern flank of the robust Mascarene High in the SH winter. Wind speeds are again large in the Arabian Sea, but not evaporation as the air is already quite saturated at this point in its journey towards the Continent. The upwelling colder SSTs extending off the Somali Coast are not helpful either.

Evaporation in the coupled simulations is not as tightly centered around the Tropic of Capricorn as in observations, since it extends northward up to the equator, especially in the western IO. The northward extension is not all due to the bias in wind speed, which is focused further to the north, since other factors can contribute in determining evaporation (e.g., near-surface vertical humidity gradients). The wind bias is connected to an anomalous vertical circulation, which manifests in the pattern of the regional upper-tropospheric divergent circulation.

5.3.7 Divergent Circulation Biases in Coupled Models

The performance of CGCMs over the South Asian sector is placed in global context in Fig. 5.7 which shows the divergent circulation at 200 hPa, the level of monsoonal outflow. As before, model biases with respect to observations (ERA-40) are displayed. Comparison of CMAP rainfall (Fig. 5.1) and ERA-40 divergent circulation shows excellent qualitative agreement between regions of strong

precipitation (i.e., strong latent heat release) and upper-tropospheric divergence in the Tropics/subtropics. The strongest upper-level divergent flow originates in the Bay of Bengal and heads northwestward (e.g., Rodwell and Hoskins 2001), westward, and southward. The southward component converges over the southern subtropical IO, strengthening the Mascarene High (Krishnamurti and Bhalme 1976; Nigam and Chan 2008). The divergence bias in the coupled simulations is consistent with the precipitation bias in the IO, especially in the GFDL and MIROC models. The analysis, unfortunately, did not provide insights into the cause of the biases in the IO. Notable biases are not confined to the IO basin alone, since equally impressive differences are present over the Maritime Continent and the Pacific ITCZ. This pattern suggests that the ITCZ and its SH counterpart are displaced in coupled simulations, often due to the existence of a double-ITCZ (e.g., Lin 2007).

5.3.8 Atmospheric Water Balance over the Southern Indian Ocean

The JJAS atmospheric water-balance over the southern equatorial IO is examined in Fig. 5.8 to gain insight into the cause of the simulated precipitation deficit. The three-leading budget terms – evaporation (E), precipitation (P), and column moisture flux convergence (MFC) – are displayed. The column moisture tendency (typically, small; ~0.1 mm day^{-1}) is not shown, and MFC does not include the transient flux contribution as sub-monthly data was unavailable for the simulations. If ERA-40 estimate of the transient MFC over the IO (~0.6 mm/ day^{-1}) is of guidance, the non-inclusion of the transient contribution is not a serious omission.

It is noteworthy that the observational budget itself is somewhat uncertain. The water balance is constructed from ERA-40 stationary MFC, CMAP precipitation, and

OAFLUX evaporation. The imbalance or residue (RES = P−E−MFC) is also plotted in Fig. 5.8. ERA-40 precipitation and evaporation fields are not used because reanalysis procedures are generally not mindful of the atmospheric or terrestrial water-balance (Nigam and Ruiz-Barradas 2006).

Over the ocean, CCSM3, HadCM3 and MIROC show E−P to be positive (and MFC of opposite sign than observations), while the opposite is true for GFDL and ECHAM (in line with observations). Despite such variation, the model budgets are balanced, attesting to the smallness of column moisture tendency and transient MFC. The negative MFC over the southern equatorial IO in the simulations exhibiting the largest precipitation biases suggest that the latter is due to the presence of divergent circulation in the lower troposphere rather than any diminished availability of moisture.

5.4 Local Air-Sea Feedbacks in the Indian Ocean

Local contemporaneous correlations among P, E, and SST are examined in this section with the purpose of investigating atmosphere-ocean feedbacks in the IO during the summer monsoon. All correlations are computed on monthly anomalies, after subtracting the monthly climatological annual cycle. Given the length of the time series (1979-1999), the 90%, 95%, and 99% confidence levels are at 0.21, 0.24, and 0.31, respectively.

As the atmosphere responds rapidly to SST, a large positive simultaneous correlation of P and SST indicates SST's influence on the atmosphere. On the other hand, a large negative correlation between P and SST-tendency is suggestive of

atmosphere's influence on SST (e.g., Wu and Kirtman 2005). The observed summer correlations shown in the top panels of Fig. 5.9a indicate generally weak links between P, E, and SST.

The P-SST correlation is weakly positive except in the eastern equatorial IO (85°-100°E, 10°S-5°N), where it is moderately large. Precipitation and SST-tendency (not shown) are positively and weakly correlated here. This suggests that SST strongly forces the atmosphere over the eastern IO, which, in turn, has a positive feedback on SSTs. A weaker SST influence on the atmosphere is found over the western equatorial and sub-equatorial IO, associated with a very weak negative precipitation-SST tendency correlation (denoting a weak negative atmospheric feedback). Over the northern IO, a negligible positive P-SST correlation associated with a significantly negative P-SST tendency correlation suggests that the atmosphere can exert control on SST here. Our finding that SST variability is influential in a very limited region of the IO is consistent with the lead-lag correlation analysis of Wu and Kirtman (2007).

Inspection of Figs. 5.9a-b shows that the simulated P-SST link is too strong in the equatorial IO, especially for three models (CCSM3, HadCM3, and MIROC). Wu et al. (2006) reported similar findings for the COLA coupled model. The P-SST correlation structure in the GFDL simulation, on the other hand, is reasonably realistic, although values are overestimated. The simulated precipitation-SST tendency correlation (not shown) is negative and quite large in the north equatorial and in the western IO, while it is positive in the eastern south equatorial IO. These patterns indicate that coupled models are characterized by an excessive oceanic

forcing on the atmosphere over the equatorial IO with mostly negative feedback except over the eastern IO, and by a too strong impact of atmospheric anomalies on the SST in the northern IO.

The second observational panel shows the variations of E and SST to be weakly and positively correlated. Significant values are found in the upwelling region off the Somali coast, reflecting the SST influence rather than the wind-speed effect.[14] The GFDL and ECHAM models have E and SST positively correlated (as in observations), but much too strongly. The other three models exhibit a band of negative E-SST correlations in the equatorial IO sector, reflecting the wind-speed influence (or atmospheric control) on E. Wu et al. (2006) have also investigated the E-SST linkage but for the whole year rather than just the monsoon season, as here. The observed evaporation-SST tendency correlation (not shown) is negative over the larger part of the domain, suggesting the predominant contribution of evaporation to SST anomalies (in agreement with the small values of the evaporation-SST correlation). Values are slightly positive in the northern IO north of 10°N and over the western IO, where the evaporation/SST correlations are positive and larger. All models show strong negative correlations over most of the IO and much larger than observations, indicating a too strong atmospheric forcing on SST.

The third observational panel (Fig. 5.9a) shows the P and E variations to be essentially uncorrelated, indicating that the variability of precipitation is only partially modulated by local variations of moisture through evaporation, and that other processes (i.e., large-scale dynamics) play an important role. This is clearly not the

[14] Stronger wind speeds would be associated with a stronger Somali jet, and thus colder upwelled SSTs. Dominance of the wind-speed effect in this region would manifest as a negative E-SST correlation.

case for the coupled simulations, though. All models, and CCSM3 in particular, show large negative P-E correlations from the Maritime Continent across the equatorial IO, indicating a too strong forcing of the atmosphere on surface evaporation.

5.5 Indian Summer Monsoon and Indian Ocean SSTs

The non-local influence of IO SSTs on precipitation over India is analyzed in this section. The antecedent and simultaneous correlations of Indian summer monsoon rainfall with surrounding SSTs are shown in Fig. 5.10. Correlations are shown for SSTs leading by 6 months, 3 months, and 0 months, and for SSTs lagging by 3 months (i.e., with previous December-February (DJF), March-May (MAM), simultaneous SSTs, and following September-November (SON), respectively). The Indian summer monsoon is, evidently, weakly linked to IO SSTs. Only previous winter's SST in the southeastern IO and the northern Arabian Sea appears to be marginally influential, consistently with findings of Clark et al. (2000). Interestingly, in the autumn following the monsoon, the correlations become significantly negative in the northern IO.

The linkage between all-India precipitation and surrounding SSTs is variedly represented in the coupled simulations, with the GFDL and ECHAM models showing significant negative correlations and CCSM3 modestly positive ones at all lags. In both cases, correlations are at variance with observations. Interestingly, HadCM3, which contains significant seasonal biases in IO precipitation and SST (cf. Figs. 5.1 and 5.5), appears more realistic from the viewpoint of Indian summer monsoon-SST links. In contrast, the GFDL and ECHAM simulations, deemed most realistic from

the local correlation analysis perspective, contain significant negative correlations in the western IO, especially at zero lag, where observed values are close to zero.

It is, of course, not difficult to envision excessive Indian monsoon rainfall as being due to stronger monsoonal flow over the western IO (and along the Somali Coast). The stronger flow would generate more evaporation and coastal upwelling, both responsible for cooling SSTs (e.g., Meehl et al. 2006). This link is supported by observations but only during the post-monsoon fall. Recently, Kulkarni et al. (2007) has also noted the influence of the Indian monsoon on fall SSTs over the Indian Ocean. Local simultaneous correlations, moreover, show E and SST to be positively correlated along the Somali coast in observations (Fig. 5.9a), indicating SST control on E in the region and not vice-versa.

5.6 Summary and Conclusion

This study examines the veracity of modeled air-sea interactions in the IO basin during the South Asian summer monsoon. Representative coupled models simulations of the 20th century climate, produced for the IPCC-AR4, are the analysis targets along with observations.

The examination is motivated by the need to assess the realism of climate variability mechanisms operating in the South Asian sector in coupled models. These models are being increasingly used to predict changes in regional hydroclimate in response to rising greenhouse gas concentrations and aerosol loadings, but without sufficient acknowledgement of the model shortcomings, especially on regional scales. The perceived overreliance on models in investigations of aerosols influence on

South Asian hydroclimate (e.g., Menon et al. 2002; Lau et al. 2006; Chung and Ramanathan 2006; and recently Meehl at al. 2008) instigated this analysis.

The seasonal variability of precipitation, evaporation, SST, near-surface winds, and moisture fluxes over the Indian Subcontinent and the IO for the period 1979-1999 was analyzed. Related published studies of Dai (2006) and Lin (2007) provided context for this analysis, which is focused on boreal summer.

Our analysis shows the presence of large systematic biases in the simulated precipitation, evaporation, and SST over the IO, often exceeding 50% of the climatological values. Many of the biases are pervasive, being common to all models.

Coupled simulations are found compromised also in representation of atmosphere-ocean interactions. Models (e.g., CCSM3, HadCM3, and MIROC) tend to strongly overestimate local air-sea coupling in the Indian basin, as reflected by their large precipitation-SST correlations at variance with the insignificant observed values. The evaporation-SST correlations are also differently represented, with the above three simulations exhibiting modest negative values (or atmospheric control) while the other two (i.e., GFDL and ECHAM) strongly positive ones (or SST control) in the equatorial IO, at odds with the modest positive correlations in observations.

Our analysis suggests that CCSM3's behavior, for example, can be best described as being local over the equatorial IO, with larger SSTs leading to more precipitation. On the contrary, evaporation is erroneously controlled by the atmosphere in this model. In nature (and to an extent in the GFDL and ECHAM models), local SSTs are not influential on precipitation, indicating the importance of non-local controls.

The relationship between SST and Indian summer monsoon rainfall also shows a distorted representation of ocean-atmosphere interactions in the coupled simulations. Indian monsoon rainfall is essentially uncorrelated or weakly correlated with both antecedent and contemporaneous IO SSTs in observations, but not so in models, especially GFDL and ECHAM.

At this stage this analysis provides rather limited insight on the cause of the models aberrant behavior. Given the myriad of dynamical and thermodynamical coupled physical processes in play in the IO during boreal summer, determining the reasons of model biases can be a challenging and arduous task. Local and non-local air-sea interactions can be differently simulated by models. For example, one is at a loss in explaining why models with distorted local air-sea interaction (e.g., HadCM3) do better in representing the non-local relationships (cf. Fig. 5.10). Answering such questions will require controlled model experimentation, which is beyond the scope of the present study.

We find that several coupled climate models used in the IPCC-AR4 are seriously deficient in their portrayal of air-sea interactions in the IO during boreal summer. In our opinion, they cannot provide durable insights on regional climate feedbacks nor credible projections of regional hydroclimate variability and change, should these involve ocean-atmosphere interaction in the IO.

5.7 Tables

Table 5.1: Climate models analyzed in this work.

Modeling Group	Model Name	AGCM resolution	OGCM resolution	Reference
National Center for Atmospheric Research	CCSM3	1.4°x1.4° L26	384x320L40	Collins et al. (2006)
Hadley Centre for Climate Prediction and Research/Met Office	HadCM3	2.75°x3.75° L18	1.25°x1.25° L20	Jones et al. (2004)
Geophysical Fluid Dynamics Laboratory	GFDL-CM2.1	2.0°x2.5° L24	1.0°x0.33° L50	Delworth et al. (2006)
Center for Climate System Research/National Institute for Environmental Studies/Frontier Research Center for Global Change	MIROC3.2	1.125°x1.125° L56	0.1875°x0.28125° L47	Hasumi et al. (2004)
Max Planck Institute for Meteorology	ECHAM5/MPI-OM	2.0°x2.5° L31	1.5°x1.5° L40	Roeckner at al. (2003)

5.8 Figures

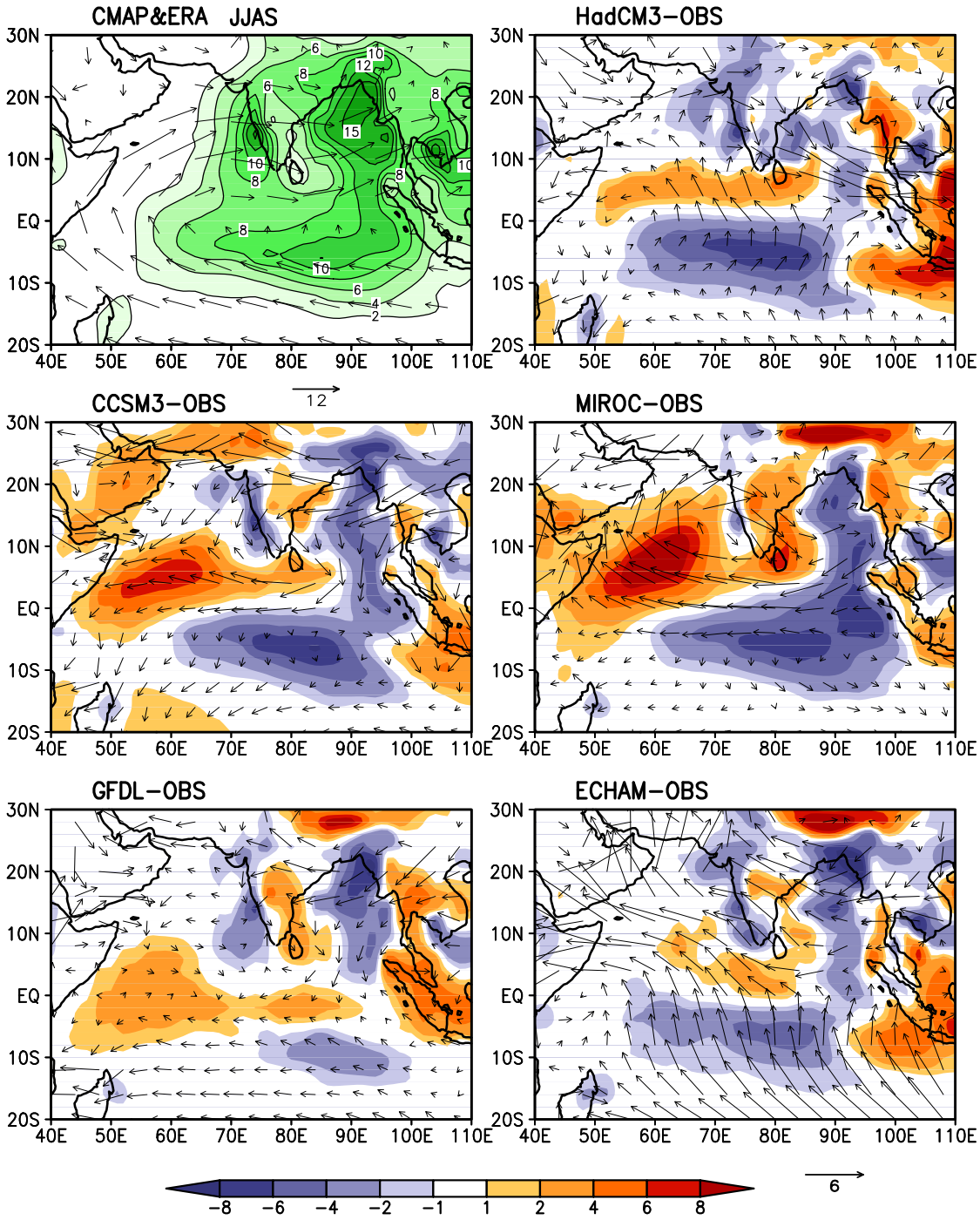

Figure 5.1: Seasonal mean (Jun-Sep; JJAS) precipitation (mm day^{-1}) and 850-hPa winds (m s^{-1}) for observations (top left) and differences model-observations (other panels).

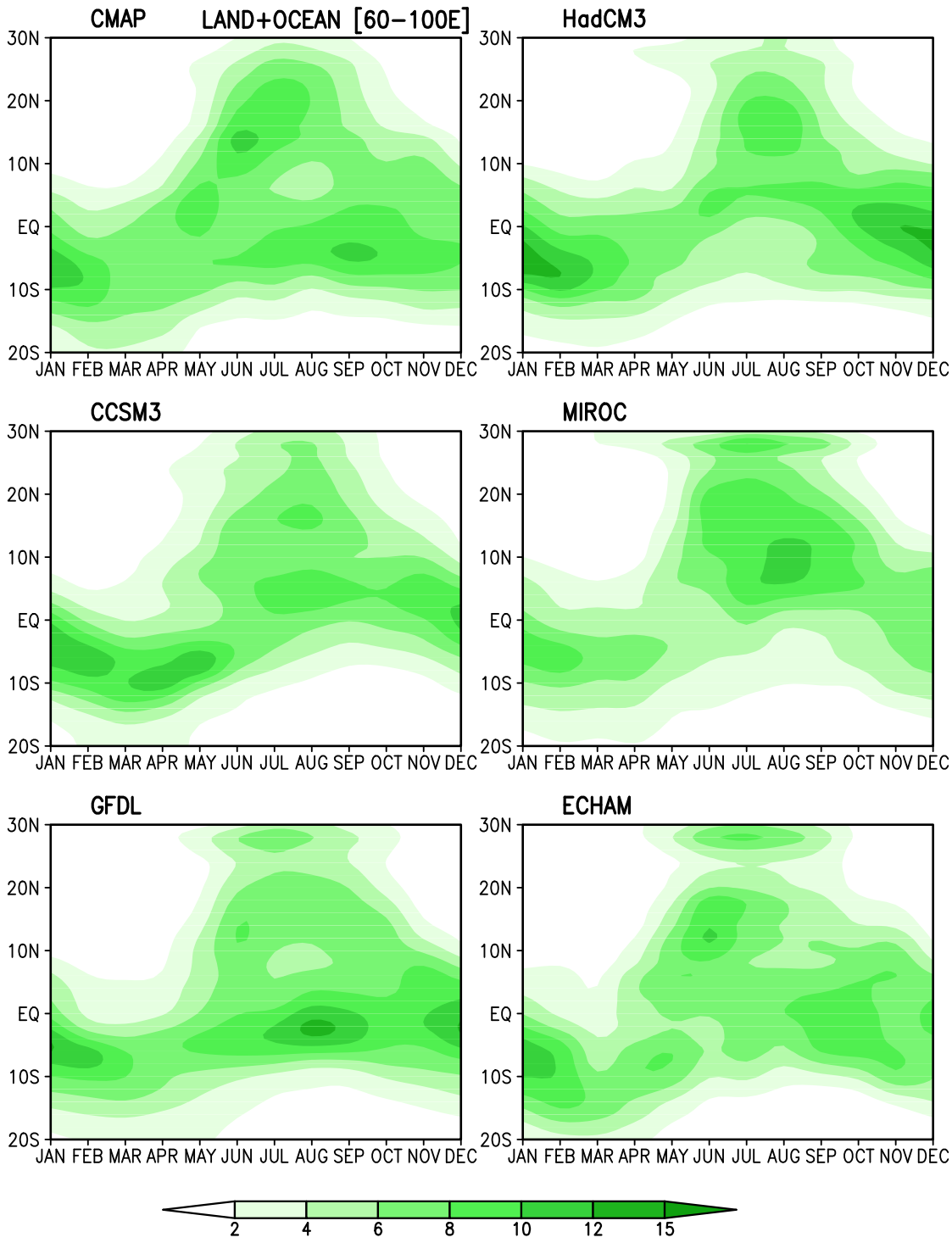

Figure 5.2: Time-latitude evolution of precipitation (mm day^{-1}) averaged over (60°-100°E; land and ocean points) for observations (top left) and coupled models (other panels).

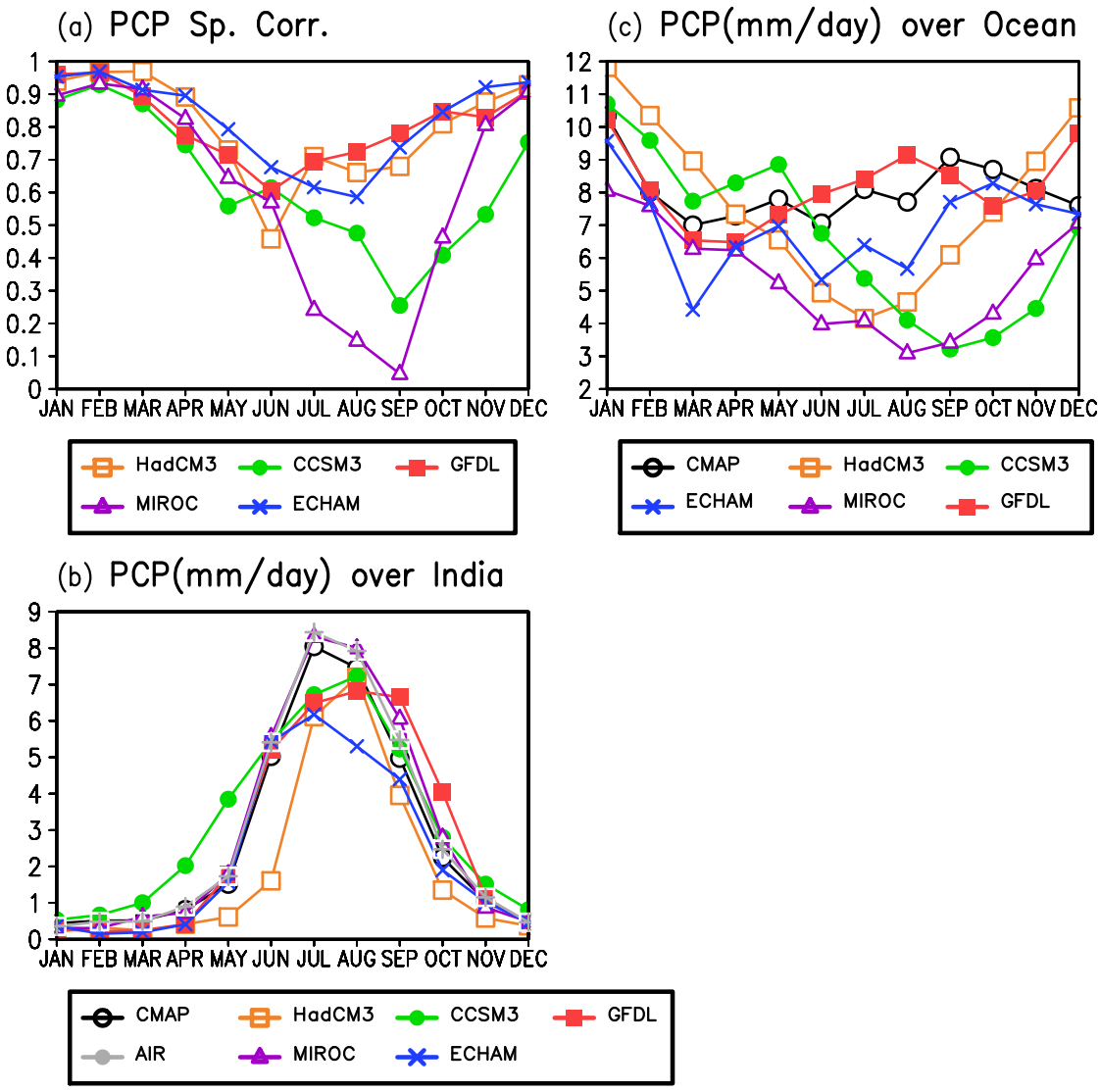

Figure 5.3: Annual cycle of (a) spatial correlation of model precipitation (averaged over 60°-100°E; 10°S-30°N; land and ocean points) with respect to CMAP, (b) observed and simulated precipitation (mm day^{-1}) averaged over India (land-only points), (c) observed and simulated precipitation (mm day^{-1}) averaged over (60°-100°E; 10°S-Equator) (ocean-only points).

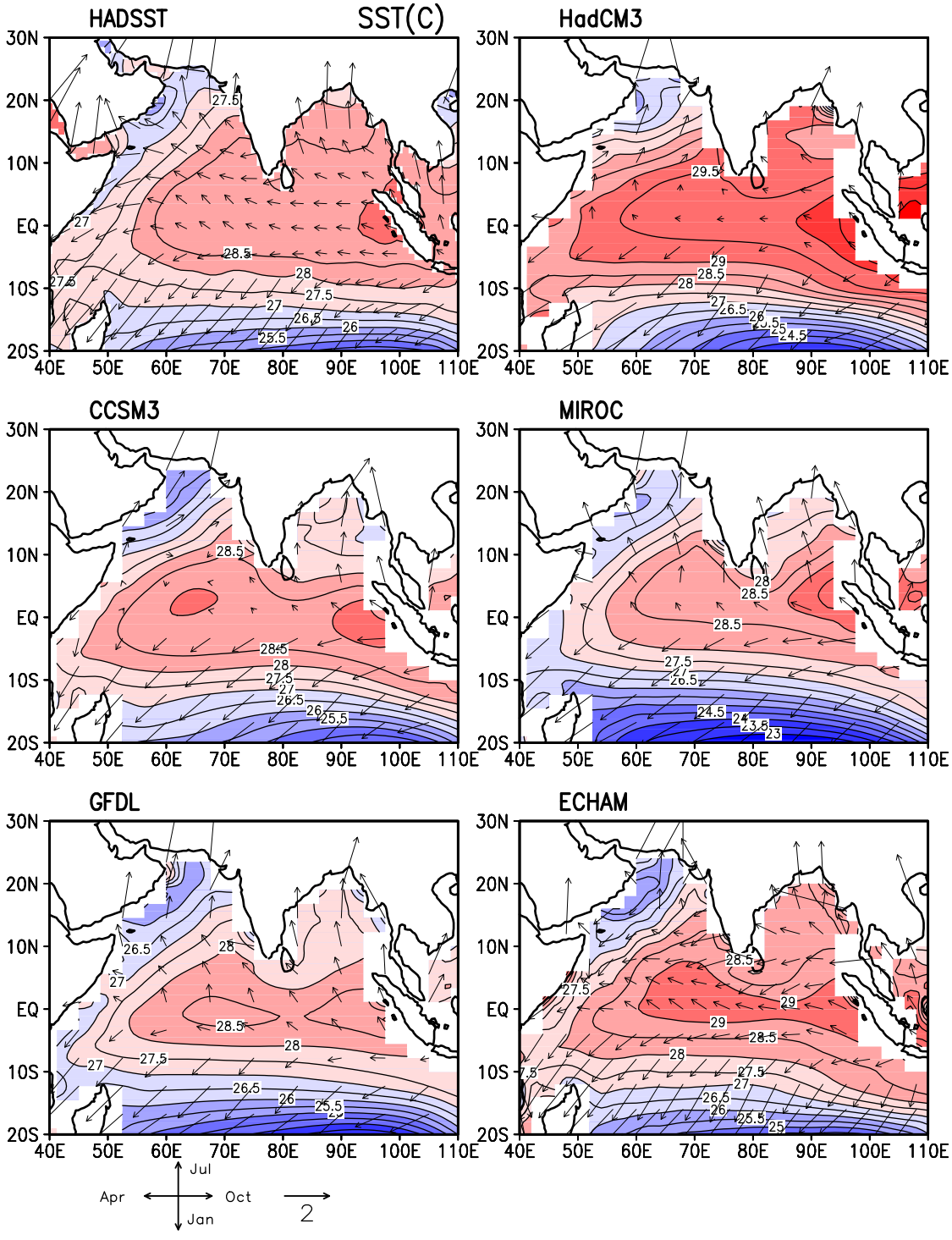

Figure 5.4: Annual mean SST (ºC, shaded) and amplitude and phase (arrows) of the annual cycle of SST over the Indian Ocean for observations (top left) and coupled models (other panels).

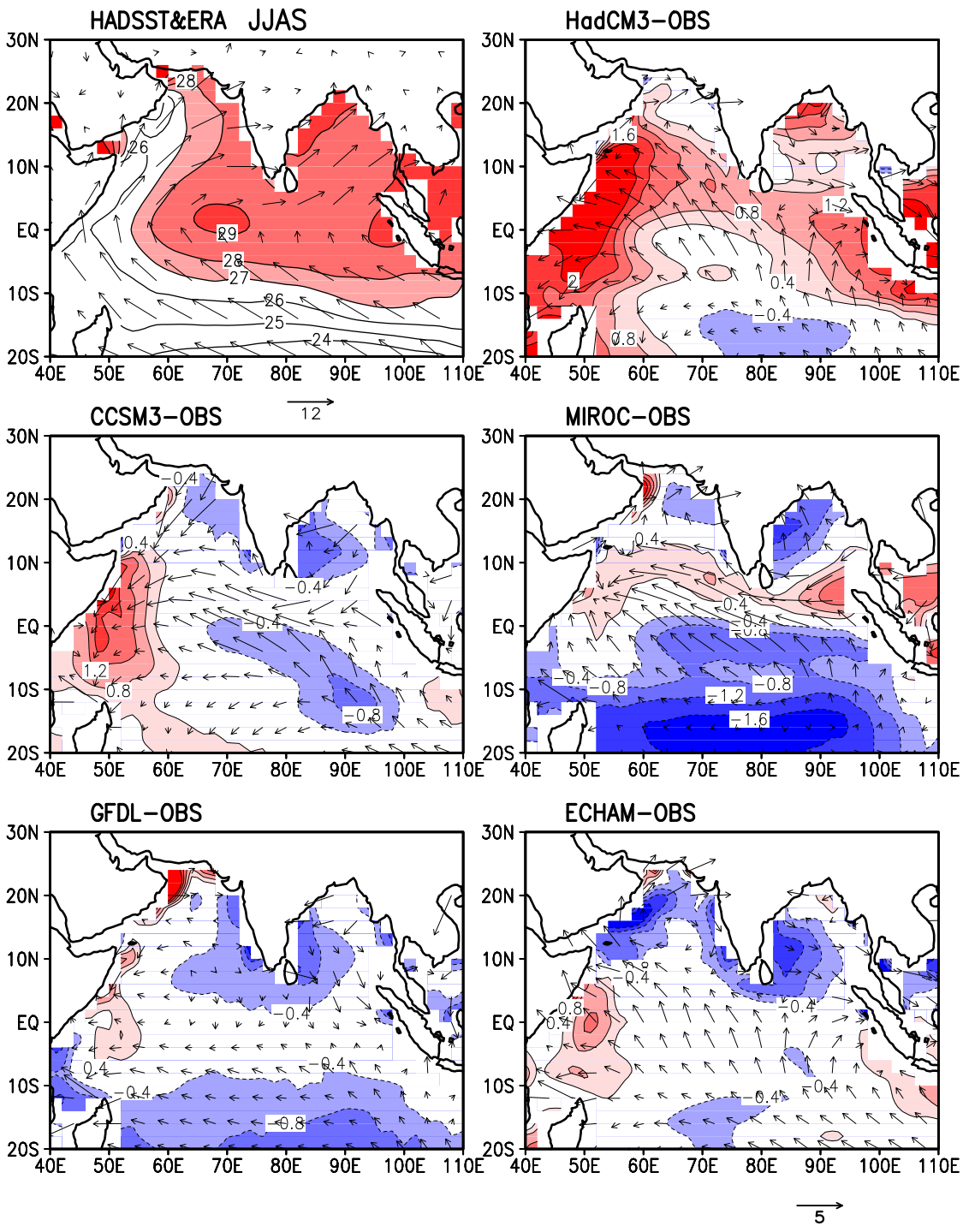

Figure 5.5: Seasonal mean (Jun-Sep; JJAS) SST (°C) and 1000-hPa winds (m s^{-1}) over the Indian Ocean for observations (top left) and differences model-observations (other panels).

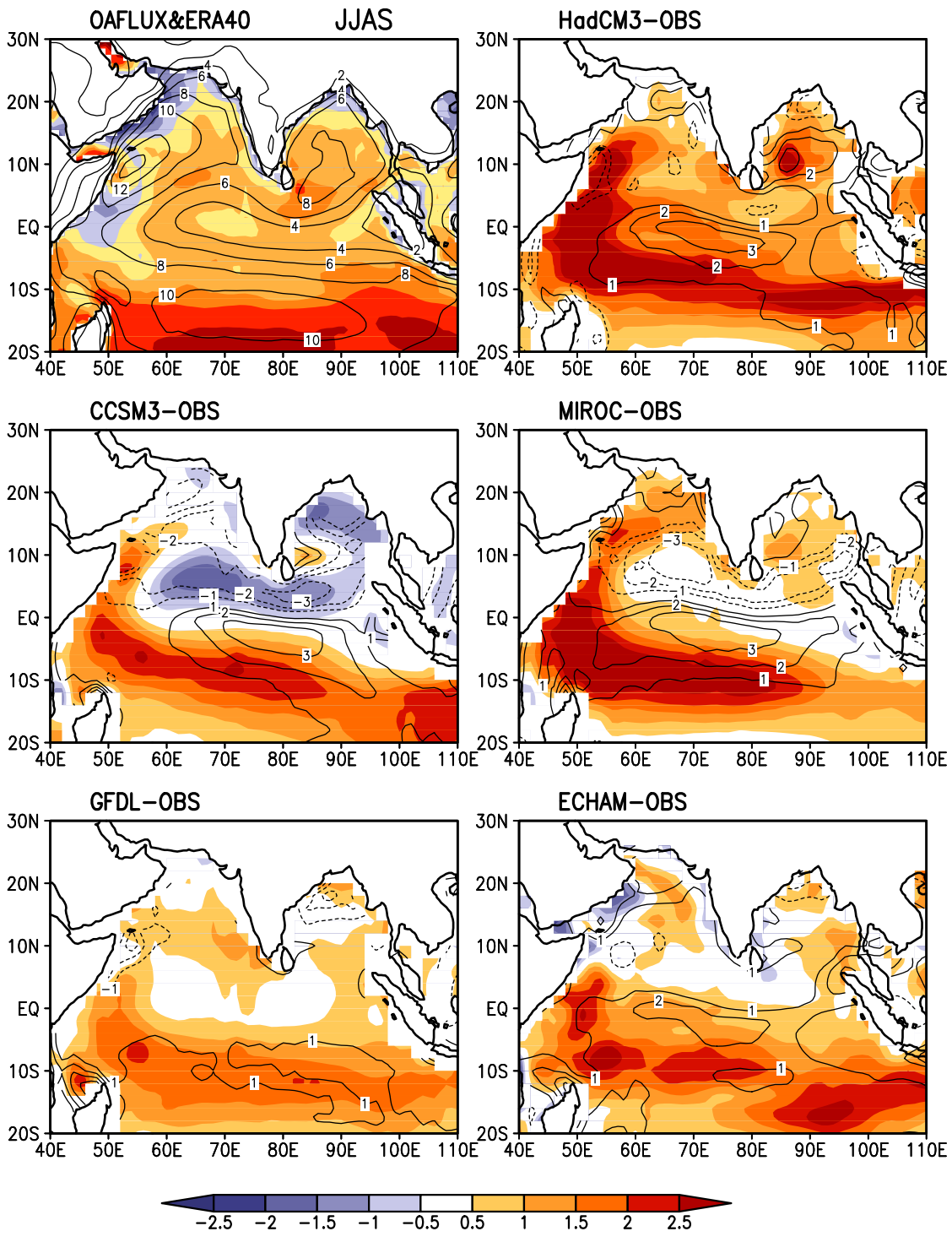

Figure 5.6: Seasonal mean (Jun-Sep; JJAS) evaporation (mm day^{-1}, shaded) and 1000-hPa wind speed (m s^{-1}, contours) over the Indian Ocean for observations (top left) and differences model-observations (other panels).

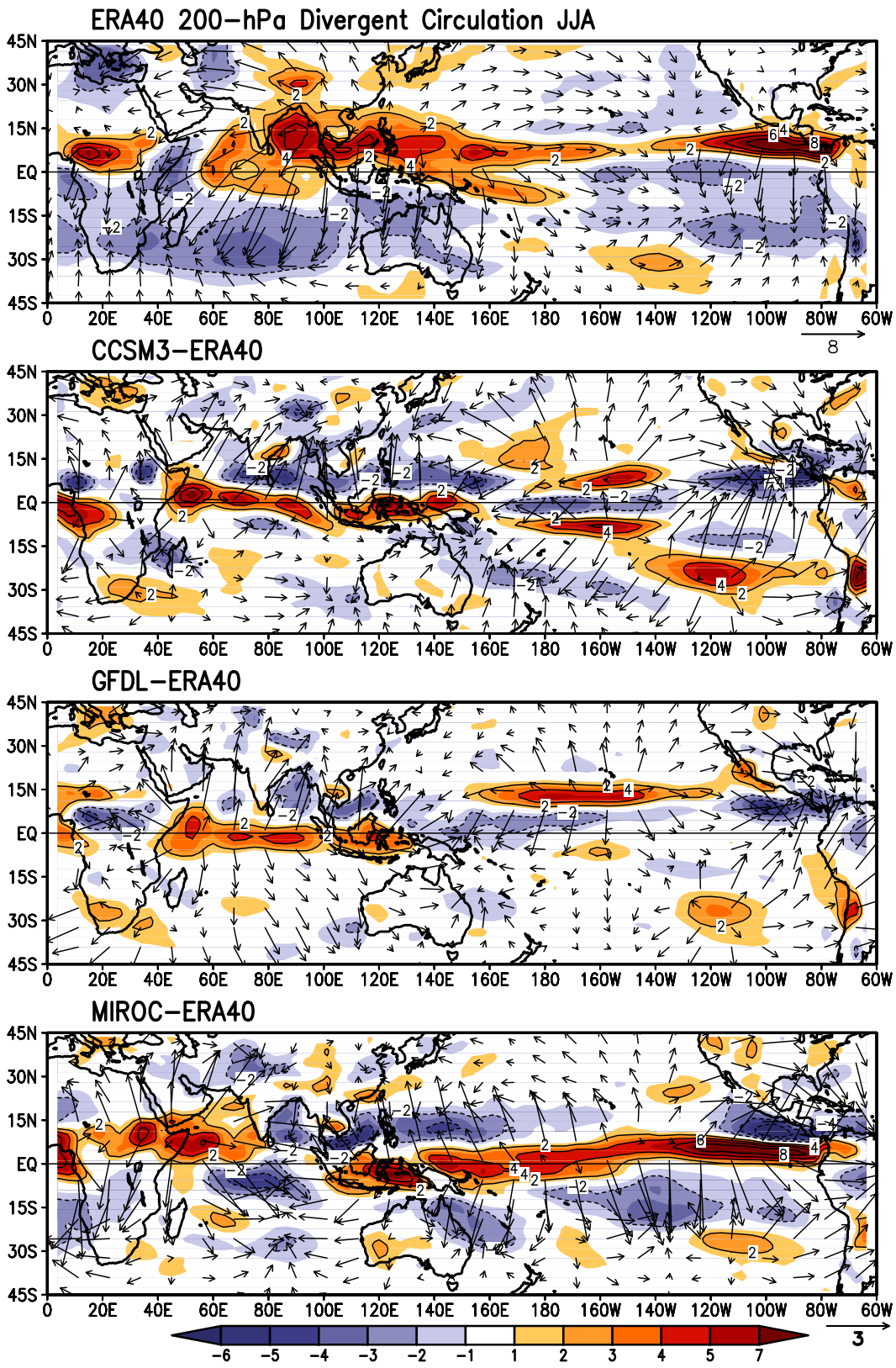

Figure 5.7: June-August mean (JJA) divergent wind (arrows) and divergence (10^{-6} s^{-1}; shaded) at 200 hPa in ERA40 (top) and differences model-ERA40 (other panels).

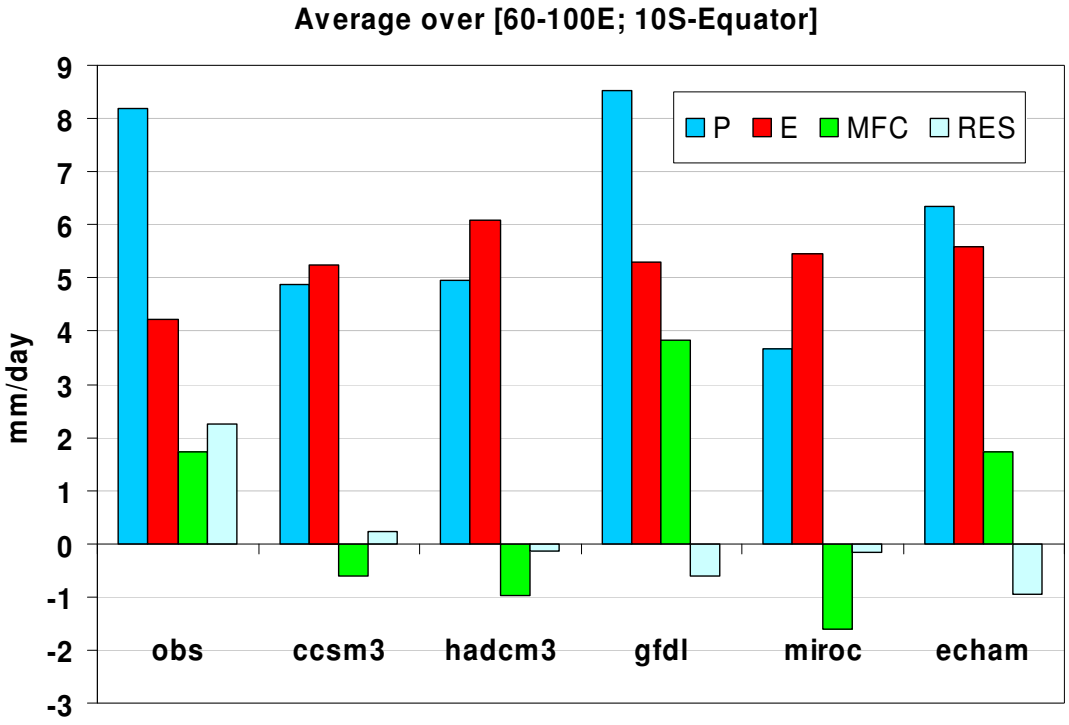

Figure 5.8: Seasonal (Jun-Sep) mean atmospheric water budget (in mm day^{-1}; P = precipitation; E = evaporation; MFC = vertically-integrated moisture flux convergence) averaged over (60°-100°E, 10°S-Equator).

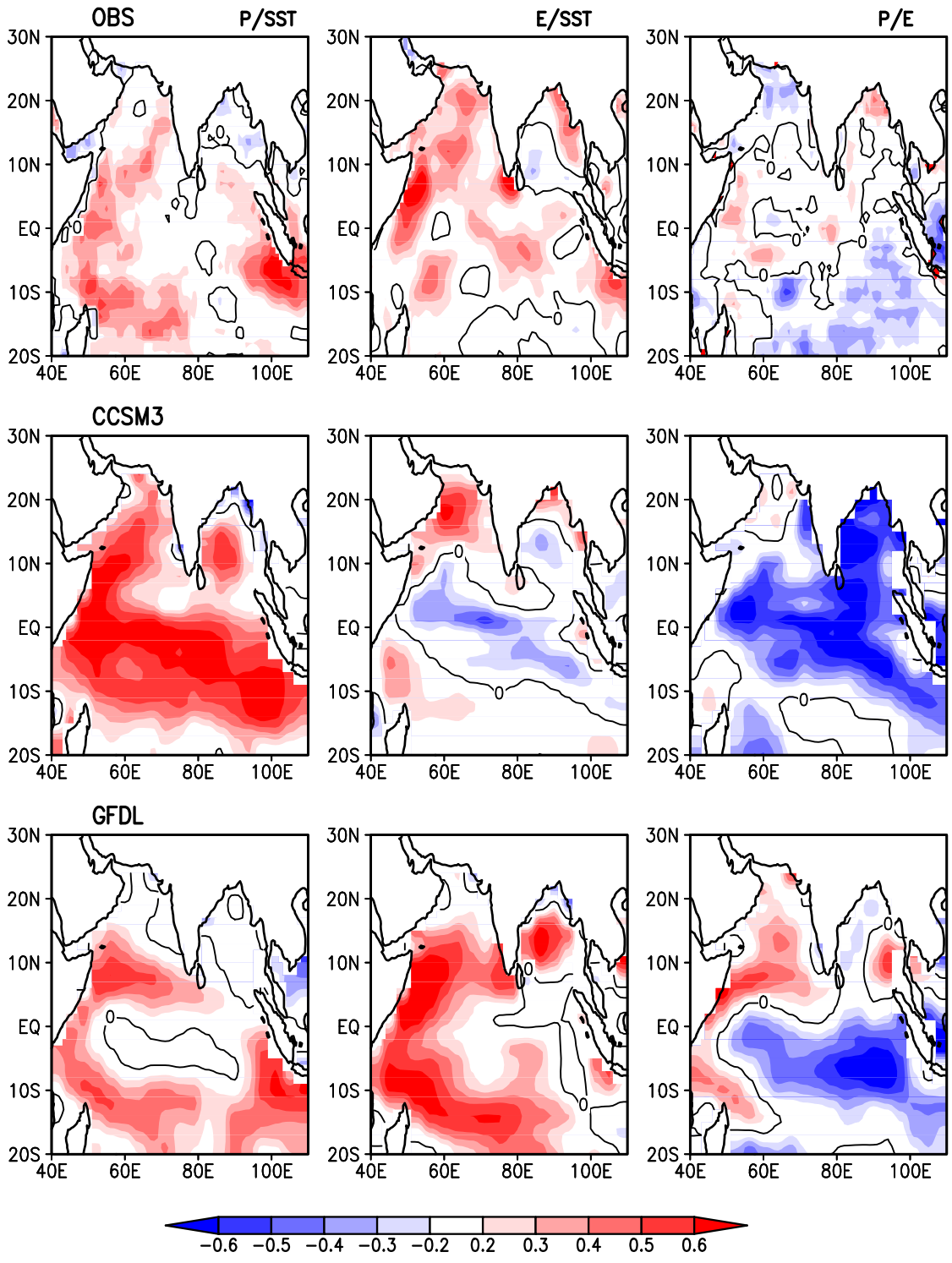

Figure 5.9a: June-August average pointwise and simultaneous correlations between precipitation and SST (left column), evaporation and SST (middle column), and precipitation and evaporation (right column) for observations (top), CCSM3 (middle), and GFDL (bottom). The zero-correlation contour is also displayed.

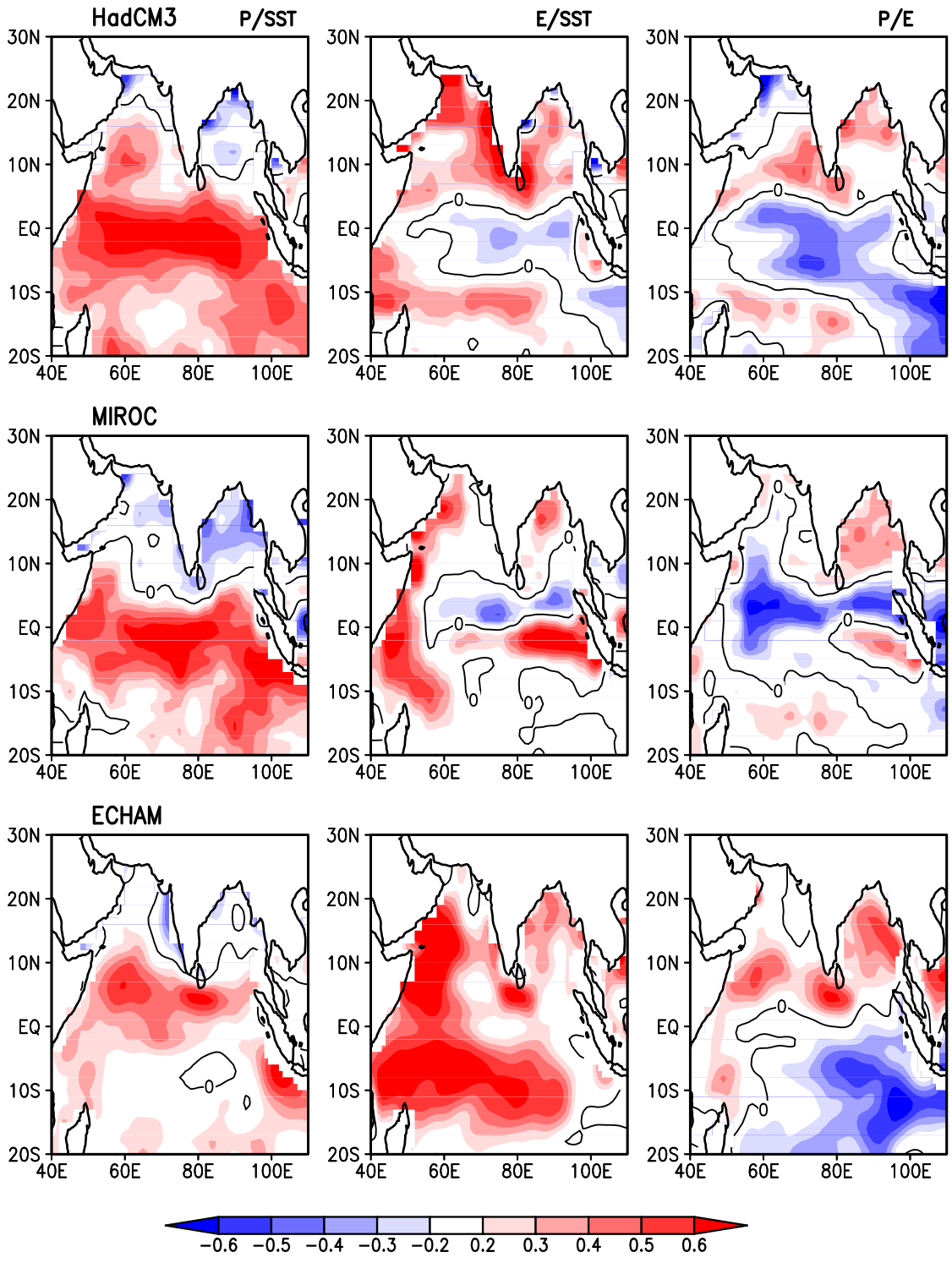

Figure 5.9b: The same as Fig. 5.9a, except for HadCM3 (top), MIROC (middle), and ECHAM (bottom).

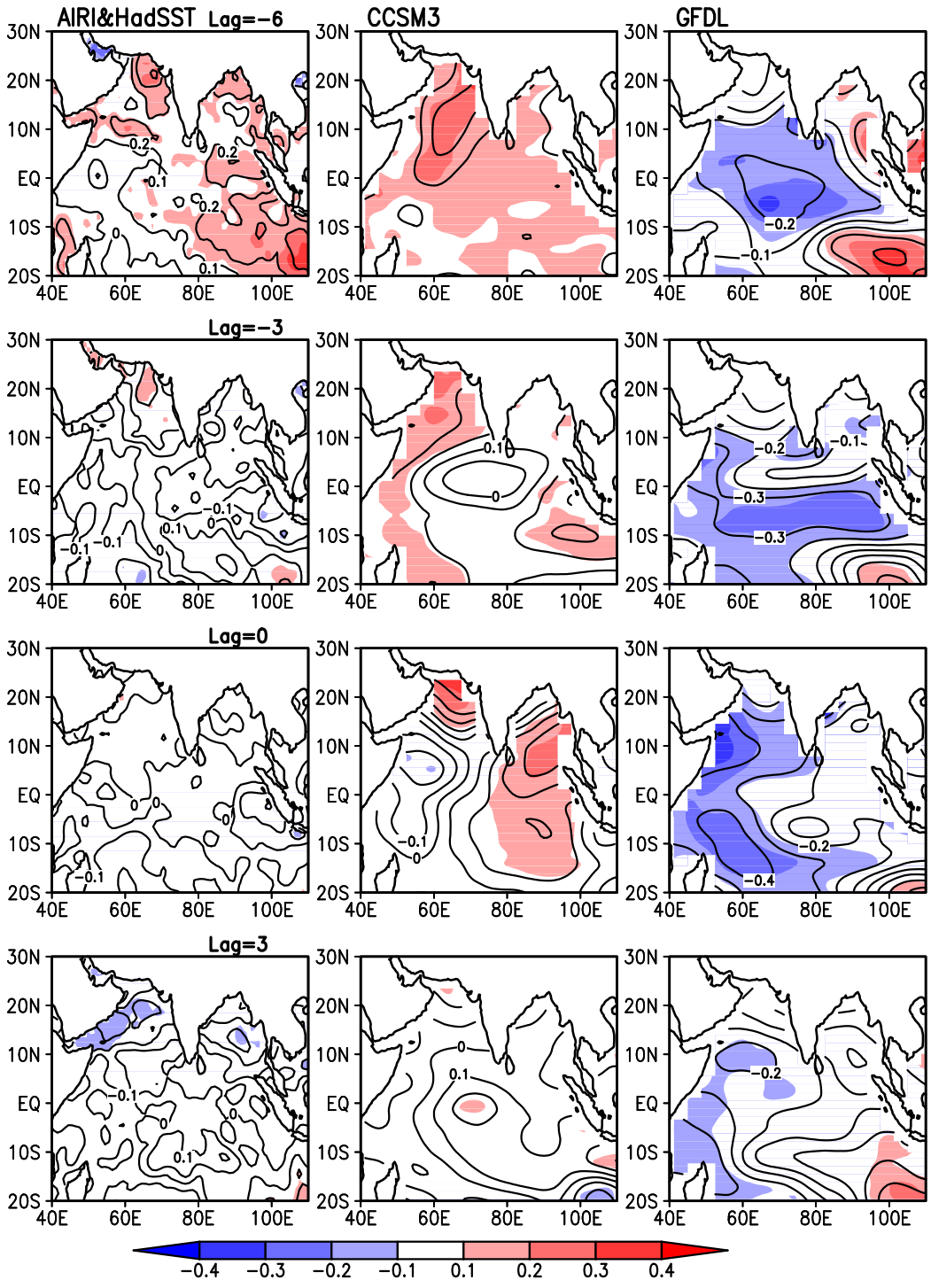

Figure 5.10a: Correlations (contour lines) and regressions (ºC; shaded) between Jun-Aug (JJA) precipitation over India and surrounding SST at (from top to bottom) lag -6, -3, 0, and +3 months (that is, SST of the previous DJF, MAM, contemporaneous JJA, and following SON, respectively) for observations (left), CCSM3 (middle), and GFDL (right).

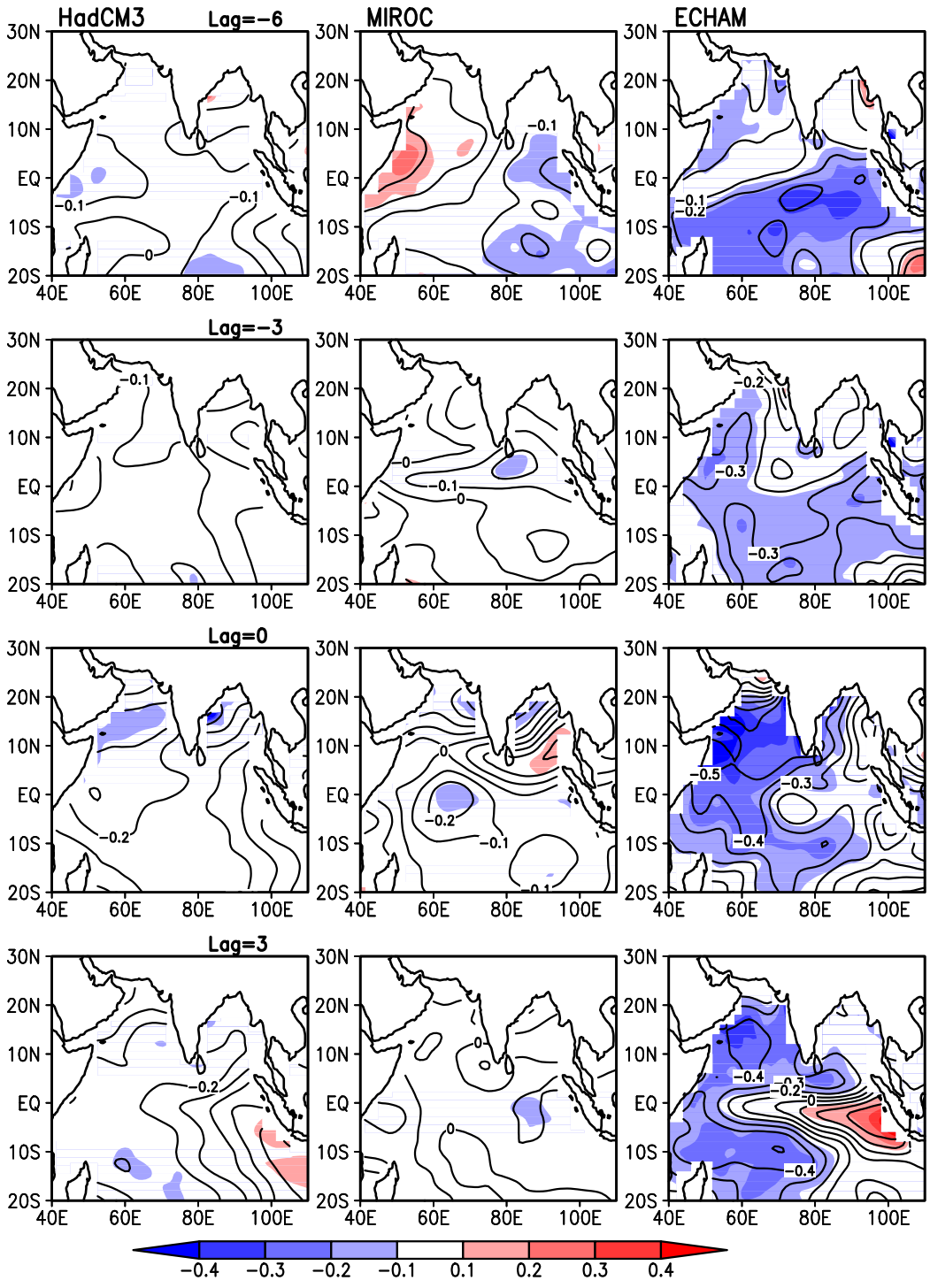

Figure 5.10b: The same as Fig. 5.10a, except for HadCM3 (left), MIROC (middle), and ECHAM (right).

Chapter 6: The Summertime "Heat" Low over Pakistan/Northwestern India: Evolution and Origin[15]

6.1 Introduction

"Heat lows" (also referred as "thermal lows") are characterized by low surface pressure (3-10 hPa lower than surrounding regions) and purportedly caused by intense heating of the land-surface (and overlying atmosphere) from solar radiation. Heat lows are found over the tropical-subtropical continents in summer when insolation is at its maximum. In particular, deep heat lows, favored by clear skies, lack of vegetation, and small evaporation, are ubiquitous features over the deserts, and as such, are found in northern and southwestern Africa, southwestern North America, central Spain, northwestern and northeastern Australia, the Tibetan Plateau, Saudi Arabia, southern Pakistan, and the Thar desert of India (e.g., Warner 1994). Key features of heat lows have been recently summarized (Johnson 2003). The dynamical aspects of the lows have been investigated using realistic (e.g., Portela and Castro 1996) and idealized numerical experiments (e.g., Rácz and Smith 1999; Spengler and Smith 2008).

The low over Pakistan and northwestern India (hereafter the Pak-India low; e.g., Ramage 1966; Chang 1972; Joshi and Desai 1985; Sikka 1997) stands out as the deepest low in the global tropics during spring and summer, and is a key element of the South Asian summer monsoon. It develops in April-May along with the low-level

[15] This Chapter has been submitted to *Clim. Dyn.* as Bollasina and Nigam (2010).

southwesterly wind regime over the Arabian Sea, a month before monsoon rains commence over western India (e.g., Ramage 1966). Monsoon depressions, the majority of which forms at the head of the Bay of Bengal move westward across the Indian Subcontinent, eventually merging and dissipating in the Pak-India low (e.g., Keshavamurty and Awade 1970). Springtime fluctuations of this low have been linked to subsequent variations of the All-India monsoon rainfall (e.g., Parthasarathy et al. 1992). Mean sea-level pressure over the low region in May is, in fact, an important parameter in the multivariate regression models of Indian summer monsoon rainfall (e.g., Singh et al. 1995). Despite the importance of the Pak-India low in the South Asian summer monsoon evolution and variability, its salient features remain to be fully characterized. Most descriptions offer a local, one-dimensional perspective, and often, in reference to the nearby Persian trough (Bitan and Sa'aroni 1992) and Saudi Arabian low (e.g., Ramage 1966; Blake et al. 1983).[16] The spatiotemporal sparseness of in-situ observations in desert regions undoubtedly hampers the characterization efforts.

The primary motivation for this study was the observation that the Pak-India low is deepest in July – not in May when the land-surface is warmer and the sensible heating stronger – questioning the prevailing view on its origin that is manifest in the commonly used "heat" label. The low is moreover nestled in the vegetated Indus River plain – not desert terrain – and just eastward of the Hindu Kush mountains (Fig. 6.1), raising further the possibility of orographic influence, which, if pertinent, finds no reference in the "heat" label. The recent availability of the European Centre for

[16] Blake et al. (1983) and Smith (1986) used intensive observations of the 1979 summer and the international Summer Monsoon Experiment to analyze the radiative and thermodynamical aspects of the heat low over the Rub'al Kahli Desert.

Medium-Range Weather Forecasts (ECMWF) 40-year global reanalysis data (ERA-40; Uppala et al. 2005) provided additional incentive to examine the 3D structure and evolution of this low, using dynamically/thermodynamically consistent fields rooted in both local and neighboring observations (in-situ and remotely sensed).

Clarification of the mechanisms generating the Pak-India low warrants a large-scale perspective on the dynamical and thermodynamical conditions as subsidence can be forced from remote regions as well (e.g., Yanai et al. 1992; Rodwell and Hoskins 1996). Subsidence over northwestern India and the Thar desert in summer has been linked to the monsoon build-up over Bay of Bengal (Das 1962). The entire Middle East, in fact, is under the influence of large-scale descent during much of the year: the Hadley cell descent is not the only contributor given the intensification and northward movement of subsidence in summer. In a seminal study, Rodwell and Hoskins (1996) showed descending motions over the Eastern Mediterranean and Middle East to be linked with the South Asian summer monsoon (the monsoon-desert link). In their modeling analysis, the Zagros mountain chain was important for the localization and intensification of the descent, through generation of regional anticyclonic low-level flow and southward advection of cold air, both leading to descending motions from Sverdrup vorticity-balance and adiabatic thermodynamic considerations, respectively.

Is the Rodwell-Hoskins' monsoon-desert mechanism of relevance in the deepening of the Pak-India low in July? Although monsoon-induced subsidence to the immediate northwest is not collocated with this low, the related low-level circulation could contribute to the low's intensification through orographic

interaction, a hypothesis investigated, observationally, in the present study. The role of regional orography in generating the Pak-India low from interaction with the zonal-mean flow is however investigated from numerical experiments with a steady linear primitive equation model. A significant role is indeed suggested in both nascent (May) and mature (July) phases of the low.

This Chapter is organized as follows: Data and model are briefly described in section 6.2. Section 6.3 describes the regional landscape and the seasonal, pentad, and diurnal variations of relevant dynamic and thermodynamic variables in the Pak-India low region, building a case for the role of non-thermal forcing (of the low) as well. Links with the large-scale atmospheric circulation, including its divergent component, strengthen the case. Diagnostic modeling of the low, in particular the orographic contribution is presented in section 6.4. Discussion and concluding remarks follow in section 6.5.

6.2 Datasets and the Diagnostic Model

The main dataset used in this study consists of atmospheric and surface variables from the ERA-40 atmospheric reanalysis. Reanalysis data is available 6-hourly on a 320 x 160 gaussian grid (horizontal resolution of about 1.125°) and at 23 isobaric levels. The 1979-2001 period data was obtained from the National Center for Atmospheric Research archives. In the following analysis, data was averaged to produce daily and pentad climatologies, in addition to monthly ones.

Monthly surface air temperatures were obtained from the Climate Research Unit (CRU) TS 2.1 dataset (Mitchell and Jones 2005) at 0.5° resolution. The study

region's land-surface is described (Fig. 6.1) using the following data sets: land topography from the National Oceanic and Atmospheric Administration/National Geophysical Data Center (NOAA/NGDC) ETOPO1 1-arc minute global relief model (Amante and Eatkins 1998); land cover from the University of Maryland/Department of Geography 1-km global classification dataset (http://glcf.umiacs.umd.edu/data/landcover/), based on 14 years (1981-1994) of imagery from the Advance Very-High Resolution Radiometer (AVHRR) which distinguishes fourteen land cover classes; land vegetation development from version-5 of the TERRA/Moderate Resolution Imaging Spectroradiometer (MODIS) Normalized Difference Vegetation Index (NDVI) monthly data at 0.05° horizontal resolution (MOD13C2.005) for the period 2000-2008 (https://lpdaac.usgs.gov/lpdaac/products/modis_products_table/vegetation_indices/monthly_l3_global_0_05deg_cmg/v5/terra).

Diagnostic Model

The steady linear primitive equation model is described in Nigam and Chan (2009) and in the references therein; only salient features are mentioned below. The model solves the eddy component (i.e., departure from the zonal average) of the linearized sigma-p coordinate ($\sigma=p/p_s$, where p and p_s are pressure and surface pressure, respectively) equations, given the zonally-symmetric basic state (temperature, zonal and meridional winds, and surface pressure). The ERA-40 orography, diagnosed 3D diabatic heating (Chan and Nigam 2009), sub-monthly transient heat and momentum fluxes, and the surface temperature constitute the model

forcing. The basic state and model forcing are all computed from the 1979-2001 period ERA-40 reanalysis (2.5° horizontal resolution, 23 isobaric levels). The diagnostic model is solved numerically, using the semi-spectral representation for the horizontal structure: 73 grid points between the two poles (i.e., $\Delta\theta = 2.5°$) and zonal Fourier truncation at wave number 60. The vertical structure is discretized using 18 full-sigma levels. Momentum dissipation is exactly as in Nigam and Chan (2009) but the thermal dissipation is slightly modified to reflect the increased sensible heating in summer, through deeper thermal diffusion in the planetary boundary layer, larger drag coefficient in the related lower boundary condition, and from reduced Newtonian damping of temperature in the lower troposphere.[17]

6.3 Climatological Features of the Pak-India Low

6.3.1 The Landscape

The physical landscape and summertime land-cover/vegetation in the Middle East and southwest Asia are shown in Fig. 6.1. Sea-level pressure is also shown using contours. The region is characterized by complex orography, with elevated mountain chains (e.g., peaks above 3000 m): the Taurus in Turkey, the Zagros to the south and the Elburz to the north in Iran, and the Hindu Kush in Afghanistan and northwestern Pakistan. The land surface is prevalently arid or semi-arid (bare ground is peach, #13, in Fig. 6.1 middle) with numerous deserts (e.g., Iranian, Karakumy, and Thar) and

[17] The thermal diffusion coefficient is $30[1+tanh\{10\pi(\sigma-0.70)\}]$ instead of $30[1+tanh\{10\pi(\sigma-0.85)\}]$; the drag coefficient is 3.0×10^{-3} as opposed to 1.0×10^{-3} earlier; the Newtonian damping coefficient is now $(25 \text{ days})^{-1}$ at all vertical levels.

some cultivated areas (principally, the Indus River plain). During July, vegetation is fully developed in the Indus River plain and western India (except over the Thar Desert; see Fig. 6.1 bottom).

A wide area of low-pressure (<1002 hPa, for instance) extends from Arabia to India during May-July, with the core of the Pak-India low defined by the lowest pressure closed contour (998 hPa). The low is located over the Indus River plain, with its western flank skirting the Hindu Kush mountain range (Fig. 6.1 top). The northern portion of the low is more dark pink than peach in Fig. 6.1 (middle), indicating a shrubland-cropland type land cover which is green during the period under consideration. Only the south-central sector is classified as bare ground. In particular, the core of the Pak-India low in July (when it is deepest, ~996 hPa) is centered over a vegetated land surface (Fig. 6.1 bottom) – calling into question its wide reference as a "heat" low.

6.2.2 Seasonal Evolution

The summertime evolution of the Pak-India low is shown in Fig. 6.2, along with surface air temperature (SAT). An expansive low, without a defined core, is present over Pakistan and northern India in May, with SAT exceeding 33°C over a wide swath of the Indian subcontinent and even 34°C over southern Pakistan. The low deepens substantially in June with the closed 996 hPa contour defining its core, and is broadly coincident with the warmest SAT region (>35°C). These distributions indicate the significance of surface thermal forcing in the deepening of the low, but not to an exclusive role. The low deepens a bit more in July, especially over southern Pakistan but, interestingly, without any further increase in SAT. The SAT, in fact,

decreases in July by 1-2°C over the core of the low, and by several more degrees over western India and the northern Gangetic Plain, the latter due to the arrival of monsoon clouds and rain. The June-to-July evolution of sea-level pressure and SAT also suggests that the Pak-India low is maintained not only by surface thermal effects.

The thermal forcing of the low is investigated in Fig. 6.3, which shows the monthly ERA-40 sensible heat flux[18] at 12Z (5 pm in Pakistan and India). The flux should capture the peak heating of the atmosphere from the underlying land-surface. Sensible heating over the Pak-India low region is evidently large in May and June but focused over southeastern Pakistan and western India, i.e., south of the core of the low. The northern lobe of the low, interestingly, is not a notable sensible heating zone (flux is 50% smaller than to the south). The heating, like SAT, is moreover diminished in July when the low is the deepest. The lack of co-location and different peak timings of sea-level pressure and surface thermal variables suggest that non-thermal processes may also be important in the evolution of the Pak-India low.

Potential temperature and vertical motion across the low are shown in a latitude-height cross-section in Fig. 6.4 (average between 70°-74°E) for May (left) and July (right). The dip in potential temperature contours, as evident between 25°-30°N in May, denotes heating of the atmosphere, which extends up to ~700 hPa. The pressure vertical velocity is negative (rising motion) beneath this level and positive (sinking motion) above it, which must generate horizontal divergence near 700 hPa. The heating of the atmosphere is evidently not as deep in July (only up to ~800 hPa)

[18] The unassimilated reanalysis variables, such as sensible heat flux, are impacted by the biases of the assimilating model, including physical parameterizations. The ERA-40 sensible heat flux is, nonetheless, analyzed here as long-term observations of this quantity are non-existent, and because of our focus on the large-scale features, especially in context of monthly evolution, i.e., relative variations.

and the sinking motions in the mid-to-upper troposphere are, notably, absent in this month, both reflecting the advance of the monsoon. Large upward velocity along the southern slopes of the Himalayas, associated with stable air, denotes strong orographic uplift.

6.2.3 Pentad Evolution

The evolution of vertical motion and horizontal divergence above the core of the Pak-India low is examined at pentad resolution in Fig. 6.5 to shed light on the steep drop in sea-level pressure between May and June (Fig. 6.2). Upward motion develops near the surface in March-April, and intensifies and extends up to 775 hPa by May. Subsidence builds up in the mid-to-upper troposphere, with a 2-3 pentad duration spike in the latter part of May. This spike is reflected in weaker upward motions near the surface (and the weakening of the low). The abatement of upper-level subsidence, interestingly, leads (by a few pentads) the intensification of near-surface upward motions (and the deepening of the low) in late June. Arrival of monsoon rains and related deep convection in the second half of July drastically alter vertical motions in the mid-to-upper troposphere, from sinking to rising. The changes are more muted near the surface. The structure of horizontal divergence – an affirmation of the continuity equation – reveals the presence of a shallow (< 100 hPa thick) convergent layer near the ground that is topped by a deep (several 100 hPa thick) divergent layer. Sea-level pressure development (not displayed) shows the Pak-India low to be deepest at the end of June. The deepening, as noted above, is preceded by rapid reduction in upper-level subsidence, suggesting that the Pak-India low, while

originating from surface heating, is influenced by larger-scale regional circulations, including the monsoon (as shown later).

The presence of multiple influences is also indicated by analysis of the position of the core of the Pak-India low. Heat lows, owing their existence principally to surface thermal forcing, are essentially stationary features. Broadly, this is the case for the Pak-India low, as well. Tracking the core's position at pentad resolution using 23 years of ERA-40 reanalysis however shows the core, located over southeastern Pakistan in late April, to migrate northeastward while intensifying.[19]. The core's position however does not track the warmest SAT region.

6.2.4 Diurnal Cycle

The diurnal variation of potential temperature and vertical motion over the northern and southern sector of the Pak-India low are examined in Fig. 6.6 in May and June when the low develops and deepens. Variations are analyzed separately in the sectors in view of differences in the underlying land-surfaces: the northern sector is classified as croplands while the southern one is more arid (cf. Fig. 6.1 middle and bottom). Nighttime and daytime conditions are represented by the 00Z and 12Z (5 am and 5 pm local time, respectively) profiles (blue and red, respectively). Only the daytime minus nighttime difference is shown in case of potential temperature.

In the southern sector, diurnal variability is robust, penetrating into the mid-troposphere. Daytime ascending motions in the 1000-800 hPa layer are replaced by

[19] The core location is identified by successive searches of the point where sea-level pressure is lower than its 8 surrounding points. Examination of 23 maps for each pentad shows the core to be located in the following area (68.625°-70.875°E, 27°-28.125°N; southeastern Pakistan) in 15 of the 23 cases during 11-15 April. About a month later (16-20 May), 17 of the 23 centers are found in the area (72°-74.25°E, 29.25°-31.5°N; northeastern Pakistan).

strong subsidence at night; the ascent is more vigorous and deeper in June, when the land-surface is warmer (cf. Fig. 6.2). These variations are typical of those encountered in desert regions (e.g., Sikka 1997; Blake et al. 1983; Smith 1986). The large near-surface diurnal range in potential temperature, in June, especially, reflects the super-adiabatic lapse rate conditions in the afternoon and a stable near-surface layer (if not an inversion during May) during nighttime.

The northern sector of the low however exhibits very different vertical velocity profiles: Both daytime and nighttime motions penetrate into the mid-troposphere, attaining maximum amplitudes much above the surface. More noteworthy is the occurrence of daytime (nighttime) descent (ascent), which is not typical even of the circulations developing over flat vegetated surfaces. The diurnal temperature range is also smaller than in the southern sector. Such diurnal variability, including deep ascent/descent, likely reflects the presence of regional-scale circulations, possibly influenced by orographic effects.

The structure of diurnal variability in the southern and northern sectors of the Pak-India low is thus quite different, with the former exhibiting desert-like structure. The distinction supports the notion that mechanisms other than surface thermal effects also contribute to the development of the Pak-India low.

6.2.5 The Large-scale Circulation Context

The evolution of the Pak-India low is examined in the context of the developing large-scale circulation in Fig. 6.7. Full fields are shown in April and the monthly

increments thereafter.[20] Sea-level pressure is lowest (~1006 hPa) along the Pakistan-India border (and in the eastern Gangetic Plain) even in April. The low-level westerlies confined to the south of the Zagros mountain range become diffluent upon entering the Indian subcontinent, with the northern stream skirting the nascent Pak-India low. Sea-level pressure drops precipitously in the subtropics in subsequent months, with the Pak-India low region as one of the foci; a 5-6 hPa decline occurs each month.

Following Rodwell and Hoskins' (1996) monsoon-desert hypothesis linking the aridity of remote northwestern regions to monsoon convection over South Asia, the impact of eastern Indian Ocean and the Bay of Bengal convection (key monsoon convection zones) on the Pak-India low region is assessed from the structure of upper-level divergent circulations (Fig. 6.8). The 200-hPa divergent outflow is notably strong over Southeast Asia in May with divergent winds directed toward a broad area from western India to eastern Iran, and primary convergence over western Pakistan and southern Afghanistan. This upper-level convergence switches to divergence at lower levels (by mass continuity), with a node at 400-500 hPa (not shown). The 700-hPa divergence (also not shown) is a mirror image of the upper-level pattern at large scales, modulated by surface effects, including orography. Deep convection and related upper-level outflow intensifies and moves northward to the Bay of Bengal in July in conjunction with monsoon onset over eastern India. Upper-level divergent flow to the northwest is now principally focused over the eastern Mediterranean (Rodwell and Hoskins 1996), but with a secondary convergence center

[20] The sea-level pressure *change* is preferred to the full field in complex orography regions as the former underemphasizes the biases introduced by the below-ground interpolation/extrapolation schemes in computation of sea-level pressure.

over Iran-Turkmenistan-Afghanistan (i.e., east of the Caspian Sea). Can the low-level divergent flow induced by upper-level convergence (and subsidence) in these regions (but ultimately by monsoon deep-convection much farther to the east) be consequential for local sea-level pressure and circulation development (e.g., the Pak-India low evolution)? The monsoon-desert hypothesis of Rodwell and Hoskins (1996) encourages pursuit of the idea that the Pak-India low may be forced, in part, by the low-level divergent (and rotational) flow. This forcing would manifest not directly, but from its interaction with regional orography.

The idea is difficult to pursue, observationally, given the challenge of attributing divergent flow to various processes, especially in complex terrain regions. The 775-hPa streamlines are nonetheless superposed on regional orography in Fig. 6.8 to broadly note the salient features: a weak anticyclonic center is present over the Karakum desert in May; in July it intensifies into a prominent ridge positioned northwestward over the Caspian Sea (with strong northerly flow over western Afghanistan), broadly tracking the movement of the upper-level convergence (low-level divergence) zone. The ridge will, of course, not be collocated with the divergence zone. Even if this remotely induced divergence were its principal forcing – unclear given the complex regional orography – the ridge placement will be determined by the nature of the vorticity balance: the large-scale (Sverdrup) balance would, for example, result in the ridge being to the west. Regardless of how this ridge is forced, it generates northerly flow over the mountains: over the western Hindu Kush in May, and more extensively, over the eastern Zagros, Elburz, and Hindu Kush ranges in July. The mountain ranges, in particular the Hindu Kush, deflect the flow,

and while it is crossing the southern slopes, if potential vorticity [≡(f+ζ)/H; with f the Coriolis parameter, ζ the relative vorticity, and H the fluid column height] is conserved, ζ will become more cyclonic (i.e., positive) for f decreasing and H increasing, not inconsistent with the observed flow structure. Such mechanisms are best investigated by a modeling analysis where the divergent flow can be attributed to various processes.

6.4 Role of Orography and Land-Surface in Development of the Pak-India Low: A Diagnostic Modeling Analysis

The steady, linear primitive-equation model used here cannot capture the interaction of the remotely-induced divergent (and rotational) flow with regional orography – of the kind posited above for deepening of the Pak-India low from intensifying Bay of Bengal convection in June and July. It can, however, provide an estimate of the role of regional orographic features in the generation of the low. Three model solutions are discussed, including the control case (CTL) which is a simulation of summer stationary waves using all forcing (cf. section 6.2). The realism of this simulation will be an indicator of the suitability of this model. The other two solutions are the "no-mountain" simulations, both generated with forcing as in CTL but after removal of regional orographic features (as marked in Fig. 6.1 top): the Taurus-Elburz-Zagros mountains extending across Turkey and Iran are removed in the first simulation (referred as 'No-Zagros Taurus') while the Hindu Kush range in Afghanistan and Pakistan is zeroed out in the second one (the 'No-Hindu Kush'). The

impact of surface thermal forcing in the Pak-India low region is also simulated in another sensitivity experiment.

6.4.1 Control Simulation

The May and July sea level pressure in the CTL simulation (Fig. 6.9, top panels) should be compared with their observed counterparts (Fig. 6.2). The Pak-India low is evident in May along with its deepening in July, with core values generally consistent with ERA-40. The model however tends to extend the low-pressure region too far westward (toward Iran), perhaps because it cannot represent the non-linear aspects of the flow's interaction with orography. The model's performance is further assessed by examining the 850-hPa streamfunction and 600-hPa vertical velocity (Fig. 6.10). As with sea-level pressure, the streamfunction trough is placed more westward (over the Iran-Pakistan border) in May, and more eastward (over the western Himalayas) in July. The mid-tropospheric vertical velocity is simulated more closely in the region except for the stronger and somewhat shifted subsidence in the western Himalayan sector. This shift is related to the eastward placement of the monsoon trough (and related upper-level Tibetan anticyclone) in the simulation.

6.4.2 Impact of Regional Orographic Features

The Taurus-Elburz-Zagros Mountains lead to lower sea-level pressure over the Middle East in both May and July (Fig. 6.9, middle panels, obtained as CTL minus 'No-Zagros Taurus' simulation): a 6-8 hPa pressure drop centered over Iran in this linear diagnosis. The effect is evident at upper levels as well, as seen in the 850

streamfunction (Fig. 6.10) which also shows a modest feature over the Pak-India low region. The mountains thus generate a cyclonic near-surface circulation with descent over the southern slopes of the Zagros Mountain and the Persian Gulf. Note, vertical motions arise from kinematic interaction with orography, and to offset thermal advection by orographically forced circulation and/or diabatic heating. The presence of descent (ascent) in northerly (southerly) regions in Fig. 6.10 (third panels from the top) reflects some contribution from the offsetting of cold (warm) advection under adiabatic conditions, applicable to the regional mountain experiments.

The Hindu Kush mountains of Afghanistan and Pakistan also generate low sea-level pressure (Fig. 6.9, bottom panels). While their contribution is comparatively modest (~3 hPa), it is in the core region of the Pak-India low, attesting to the relevance of non-thermal forcing mechanisms as well. The Hindu Kush impact on sea-level pressure is focused in northern Pakistan in May and over Afghanistan in July. In both months, these mountains generate descent over southern Pakistan and eastern Afghanistan, leading to severe aridity and lack of vegetation in these regions (cf. Fig. 6.1), which must feedback on the low's intensity.

6.4.3 Influence of the Warm Land-Surface

As noted earlier, the Pak-India low is often refereed as the 'heat" low, reflecting the view that its origin is rooted in the heating of the underlying land-surface and attendant sensible heating of the planetary boundary layer (together, surface thermal forcing), a view contested in this paper. The influence of surface thermal forcing in the Pak-India low region is computed from the difference of two model solutions: the control simulation and another in which surface air temperature in the Pak-India low

region (62.5°-75°E, 22.5°-32.5°N) is capped at 30°C and diabatic heating (and transients) switched off in the planetary boundary layer ($\sigma \geq 0.85$).[21] The surface temperature forcing in May and July (Fig. 6.11 top panels) fully covers the area of interest and is ~5K in the core region of the low. The response to surface thermal forcing (Fig. 6.11 bottom panels), consisting of a 1-2 hPa signal over southwestern Pakistan, shows it to be consequential but only modestly compared to the Hindu Kush mountains, which generate a stronger signal (up to 3-4 hPa) over this region and Afghanistan and northern Pakistan (Fig. 6.9 bottom panels). The orographic signal is, comparatively, even stronger further to the west where the Taurus-Elburz-Zagros mountains generate a sea-level pressure response of 6-8 hPa. The surface thermal effects are expected to be of the same order as before.

6.5 Discussion and Concluding Remarks

The study was instigated by the hypothesis that the arid land-surface of southwest Asia plays a role in the development of the South Asian summer monsoon through generation of lower sea-level pressure from surface thermal effects. One can envision the resulting pressure distribution to generate southerlies in the Tropics, and southwesterlies beyond when the Coriolis force becomes significant: the southwesterly monsoon flow over the Arabian Sea and peninsular India. Subsequent interaction with regional orography – Western Ghats along the coast, regional plateaus in the interior and, of course, the Himalayan-Tibetan complex to the north –

[21] Ideally, the planetary boundary layer heating should be set to the surrounding region value, just as with surface air temperature. It was removed all together, however, to provide an upper estimate of the surface thermal impact.

would influence the rainfall distribution. The hypothesis is conceptually appealing as it complements the monsoon-desert hypothesis of Rodwell and Hoskins (1996). If tenable, it would impart an element of symmetry to the monsoon-desert linkage. Interest in this hypothesis led us to investigate the Pak-India "heat" low, especially its evolution during the summer monsoon season which could be insightful on its origin.

Although drawn to this near-surface circulation feature because of its "heat" label which conveys the prevailing view on its origin – from surface thermal effects – , we soon noted several observational aspects that encouraged questioning the suitability of this descriptive label. In particular:

- The Pak-India low is deepest in July, not in May when the land-surface is warmer and sensible heating stronger;
- The low is nestled in the vegetated Indus River plain, not over desert terrain;
- The low is positioned just eastward of the Hindu Kush mountains, raising the possibility of orographic influence;
- Sensible heating in early summer is focused over southeastern Pakistan/western India, i.e., south of the core of the low. Its northern sector, interestingly, is not a notable heating zone;
- Tracking the steepest monthly deepening of the low (May-to-June) at pentad resolution showed the deepening to be preceded by rapid reduction in upper-level subsidence, indicating the influence of larger-scale regional circulations;
- Diurnal variability in the northern and southern sectors of the Pak-India low is quite different, with only the latter exhibiting desert-like, day-to-night time differences;

- The upper-level divergent flow to the northwest of deep monsoon convection over Bay of Bengal/eastern India is focused over eastern Mediterranean and also Iran-Turkmenistan-Afghanistan (Rodwell and Hoskins 1996). The remotely forced descent over the latter region (and related rotational response) is not factored in current explanations of the Pak-India low, especially its summer evolution.

Our analysis, rooted in observations (principally ERA-40 reanalysis) and diagnostic modeling, suggests that the Pak-India low is forced both by regional and remote forcing. Regionally, the influence of Hindu Kush mountains is found to be stronger than the impact of land-surface heating and attendant sensible heating of the planetary boundary layer (referred, together, as surface thermal forcing) by a factor of 1.5-2.0, questioning the suitability of the "heat" label in canonical references to this circulation feature.

Our observational analysis indicates that the notable May-to-June deepening of the Pak-India low and its further deepening in July, however, arises from remote forcing – development of monsoon deep-convection over the Bay of Bengal and eastern India in June and July. The importance of monsoon convection for the upstream (northwest) region aridity was noted in the seminal analysis of Rodwell and Hoskins (1996). Here we hypothesize that the upstream descent over Iran-Turkmenistan-Afghanistan (i.e., east of the Caspian Sea; noted in Rodwell and Hoskins' paper as well) and related low-level northerlies over the Elburz-Zagros-

Hindu Kush mountains also contribute to the strengthening of the Pak-India low in June (and July) – not directly, but from interaction with regional orography.

In summary, we find surface thermal forcing to have a limited role in the development of the Pak-India low; the forcing is somewhat influential in the low's southeastern sector (which has desert-like characteristics), principally, in its nascent phase. The study argues for a reconsideration of the physical processes important for the development of the Pak-India low. Advancing understanding of the development mechanisms of this summertime circulation feature is essential given its strong precursor links to the summer monsoon rainfall, a link captured in statistical prediction models, as noted in the Introduction.

6.6 Figures

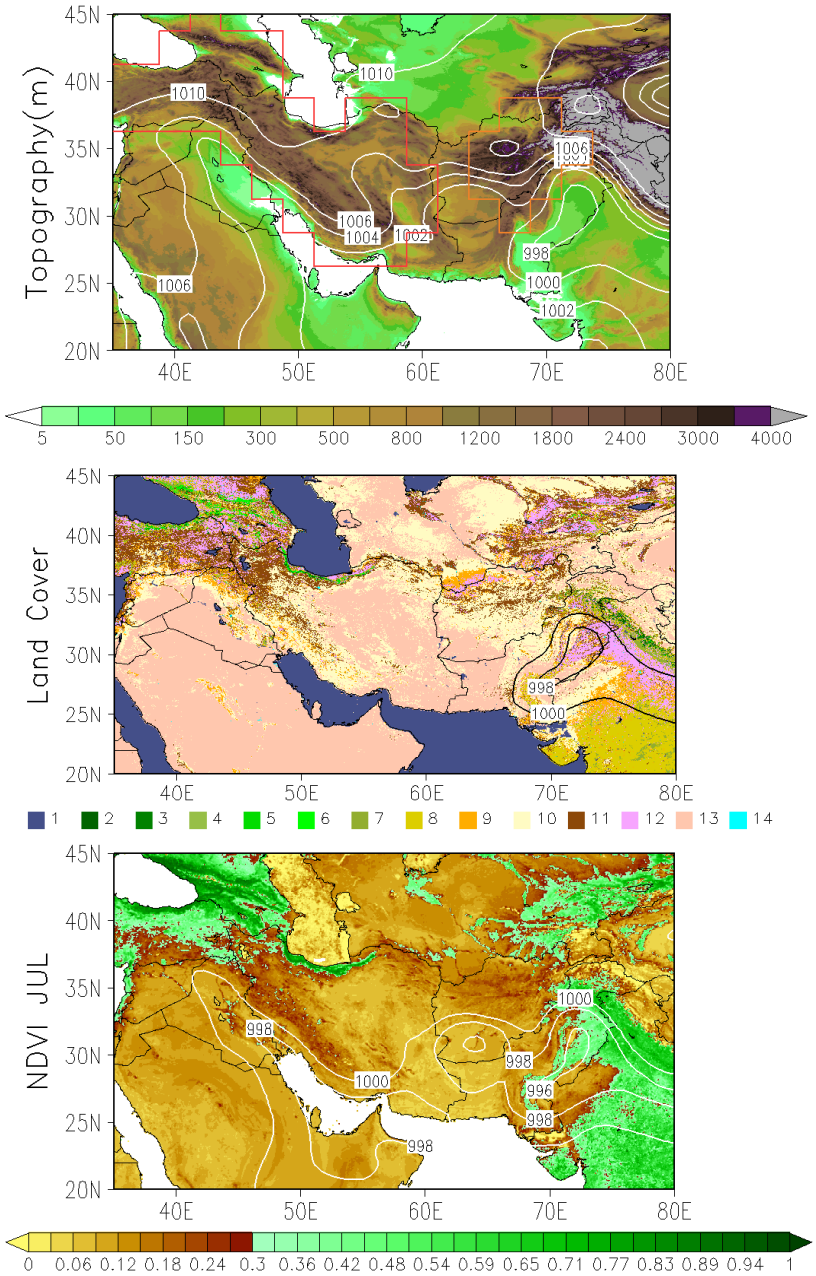

Figure 6.1: From top to bottom: ETOPO1 1-minute topography (m; colors) and May-July average sea-level pressure (hPa, white contours); UMD AVHRR 1-km land-cover classification and May-July average sea-level pressure (hPa; black contours, only values below 1000 hPa are shown); July mean MODIS NDVI and July average sea-level pressure (hPa; white contours, only values below 1000 hPa are shown). Land cover classes are: 1 = water, 2 = evergreen needleleaf forest, 3 = evergreen broadleaf forest, 4 = deciduous needleleaf forest, 5 = deciduous broadleaf forest, 6 = mixed forest, 7 = woodland, 8 = wooded grassland, 9 = closed shrubland, 10 = open shrubland, 11 = grassland, 12 = cropland, 13 = bare ground, 14 = urban and built. The color lines in the top panel delineate the areas where orography (red: Taurus, Zagros and Elburz; orange: Hindu Kush) is removed in the model experiments. The red area actually extends to 28°E (the area is restricted in the picture to focus on regional details).

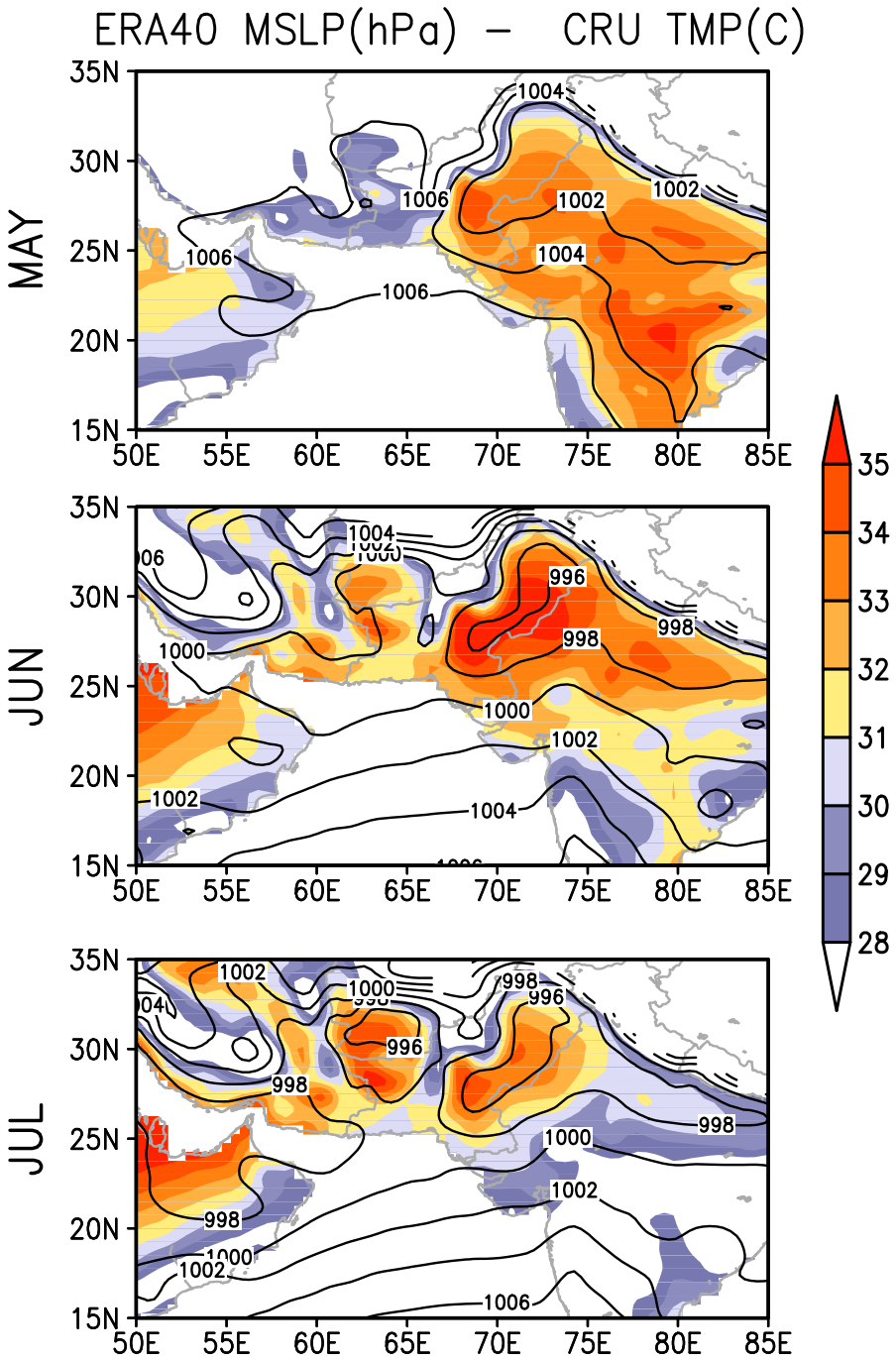

Figure 6.2: ERA-40 sea-level pressure (hPa, contours) and CRU surface air temperature (°C, shaded) for (top to bottom) May, June and July.

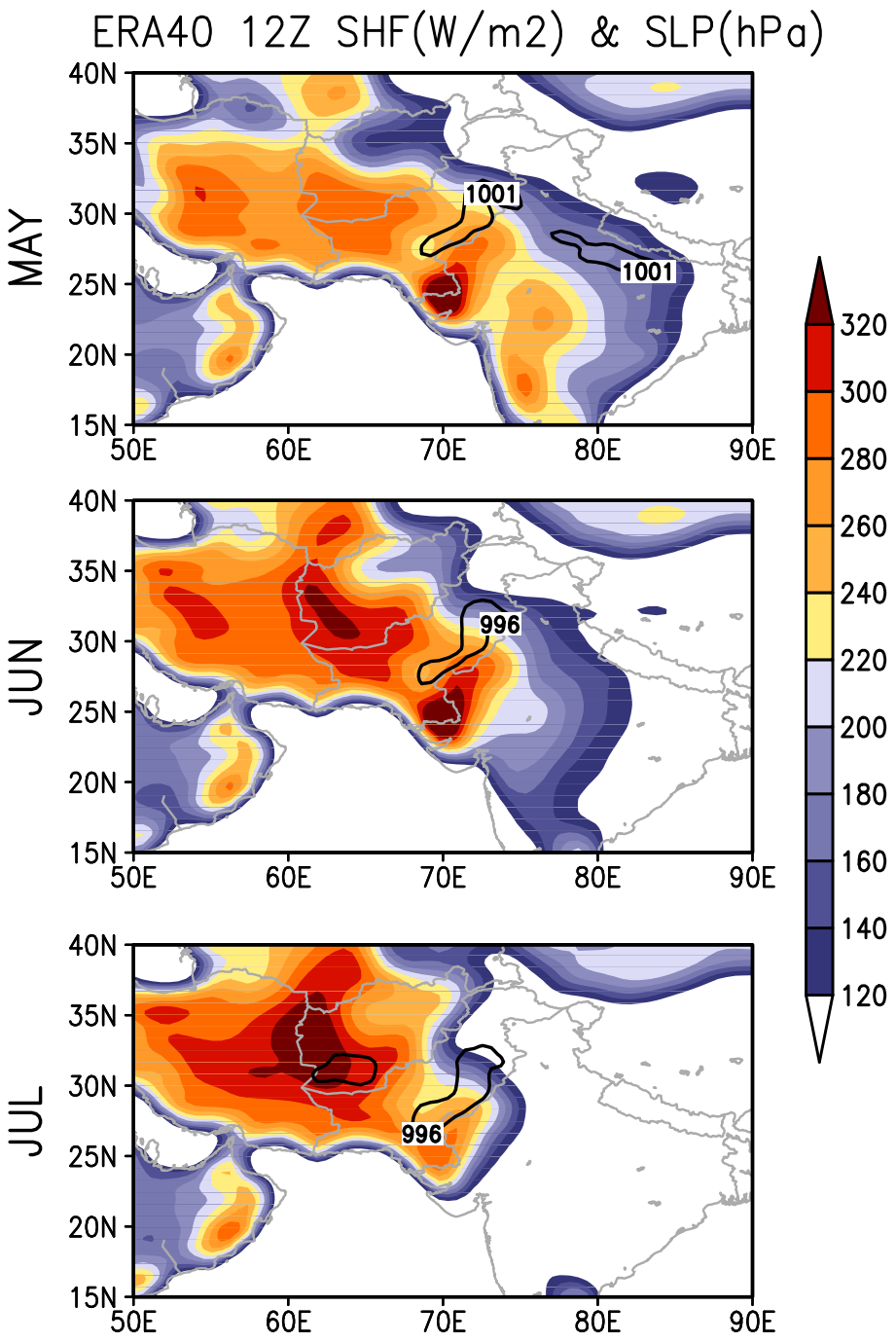

Figure 6.3: Sensible heat flux at 12Z (W m^{-2}, shaded) and sea-level pressure (hPa, contours) for (top to bottom) May, June and July. Sea-level pressure is represented as the lowest closed contour.

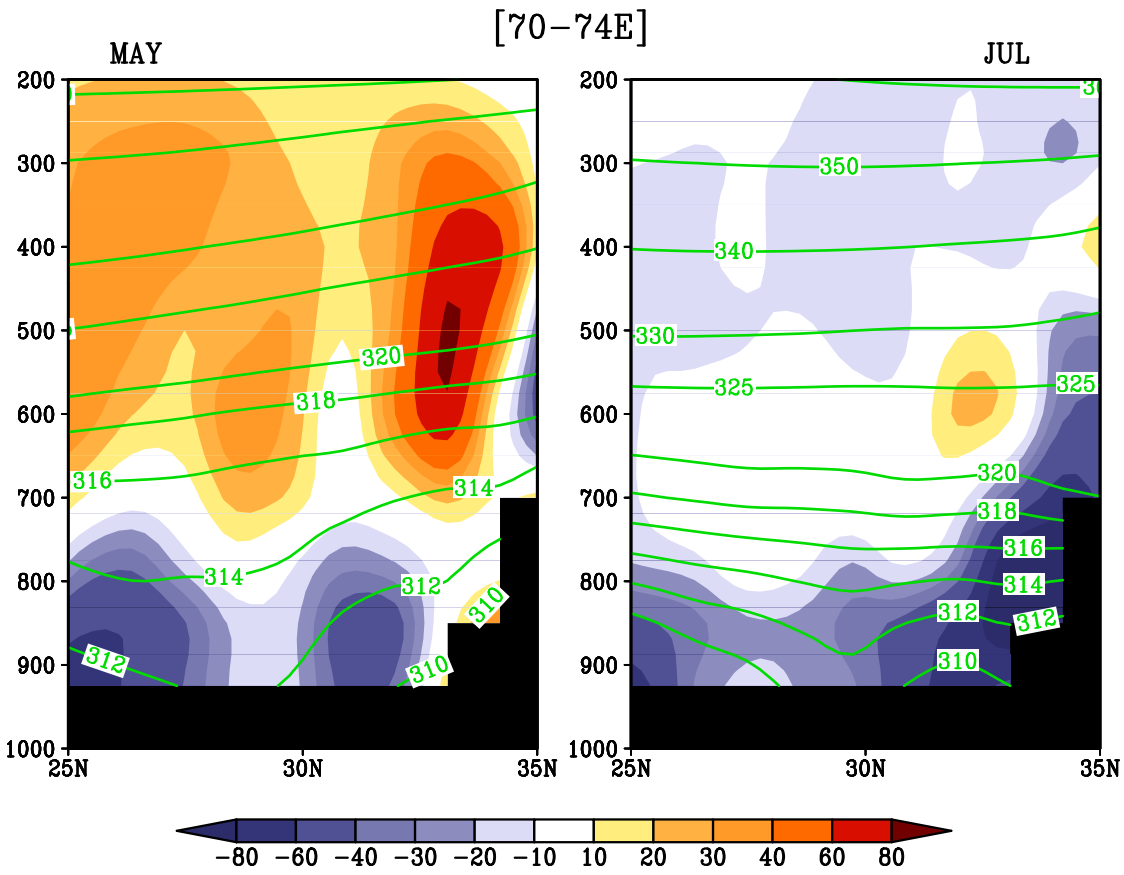

Figure 6.4: Latitude-vertical cross-section of pressure-vertical velocity (hPa day^{-1}, shaded), and potential temperature (°C, green contours) longitudinally averaged between 70°-74°E for May (left) and July (right). Vertical velocity in z-coordinates has opposite sign to the velocity displayed here.

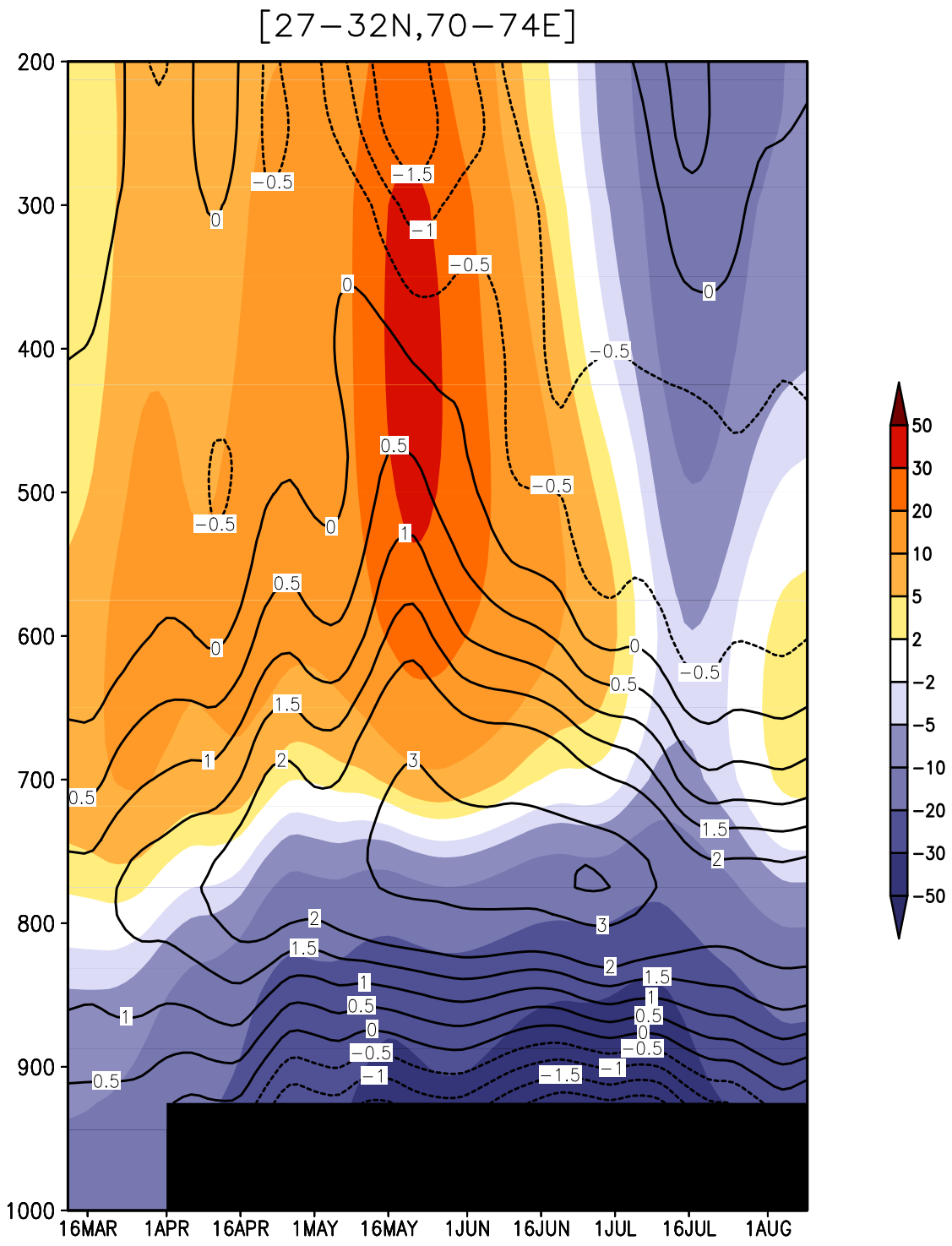

Figure 6.5: Pentad evolution of the vertical profiles of pressure-vertical velocity (hPa day^{-1}, shaded) and horizontal divergence (x10^{-6} s^{-1}, contours) averaged over the area (70°-74°E, 27°-32°N).

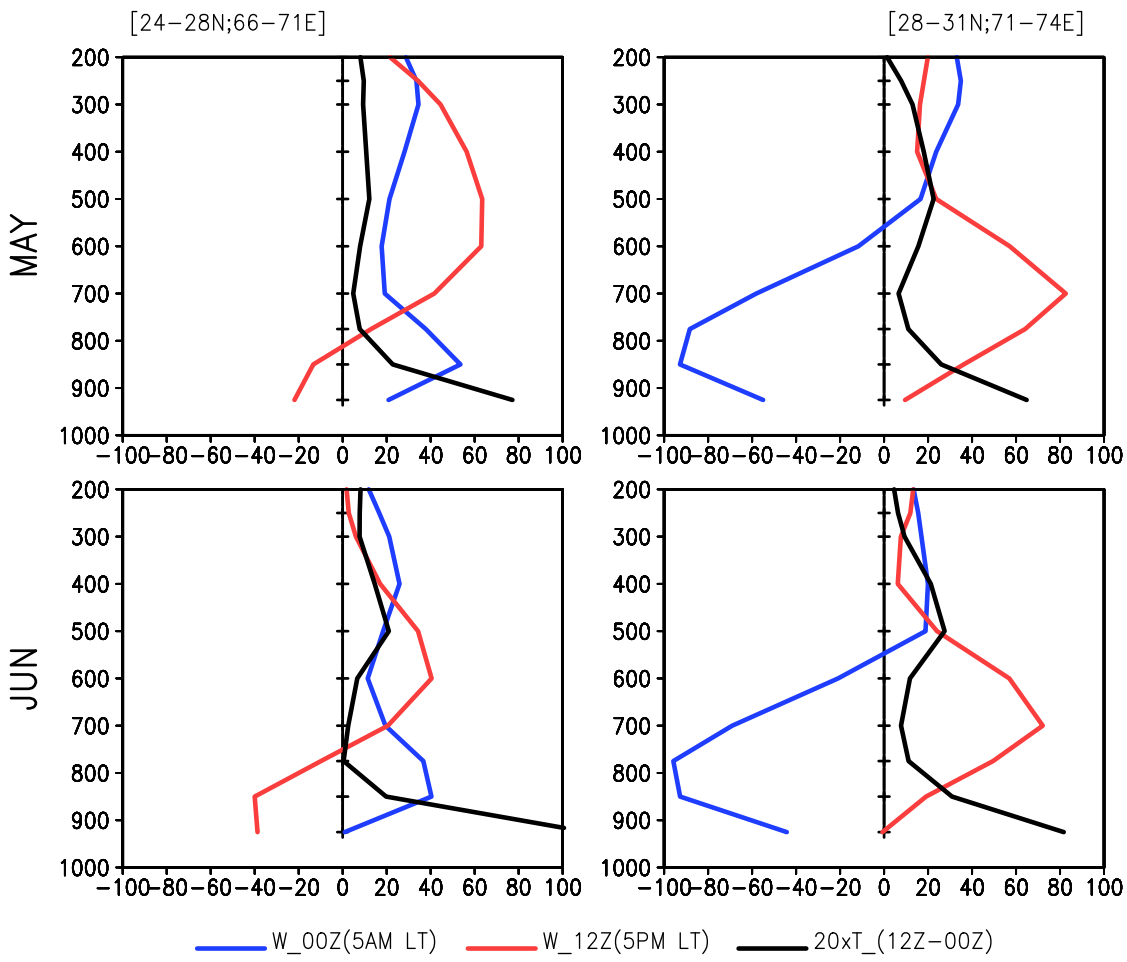

Figure 6.6: Diurnal variation of the vertical profiles of pressure vertical velocity (hPa day^{-1}) and daily range of potential temperature (°C, black) averaged over (left) the southern sector of the low (66°-71°E, 24°-28°N) and (right) its northern sector (71°-74°E, 28°-31°N). For vertical velocity, the 00Z and 12Z profiles are displayed (blue and red, respectively). The temperature range is defined by the difference 12Z minus 00Z, and it has been multiplied by 20 in order to fit to the same scale. Local time is UTC + 5.

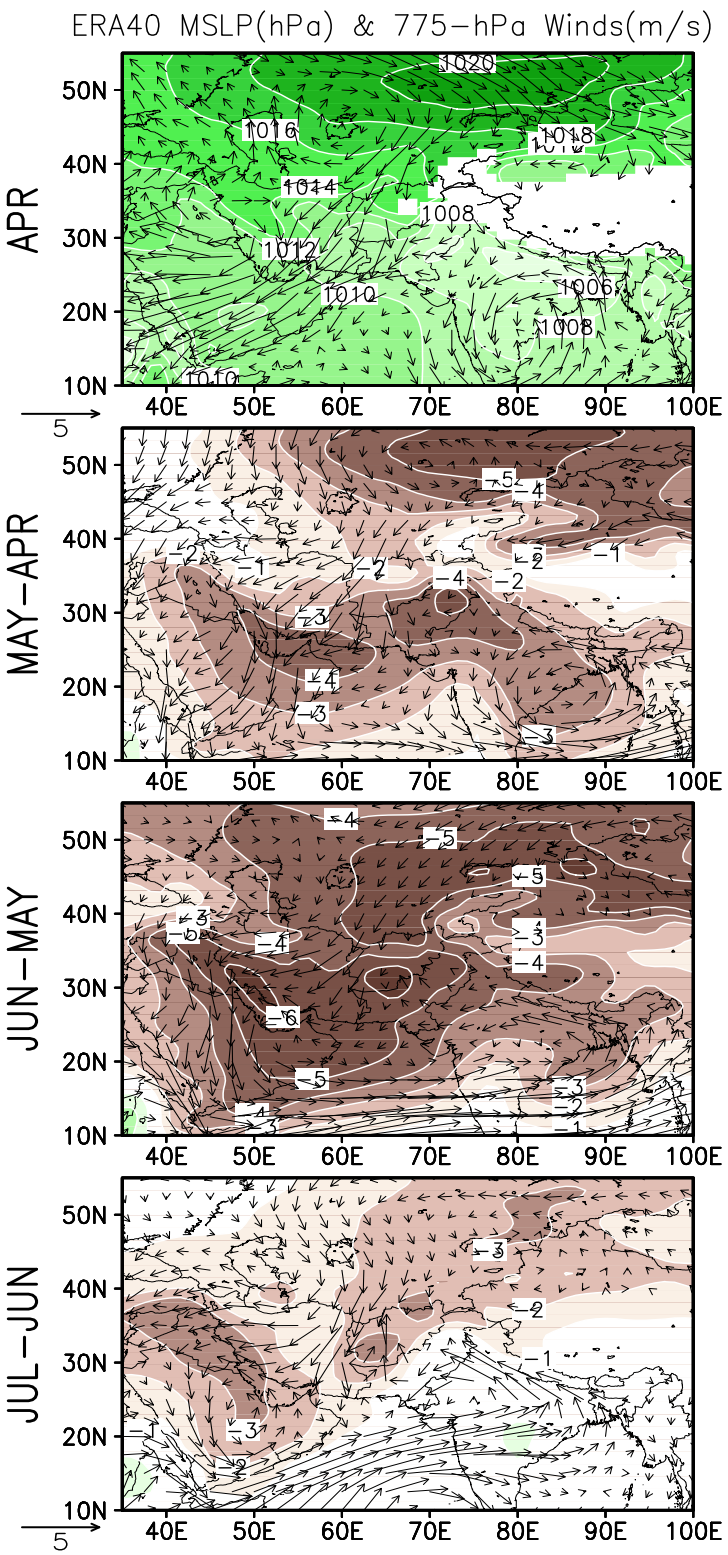

Figure 6.7: Sea-level pressure (hPa, shaded), and 775-hPa winds (m s^{-1}) for April (top), and differences (top to bottom) May-April, June-May, July-June.

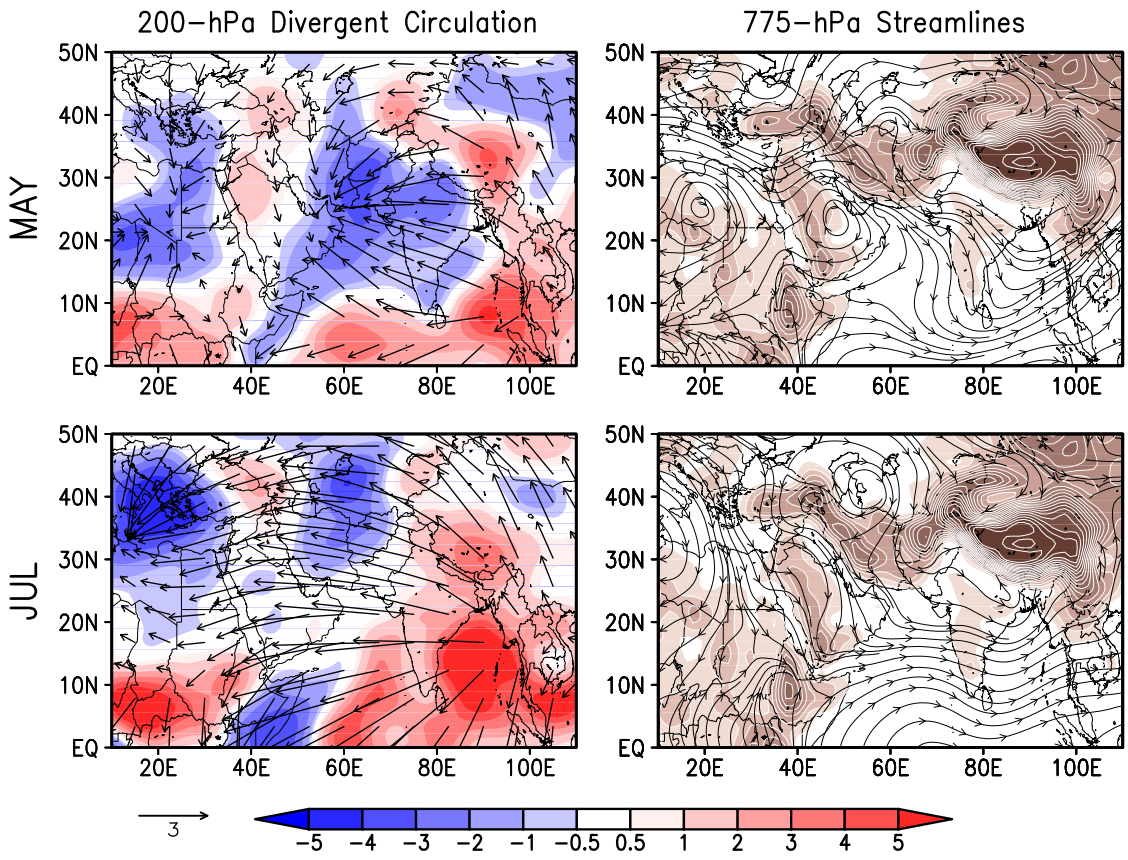

Figure 6.8: Left: Divergent wind (m s^{-1}, arrows) and its divergence (x10^{-6} s^{-1}, shaded) at 200 hPa for May (top) and July (bottom). Right: 775-hPa streamlines on ERA-40 orography (m, brown shades with white contours every 300 m) for May (top) and July (bottom).

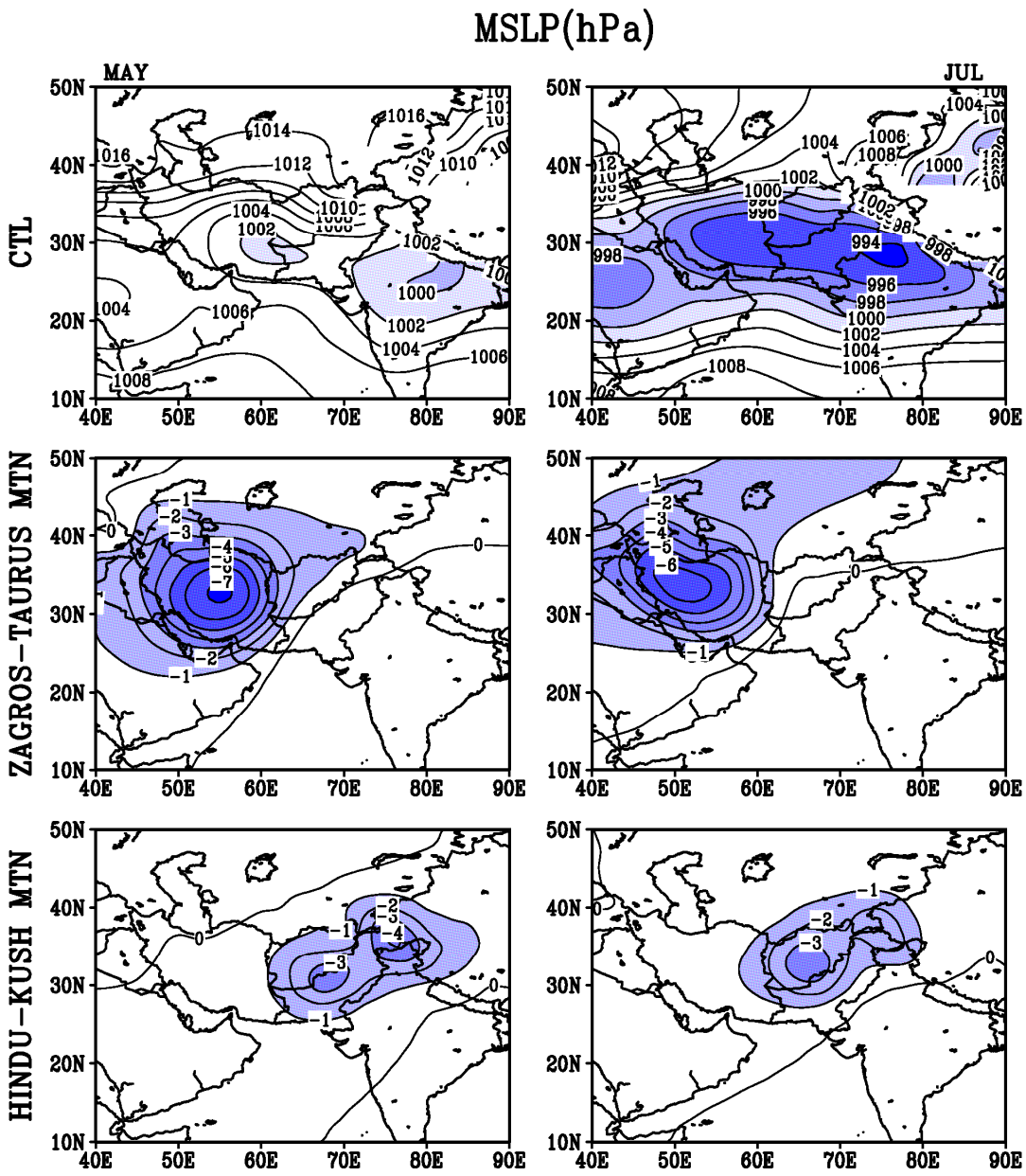

Figure 6.9: May (left) and July (right) sea-level pressure (hPa) from the linear primitive equation model control run (CTL, top; values below 1000 hPa are shaded) and (middle and bottom) differences between CTL and the two no-mountain sensitivity runs (No Zagros-Taurus and No Hindu Kush, respectively; differences greater than 1 hPa are shaded). The effect of the mountains (Zagros-Taurus and Hindu Kush, respectively) is therefore represented.

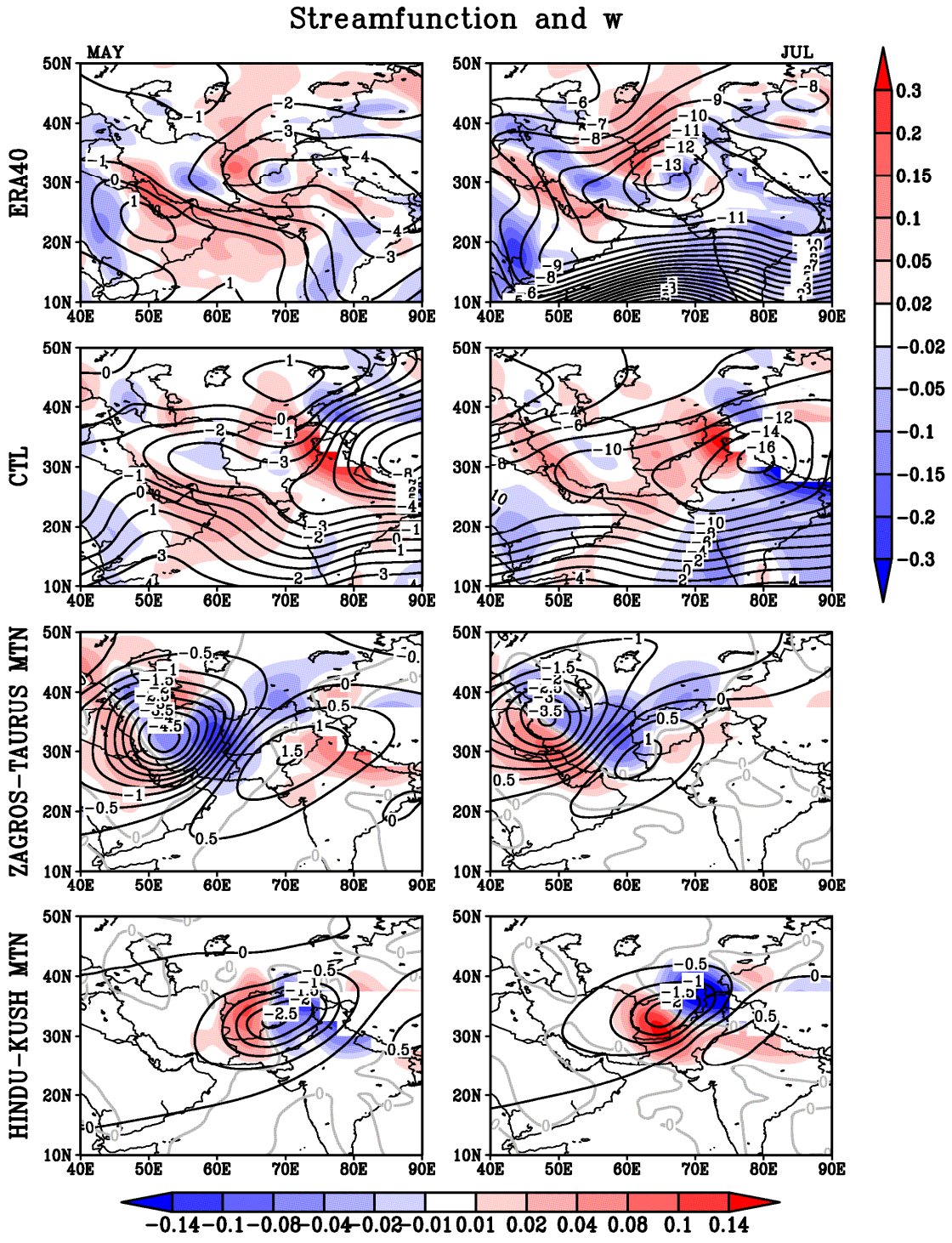

Figure 6.10: May (left) and July (right) 850-hPa streamfunction (x10^{-6} m^2 s^{-1}, contours) and 600-hPa vertical velocity (Pa s^{-1}, shaded with the zero-contour line in grey) for (top to bottom) ERA40, CTL, and differences between CTL and the two no-mountain sensitivity runs (No Zagros-Taurus and No Hindu Kush, respectively). The streamfunction is displayed as deviation from the global average, which corrects for model global biases.

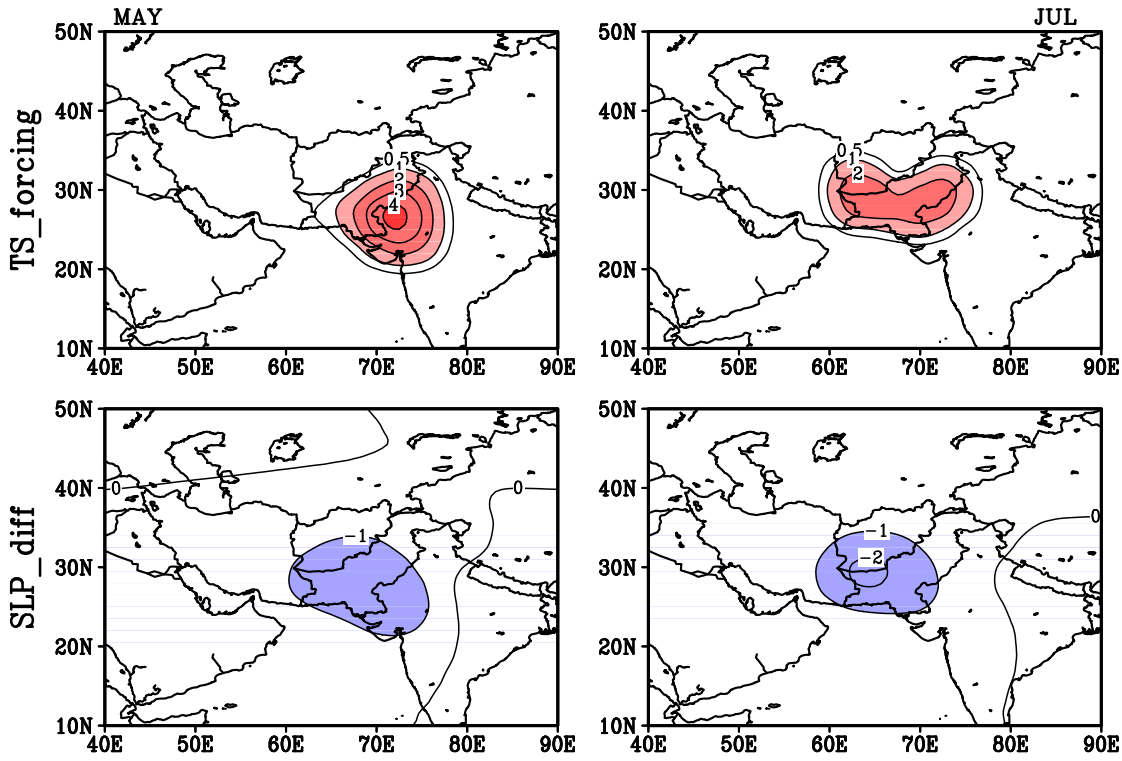

Figure 6.11: May (left) and July (right) surface temperature forcing (°C, top), a component of surface thermal forcing. The latter's response, from the difference of CTL and surface-forcing runs, is shown in the bottom panels (hPa). In the surface-forcing run, the prescribed surface temperature is capped at 30°C and diabatic heating and transient fluxes are removed in the planetary boundary layer over the Pak-India low region (62.5°-75°E, 22.5°-32.5°N).

Chapter 7: Modeling of Regional Hydroclimate Change over the Indian Subcontinent: Impact of the Expanding Desert[22]

7.1 Introduction

The Thar (or Great Indian) Desert is located between northwestern India and Pakistan. It receives an average annual precipitation between 150 and 450 mm (from west to east), 90% of which occurs during summer (Sikka 1997; Chauhan 2003). In summer the Thar Desert is the center of the most intense surface low-pressure system in the global tropics. Several crops are cultivated in the area surrounding the Thar Desert, with major harvesting in winter or early spring (when maximum greenness is observed), benefitting from monsoon precipitation (e.g., USDA 1994; see also Fig. 7.1). The Thar Desert itself appears darker on global albedo maps compared to other deserts (e.g., the Sahara), given the presence of dry open grassland vegetation (Rahmani and Soni 1997). To the west, the Desert is bounded by the Indus River and its relatively green valley from which many irrigation canals depart. The Thar Desert territory is the most densely populated desert region in the world and vast areas of northwestern India are affected by rapid soil degradation and vegetation loss (e.g., Ravi and Huxman 2009). Maps of soil moisture regions show a drastic westward expansion of the "arid" regime in recent years (Singh et al. 2005). It has also been shown (Rodell et al. 2009) that, as a result of population growth and extensive agricultural practices, groundwater over northwestern India is progressively being

[22] Manuscript in preparation for *J. Climate*.

depleted. The region is under the threat of future desertification (e.g., Goswami and Ramesh 2008).

Land-surface processes affect climate through the exchange of heat, moisture, and momentum between the earth's surface and the atmosphere. Land use/land cover changes over Northwestern India (i.e., from croplands to desert), by altering the surface water and energy budgets through changes in albedo, soil moisture, surface roughness, are expected to have significant impacts on monsoon hydroclimate, not necessarily confined to the local region. A global perspective of the impact of land-use changes on climate is given by Pielke et al. (2002).

Among the various effects of vegetation degradation, two factors have been shown to have a major influence on the energy and water balance: (i) an increase in surface albedo, and (ii) a decrease in surface roughness. An increase of albedo leads to less solar radiation absorbed by the ground (thus surface cooling) and to a net radiation decrease at the top of the atmosphere, which induces compensating subsidence aloft and inhibits precipitation development. Surface roughness reduction negatively affects the fluxes of momentum, heat, and moisture from the surface to the atmosphere, and therefore convection too. Furthermore, soil moisture decrease by vegetation reduction affects evapotranspiration and therefore moisture availability in the atmosphere, which in general also negatively impact precipitation. The three mechanisms sustain positive feedback loops, since in all three cases precipitation decrease in turn leads to more desertification. It is also clear that in nature all these processes interact with each other and have positive and negative feedbacks with other processes too (e.g., Nicholson 1988; Warner 2004).

The impact of vegetation changes on climate either due to anthropogenic forcing or climate change has been widely investigated, especially for the Sahel area. Charney (1975) and Charney et al. (1977) first investigated the effect of overgrazing on land-surface albedo over northern Africa and highlighted a positive feedback mechanism acting to perpetuate drought conditions (e.g., Dickinson 1992). The importance of latent-heat fluxes over vegetated areas, initially ignored, was subsequently noted (e.g., Ripley 1976). More complex modeling studies confirmed these findings (e.g., Ellsaesser et al. 1976; Chervin 1979; Sud and Fennessy 1982; Laval and Picon 1986). Realistic albedo derived from satellite measurements has also been used (Knorr et al. 2001). Other studies (e.g., Shukla and Mintz 1982; Sud and Fennessy 1984) focused separately on the effect of reduced evapotranspiration over Northern Africa. The combined effect of albedo and soil moisture (e.g., Sud and Molod 1988) and of surface roughness (e.g., Sud et al. 1988) has also been investigated. More realistic desertification experiments have been conducted, where multiple parameters were simultaneously changed in the land-surface model by changing the vegetation cover (e.g., Mylne and Rowntree 1991; Lean and Rowntree 1993; Xue and Shukla 1993, 1996; Xue 1996; Dirmeyer and Shukla 1996, hereafter DS96; Zeng et al. 1996; Clark et al. 2001; Xue and Fennessy 2002; Oyama and Nobre 2004; Sen et al. 2004; Gupta et al. 2005). However, almost all of these studies used a general circulation model (GCM). Furthermore, at our knowledge, the impact of desertification over the Indian Subcontinent has been addressed only by DS96.

There is almost consensual agreement among GCMs studies that land cover degradation (i.e., desertification) would result *locally* in precipitation decrease,

regardless of the geographical location of the target region, together with significant changes in the circulation and of the three-dimensional thermodynamical structure of the atmosphere in the *surrounding* areas. However, not necessarily surface temperature (surface pressure) increases (decreases) over the degraded land, leading to the formation of a surface low, since the outcome depends on the predominance of the impact of reduced absorbed surface radiation versus reduced evaporation (e.g., DS96; Oyama and Nobre 2004; Gupta et al. 2005). In principle, it is also reasonable to expect the atmospheric response to be different from region to region, depending on the relative role of local versus remote forcing factors on the climate of the region.

The primary goal of this work is to investigate the impact of the expanded desert over northwestern India and Pakistan on the South Asian summer monsoon hydroclimate. A somewhat extreme scenario is prescribed, in which all the area between eastern Pakistan and northwestern India has undergone extensive desertification due to a decrease of water availability (e.g., by retreat of the Karakorum glaciers, over-irrigation over its northern part), including a significant reduction of the Indus River flow and dry-up of its Valley (already identified as a "hot-spot" in several studies; see UNEP1998; WRI 2003; Wong et al. 2007), at least its southern sector.

The Chapter is organized as follows: section 7.2 describes the regional model, the design of the experiment and the observational data used for model verification. The control simulation is analyzed in Section 7.3, while the impact of desertification is discussed in Section 7.4. Summary and conclusions follow in Section 7.5.

7.2 Model, Experiments, and Data

7.2.1 WRF

The Weather Research and Forecast (WRF) model, specifically the Advanced Research WRF (ARW, version 3.1.1 released on July 31, 2009), was used in this study. Its core is based on an Eulerian solver for the fully compressible nonhydrostatic equations in flux (conservative) form, using a terrain-following hydrostatic pressure-vertical coordinate. The model has a two-nesting capability and numerous physics options. A full description of the modeling system is given in Skamarock et al. (2008). WRF has been successfully used in several works, from case studies to long-term simulations (e.g., Das et al. 2008; Zhang et al. 2008; Caldwell et al. 2009; Decharme et al. 2009; Kwun et al. 2009; Leung and Qian 2009; Qian et al. 2009; Wu et al., 2009; Routray et al. 2010).

In this study, WRF-ARW was implemented with the WRF Single-Moment 5-class microphysics scheme (WSM5; Hong et al. 2004; Hong and Lim 2006), a modified version of the Kain-Fritsch scheme for cumulus convection (Kain 2004), the spectral-band scheme (Collins et al. 2004) used in the NCAR Community Atmosphere Model (CAM 3.0) for both shortwave and longwave radiation, the fifth-generation Pennsylvania State University–NCAR (PSU–NCAR) Mesoscale Model 5 (MM5) surface-layer scheme based on the Monin-Obukhov similarity theory, the Noah land-surface model (LSM; Chen and Dudhia 2001) with soil temperature and moisture in four layers, fractional snow cover and frozen soil physics, the Yonsei University (YSU) Planetary Boundary Layer model (PBL; Hong et al. 2006). This configuration represents one of the most common land-surface, surface-layer and

PBL configurations used by the WRF community. Several tests were conducted prior to the final runs in order to investigate the sensitivity of the performance of the model to the choice of cumulus, microphysics, and radiation parameterization schemes. The chosen configuration resulted in the most realistic representation of the summer monsoon hydroclimate.

The desert impact was investigated by means of 7-month simulations initialized on successive days of February (00Z February 1, 2, 3, 4) until 00Z September 1 for the 2006 year. WRF was run at 36 km horizontal resolution with 28 vertical levels over an area spanning from Eastern Africa to Indochina in the zonal direction, and from the Equator to north of the Tibetan Plateau in the meridional direction (Fig. 7.1). All the significant geographical features of the area are therefore included in the domain. The Noah LSM is configured to use the United States Geological Survey (USGS) 24-category land use dataset and a 16-category soil texture dataset based on the FAO maps, both interpolated to the model grid from the original 2 arc minute (~3km) horizontal resolution. Heterogeneous vegetation greenness fraction and background surface albedo data are taken from monthly climatological datasets at 0.144° horizontal resolution provided by National Centers for Environmental Prediction (NCEP; Gutman and Ignatov 1997; Csiszar and Gutman 1999). The dominant vegetation types over northwestern India are represented in Fig. 7.1.

Two types of experiments were run, each consisting of a 4-member ensemble: the control run (CTL), and the desertification scenario (DES). In the latter case, the area of the Thar Desert was extended by changing the vegetation type over a defined region (delimited by the blue contour in Fig. 7.1, which approximately encloses the

Indian States of Gujarat, Rajasthan, Haryana, and Punjab, and the eastern territories of the Pakistan Provinces of Sindh and Punjab; the extended area is roughly nine times the original area of the Thar Desert) to barren or sparsely vegetated (class 19). Correspondingly, vegetation fraction, roughness length and albedo were modified too. Vegetation fraction and albedo of the expanded desert were assigned by attributing the average values prescribed over the Thar Desert in the input datasets. The former is constant throughout the year (at 0.01, that is 1%), the latter varies between 0.23 (fall and winter) and 0.25 (spring). Roughness length is prescribed according to table values and it is fixed at 0.01 m for class 19. By changing vegetation type, several other parameters in the LSM are automatically changed according to table values, such as root depth (reduced to the upper soil layer), stomatal resistance, leaf area index, emissivity. Soil moisture was initialized in the same way as for vegetation fraction and albedo to represent widespread desert conditions (only the moisture in the upper layer is actually used in the desertification scenario given the reduced root depth). Since the area is already very dry during springtime, soil moisture is actually reduced only slightly (few percent) over the original non-desert area, and it is expected that soil moisture will rapidly adjust to equilibrium values. Indeed, to check the effect of soil moisture initial values, few simulations were also repeated without correcting the initial soil moisture over the expanded desert. The results were only slightly different, attesting the secondary impact of soil moisture *initial* anomalies on the results for these specific experiments.

The large-scale intial and lateral boundary conditions were provided by the NCEP Final Analysis (FNL) every 6 hours and at 1° resolution. Observed SST was

also prescribed according to the NCEP real-time global daily SST analysis (RTG_SST; Gemmill et al. 2007). All the simulations were carried out for the year 2006, which was characterized by normal monsoon rainfall over India as a whole (Jayanthi et al. 2006). This work should be considered as a pilot study, as we focus only on one particular year. It is fair to notice that other regional and large-scale factors (e.g., SST, land-surface conditions) affect land-atmosphere interactions over the investigated area and the subsequent monsoon evolution as well, and that their impact may vary from year to year. However, these factors are expected to modulate the response, with the desert-driven anomalies qualitatively consistent with the findings reported below, and it is reasonable to consider the following discussion to be valid regardless of the simulated year. The first two months of the simulations were considered as spin-up and were discharged. The significance of the difference DES-CTL was evaluated by means of the Student's *t*-test.

7.2.2 Observational Data

Atmospheric and surface variables are compared to the driving FNL data and to the European Centre for Medium-Range Weather Forecasts (ECMWF) Interim Reanalysis (ERA-Interim, ERAI in the figures; Simmons et al. 2006) daily and monthly data at on a 1.5° x 1.5° grid and at 37 vertical isobaric levels obtained from the ECMWF data portal.

Precipitation observations came from several datasets: the Tropical Rainfall Measuring Mission (TRMM) 3B42 daily and 3B43 monthly datasets both at 0.25° resolution (Huffman et al. 2007), the Global Precipitation Climatology Project (GPCP) version 2.1 2.5° x 2.5° monthly average (Adler et al. 2003) and version 1.1

1° x 1° daily (1DD; Huffman et al. 2001) precipitation, and the University of Delaware (UDEL) gridded monthly station land precipitation version 2.01 at 0.5°x0.5° resolution (Matsuura and Wilmott 2009a; data downloaded from the web site: http://jisao.washington.edu/data/ud/).

Observed surface temperature was also obtained from UDEL (Matsuura and Wilmott 2009b).

7.3 Model Validation

As first step, the performance of the model in simulating the mean summertime (June-August, JJA; i.e., the mature phase of the monsoon) hydroclimate over South Asia is evaluated against observations and reanalysis data.

Seasonal (June-September) precipitation, for the country as a whole, was 100% of the climatological average (87% in June, 98% in July, and 107% in August). However, the monsoon went through a series of wet and dry phases: an early onset with above-normal precipitation, a long break period in the second and third weeks of June (due to anomalous subsidence over the Indian Subcontinent caused by above-normal SSTs and enhanced convection over the equatorial Indian Ocean), a recovery until a new hiatus during the second and third weeks of July, followed by a long active phase until September. June-August rainfall was normal (above normal) for central India (western regions, including Gujarat and Rajasthan), below normal for much of the northern and, especially, northeastern regions (Jayanthi 2006; see also the web at: http://www.tropmet.res.in/~kolli/mol/Monsoon/frameindex.html).

CTL captures the main features of the observed JJA precipitation amounts and distribution (Fig. 7.2), and it is in reasonable agreement with observational datasets over most of the domain. The orographic precipitation along the Western Ghats (and its associated shadow effect over southern India), the Himalayas and over northeastern India, as well as the core over central India and the deficient rainfall at the north, are well-simulated. The westward limit of precipitation, with the minimum over the Thar Desert region, is realistic. However, CTL overestimates the maximum over Indochina (indeed overestimated also by ERA-Interim, while TRMM shows ocean-locked precipitation) and also produces excess precipitation over the equatorial Indian Ocean and off the Western Ghats.

The time evolution of the observed and simulated daily precipitation, averaged between 75° and 95°E (the core region of the Indian monsoon), is shown in Fig. 7.3. The model realistically simulated most of the precipitation events and the onset of the monsoon by the end of May, as well as the northward extension of precipitation during the mature phase of the monsoon. There is however a certain amount of disagreement on the location of the northern limit of precipitation in the second half of May (15°-20°N instead of the observed 25°N) and during the dry period in the first half of June, which appears to be more intense in CTL than in observations. The excess precipitation along the equatorial Indian Ocean is also evident as an almost constant feature throughout the season.

Water vapor transport is a very important source of moisture and precipitation for the monsoon and Fig. 7.4 shows that CTL is in remarkable agreement with observations both in terms of magnitude and distribution of moisture fluxes.

Convergence tends to be overestimated along the equatorial Indian Ocean (associated with the meridional gradient of the *v*-component of the wind) and over the Maritime Continent (excessive zonal wind), generating the excess precipitation. CTL appears to produce a stronger cyclonic circulation over northwestern India (presumably affected by orography) which advects dry desert air from the Middle East (see the slight precipitation deficit in Fig. 7.2).

The lower tropospheric circulation, represented by the 850-hPa winds, together with the middle tropospheric (i.e., 500 hPa) vertical motion allow to better estimate the model's dynamical skill in relation to precipitation and moisture fluxes distribution (Fig. 7.5). The agreement is certainly satisfactory, although there are some regional deficiencies. As noted above, the excess precipitation over Indochina is associated with stronger converging wind and more intense upward motion than observations. In the Arabian Sea, the Somali jet is confined to lower latitudes, with the northerly dry subsiding flow from the Middle East infiltrating over northwestern India and Pakistan (see also Fig. 7.6). This anomaly allows more radiation to reach and heat the ground (not shown), with a consequent deeper core of the low in the sea-level pressure field (Fig. 7.6). Sea level pressure is lower than in observations due to a warm bias over the land-mass (not shown); note however that the horizontal gradient, which is what actually counts, is in good agreement.

The model performance over two key regions (i.e., the semi-arid region over northwestern India and the maximum precipitation area over Central India, respectively) and can be estimated looking at vertical profiles of vertical velocity and relative humidity (Fig. 7.7). May and July are chosen because the former is the month

before the monsoon onset, when the conditions are set up for the arrival of precipitation, while the latter is the month of full development of the monsoon, with strong convection and widespread precipitation. The simulated profiles are realistic and compare well with observations, with the main features consistently reproduced, especially over Central India. CTL tends to generate enhanced subsidence over northwestern India, especially in July, which results in lower relative humidity. As a result, the simulated precipitation is also deficient (cf. Fig. 7.2).

In general, the model is shown to realistically reproduce most of the features of monsoon hydroclimate over South Asia, and it is therefore adequate to carry out the desertification sensitivity experiment.

7.4 Impact of the Expanding Desert

Changes in the main components of the atmospheric water balance induced by the expanded desert during JJA are shown in Fig. 7.8, which displays the anomalies (i.e., differences DES-CTL) of precipitation, evaporation, vertical integrated moisture fluxes, and upper-layer soil moisture. The most remarkable feature is the large-scale significant response of monsoon hydroclimate to the increased desert, which extends well-beyond the area of the imposed forcing across the whole Indian Subcontinent. *Locally*, the replacement of current vegetation with bare ground induces significant and consistent negative anomalies for all variables, further reinforcing the forcing mechanism. *Regionally*, the response is even more intense and is characterized by a somewhat northwest-southeast band pattern with an evident large-scale anomalous anticyclone over northeastern India. This flow opposes the southeasterly moisture

advection from the Bay of Bengal toward the Indo-Gangetic Plain, and brings moist air toward the southern part of the peninsula (a relatively dry region under the rain shadow effect; see Figs. 7.2 and 7.4). Precipitation is therefore reduced (increased), respectively. Interaction with orography (the eastern Himalayas) over northeastern India and Burma enhances the westerly flow; convergence and precipitation is then generated when this current impacts on the mountains of Southern China (see Fig. 7.1). Evaporation and soil moisture anomalies are linked to precipitation anomalies, being for example strongly positive over south-central peninsular India and mostly negative over the northern regions.

Interestingly, surface skin temperature (not shown) has a dipole pattern, with, broadly speaking, decreased (increased) values over the west (east and northeast) sector, the separation line being approximately along 72°E. The heating is not however communicated to the atmosphere given the clear reduction of sensible heat flux (as we will see hereafter), resulting in atmospheric cooling above the entire desert (Fig. 7.10c). The JJA average anomalies of various components of the surface energy budget are represented in Fig. 7.9. Downward shortwave radiation increases, not only over the desert but also over the central regions, in agreement with cloudiness reduction (see Fig. 7.10d) and precipitation decrease. Associated with increased precipitation (and cloudiness), surface downward shortwave radiation is reduced over Indochina and, consequently, upward shortwave radiation too. Upward shortwave radiation increases especially over the expanded desert as a result of the increased albedo. Both longwave components decrease over the desert: the upward component (dominating the net longwave balance) because of surface cooling (to the

west) and the effect of the variation in surface emissivity (lower for desert), which overcomes the slight warming (to the east); the downward component due to cloudiness decrease. The net radiation budget is negative to the west and positive above the area of the original Thar Desert, reflecting the pattern of albedo change between CTL and DES (which can be estimated by the ratio between the upward and the downward component of shortwave radiation, i.e. SWUPB/SWDNB in Fig. 7.9). Sensible and latent heat fluxes, both negatively affected in the desertification experiment by the increased surface resistance (reduced surface roughness), also show a dipole pattern: the former strongly decreases (slightly increases) to the west (east), while the latter greatly decreases to the east and in a less significant way to the west. The maximum (negative) values of sensible and latent heat fluxes are comparable. These patterns suggest that different processes are competing over this region, the relative predominance coming from the distribution of precipitation in CTL, in particular the increase to the East. On the west, where precipitation is very scarce (cf. Section 7.1 and Fig. 7.2), the effect of albedo change prevails, leading to surface cooling and reduced sensible heating. Latent heat reduces too (but not significantly) because of lower surface roughness (and reduced vegetation). On the (slightly) wetter east, precipitation is significantly reduced in the desertification experiment, leading to a more significant soil moisture deficit and evaporation decrease (see Fig. 7.8). In turn, the marked reduction of evaporative cooling offsets the effect of albedo change, leading to a warmer ground (and consequent positive anomalous sensible heat flux).

Both longwave components are positive over eastern India, reflecting the positive temperature anomaly (see Fig. 7.10) and the cloudiness decrease, with the upward component again dominating in the net balance. The net radiation budget is positive over central India and negative over northeastern India and Indochina, in both cases dominated by the contribution of the downward shortwave anomaly (therefore by cloudiness anomalies). It is intuitive that over south-central India, for example, increased latent heat flux is associated with higher soil moisture and larger precipitation, which in turn cools the ground and reduces sensible heat flux.

Sea-level pressure (Fig. 7.10) shows a clear dipole pattern, with positive anomalies across India toward southern Indochina and negative to the north. The correspondence with the pattern of anomalous vertical motion is evident over central India. Note that pressure increases all over the desert area, including over areas of (albeit slight) warming, indicating that the evaporation suppression and attendant processes (Sud and Fennessy 1984), which would lead to a thermal low, are not sufficiently strong. Subsidence anomalies take place over all northwestern India above 550 hPa, while in the lower Troposphere it is confined to the north since the northwesterly subsiding flow impacts almost perpendicularly on the Aravalli Range (see Fig. 7.1) generating orographic-forced uplift.

Noticeable is a core of high pressure located over eastern India (which is associated with moisture divergence and precipitation suppression, see Fig. 7.8). The anticyclonic anomaly extends throughout the whole atmospheric column up to 200 hPa (where it is replaced by a large-scale anomalous cyclone centered over the Tibetan Plateau), with the most intense circulation at 700hPa. The whole column is

drier and cooling is also seen above 700 hPa, clearly related to the decrease of diabatic heating. To keep atmospheric thermal balance, adiabatic warming increases, and, indeed, large-scale anomalous subsidence dominates at all levels, with peak at 500 hPa. In the boundary layer, a positive temperature anomaly originating from the heated ground (as a result of reduced cloudiness) exists, which contributes to damping the downward motion.

Figure 7.11 helps to relate the circulation anomaly over eastern India with the desert forcing to the west and suggests a possible mechanism to explain the regional-scale response to the expanded desert: the dry air subsiding to the west is advected toward northeastern India, where it opposes the prevailing cyclonic southeasterly humid flow (indeed drier conditions are seen throughout the whole Troposphere west of 90°E). The cyclonic circulation weakens (i.e., an anomalous anticyclone is formed), which reduces precipitation and latent heat release in the middle troposphere. Fewer clouds allow more radiation to reach the ground, where a positive temperature anomaly forms. The low-level anomalous flow, as mentioned above, impacts on the mountains of Southern China together with the humid air coming from the Bay of Bengal and is deflected eastward, where strong convergence, orographic ascent and precipitation occur. The release of latent heat there warms the air at upper levels, as seen in Fig. 7.11c.

7.5 Summary and Conclusions

The impact of desertification over northwestern India (i.e., expansion of the Thar Desert around its present-day location) on the South Asian summer monsoon

was studied by mean of ensemble sensitivity experiments with the ARW-WRF model. Desert conditions were prescribed by changing the distribution of vegetation types and associated parameters (e.g., albedo, vegetation greenness, roughness length, etc.) over a large area located between Pakistan and northwestern India. As previously shown by other desertification studies (e.g., Xue and Shukla 1993; DS96; Xue and Fennessy 2002; Sen et al. 2004), there is a strong link between anomalous surface conditions and overlying atmospheric circulation.

Indeed, intensive exploitation of natural resources (water in particular) has been taking place over the relatively dry northwestern India, as a result of rapid population growth and expansion and, as a result, the region is under the threat of future desertification. This argument provided the motivation for the present study. The occurrence of a large-scale phenomenon such as the South Asian summer monsoon makes the problem both challenging (given the numerous feedback processes in place) and of primary interest (given the potential modification and/or redistribution of the monsoon water availability for the most populated region of the world). The area by itself is particularly complex, bounded by an extensive mountain range to the east and north, and with the ocean immediately to the south.

Our findings suggest that the expansion of the desert at the expense of cultivated land results in significantly impacting summer monsoon hydroclimate and circulation both locally and at large scale over the whole Indian Subcontinent. Due to interactions with the surrounding topography and feedbacks within the developing monsoon, the effect of an expanded desert leads, for example, to both increase and decrease of monsoon precipitation, depending on the specific area considered.

Overall, the key results can be summarized as follow:

- *Locally*, the atmospheric water cycle weakens, since precipitation, evaporation, and atmospheric moisture convergence all decrease. Soil moisture and runoff reduce too. Air temperature cools due to the overall dominant impact of albedo increase and because of the reduction of surface turbulent fluxes. Subsidence is generated by thermodynamic balance, which increases sea-level pressure and induces a low-level northwesterly flow over the IGP.
- *Regionally*, moisture advection from the head of the Bay of Bengal towards the IGP is weakened by the anomalous horizontal circulation set up by the desert to the west. This reduces precipitation over eastern India, with consequent cooling of the middle Troposphere by decrease of the latent-heat release and related vertical motion, with the formation of an anomalous anticyclone. The ground heats up.
- *At larger scale,* the cooling over northwestern India extends throughout the Troposphere, the Tibetan High weakens in order to provide anomalous convergence to compensate for the widespread subsidence. On the east, the anomalous flow from the IGP intensifies and is deviated toward the eastern Himalayas and southern China. Orographic uplift and precipitation is generated.

Several findings of this study support and extend the results of DS96, keeping in mind that they used a low-resolution global atmospheric model (and therefore processes like orographic uplift and precipitation may be less accurate) compared to the high-resolution regional model used in this study. On the other hand, a multi-year

simulation is carried out by DS96, while this work is limited to one year only (albeit ensemble members are considered). The increase (decrease) of June-August precipitation in the Indian sector south (north) of approximately 15°N (their Fig. 14) is also evident in Fig. 7.8, especially the negative contribution over the Bay of Bengal. The large-scale cooling and the negative 850-200 hPa thickness anomaly centered over northwestern India (their Fig. 7) is also a common element to this study. DS96 found that latent-heat flux seems to play a secondary role compared to sensible heat flux over Asia, given the small values even in the control case. Evaporation decrease (which, together with sensible heat flux decrease, reduces the removal of energy away from the surface) over the desert should contribute to control the cooling due to albedo increase. This feedback however appears to be sufficiently strong only over the northeastern sector of the desert region, since summertime latent heat flux in CTL is already low (~10W m^{-2}, equivalent to an evaporation ~0.3 mm day^{-1}). In some aspects, the anomalies induced locally by the expansion of the Thar Desert contrast with the findings over other regions (e.g., the Sahel), where a warming was simulated. As mentioned above, the latent heat contribution to the surface energy budget is however also higher there (e.g., Xue and Shukla 1993) due to a different original vegetation and moisture availability. Briefly, the evaporation efficiency as controlling factor of the reduction of absorbed solar radiation is quite marginal over the region investigated here (see Zeng and Neelin 1999). Topography and the geographical features of the region are also expected to play an important role and to make differences with similar experiments carried out over other areas of the world.

To our knowledge, this study is the first using a regional model and the conclusions are far from being definitive. More simulations (for example multi-year runs) are necessary to make the case robust, and, as such, these findings represent a first attempt to assess the magnitude of the impact of the expansion of the Thar Desert on the South Asian summer monsoon.

It is possible that some surface parameters in the land-surface model (e.g., surface roughness) are not properly tuned for the area investigated. It has to be noted that many of these parameters are still not known with enough confidence and their distribution is highly heterogeneous, even for the same surface type. As a result, outcomes may vary depending on the prescription of these vegetation/surface parameters. Sensitivity studies to the variation of the parameters and/or to specific processes are not numerous (e.g., Hales et al. 2004; Li et al. 2007).

Finally, desertification is responsible for the production (through wind erosion of the bare ground) and emission of large quantities of dust particles in the atmosphere, which can then be transported at large distance. Dust aerosols are known to have important effects on the radiative balance and thus on climate, and may lead to significant feedbacks over desert areas (e.g., Rosenfeld et al. 2001). The inclusion of dust effects in land-use experiments is an important step toward a comprehensive simulation of the impact of desertification on climate (e.g., Yoshioka et al. 2007).

Bearing this in mind, the conclusions of this work suggest the possibility of a significant and pronounced large-scale impact of desertification over northwestern India.

7.6 Figures

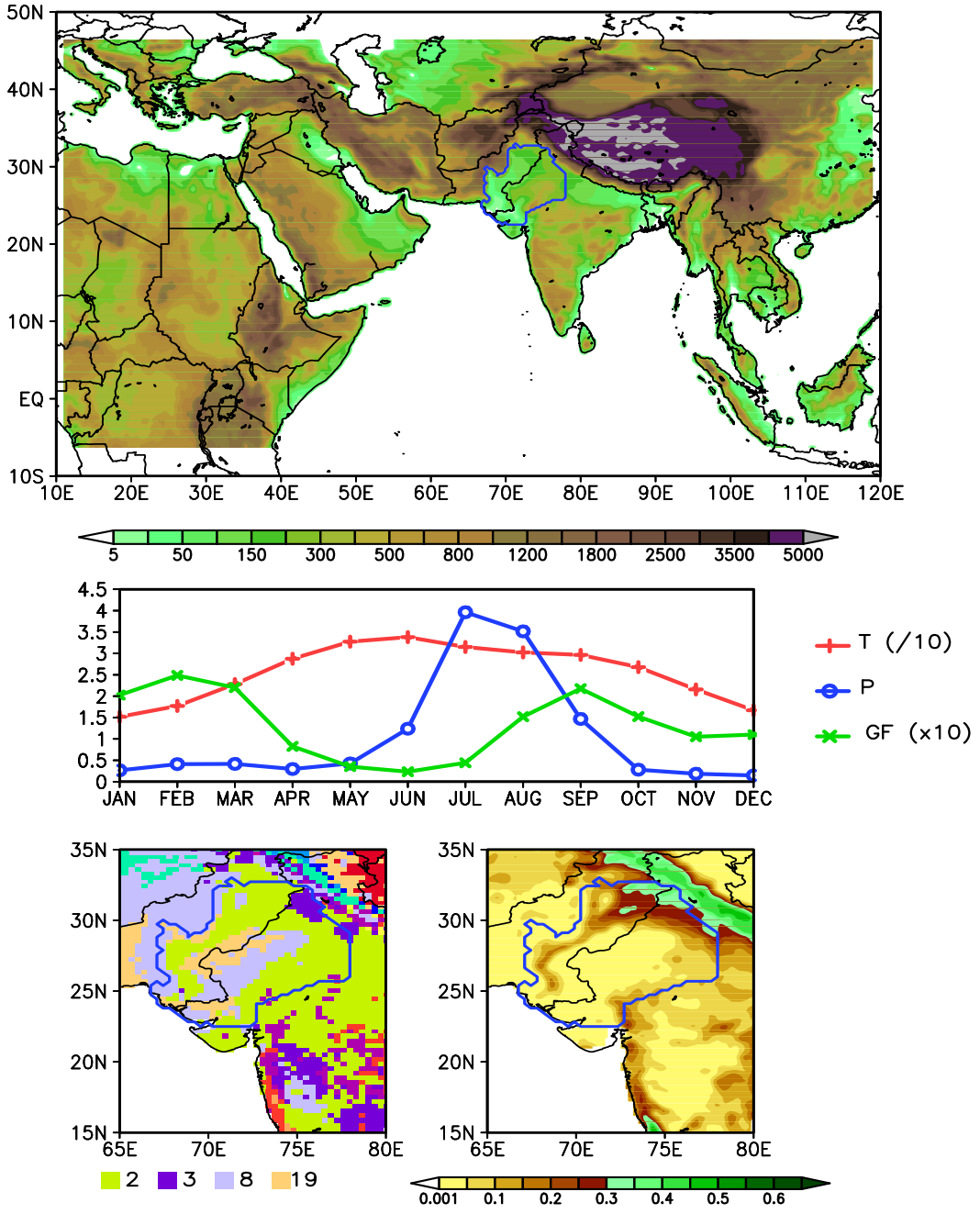

Figure 7.1: Top: model domain and topography (m), with the blue line enclosing the area of the expanded desert in the DES experiment. Middle: annual cycle of model vegetation fraction (green; x10), and of observed surface temperature (red; °C) and precipitation (blue; mm day^{-1}) from CRU averaged over the extended desert are for the period 1979-2001. Bottom: model vegetation types (left; 2 = dryland cropland and pasture; 3 = irrigated cropland and pasture; 8 = shrubland; 19 barren or sparsely vegetated) and March-June average greenness fraction (right).

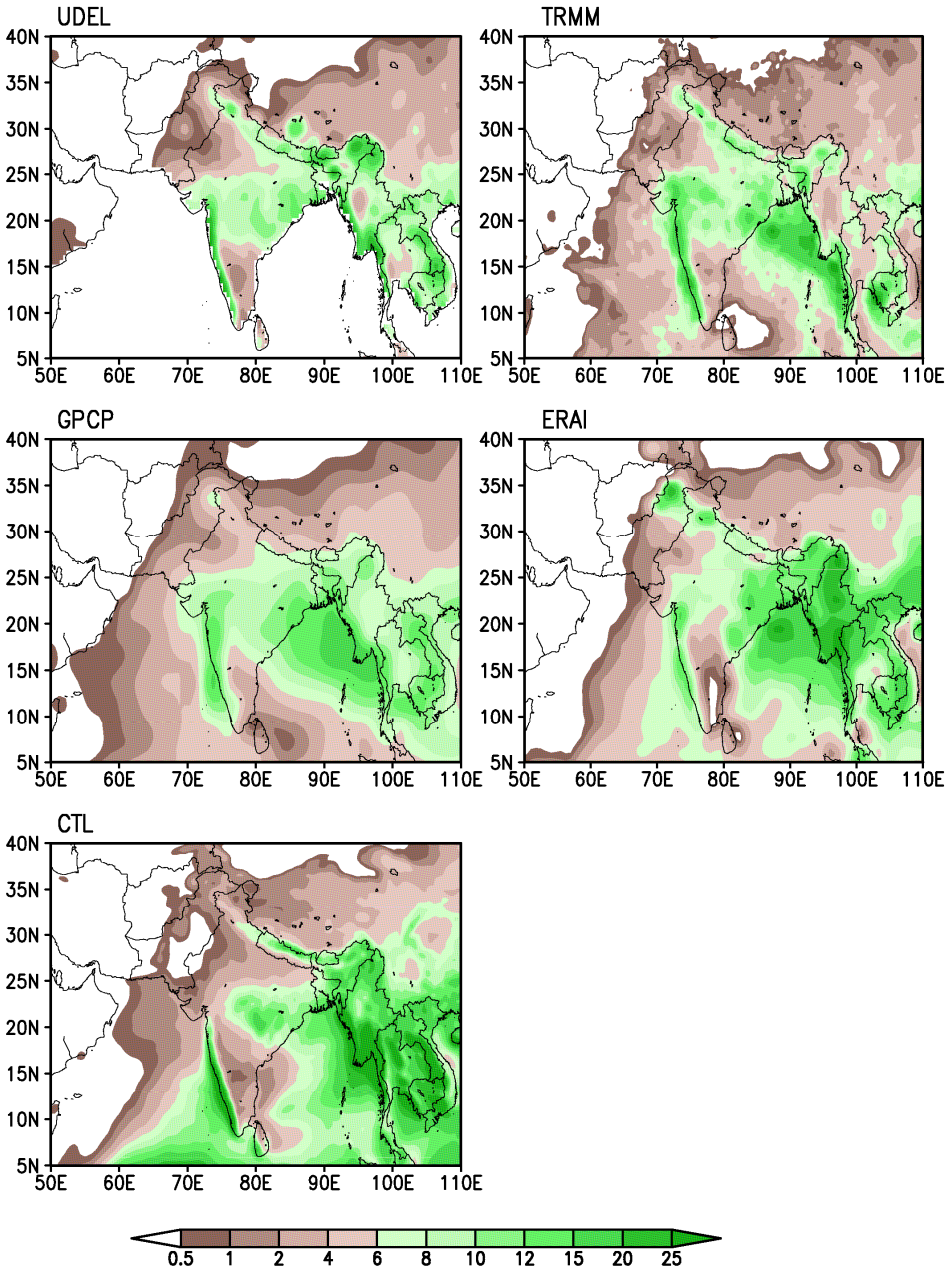

Figure 7.2: June-August average precipitation (mm day^{-1}) in observations, reanalysis, and the control simulation.

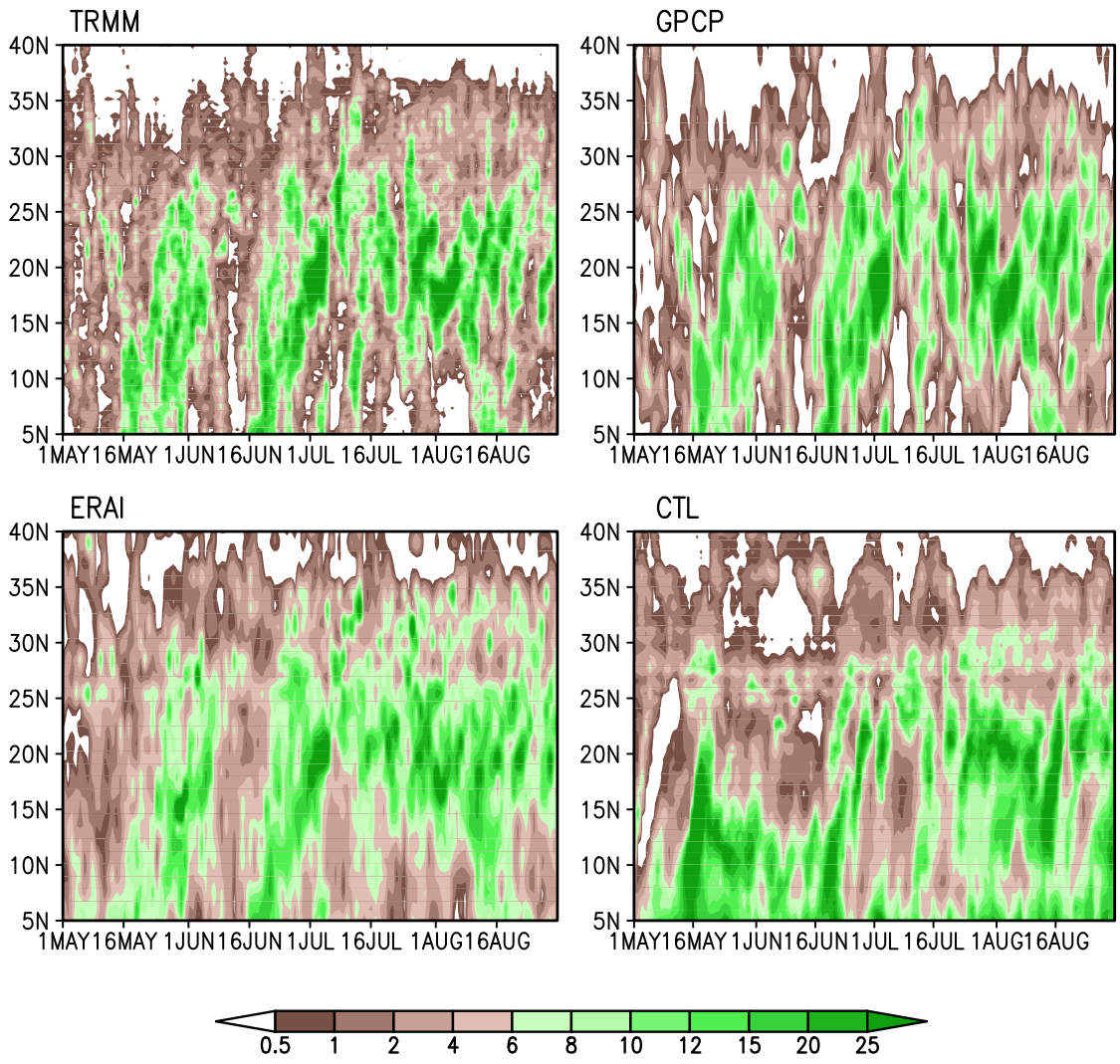

Figure 7.3: Latitudinal evolution of May-August daily precipitation (mm day^{-1}) averaged between 75°-95°E.

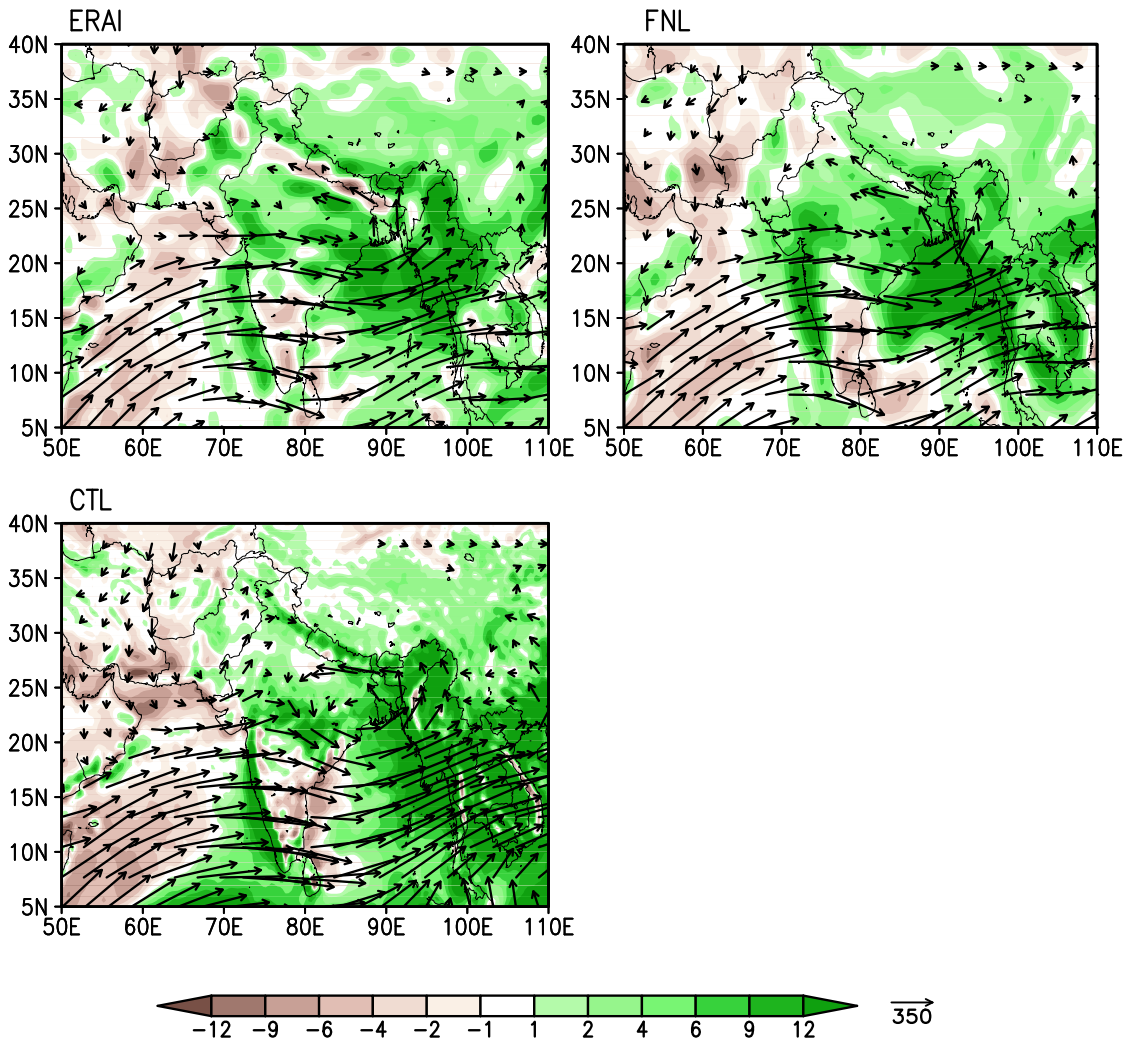

Figure 7.4: June-August moisture flux (kg m^{-1} s^{-1}) and its convergence (mm day^{-1}; shaded, positive green values representing convergence) mass-weighted vertically integrated between the surface and 100 hPa.

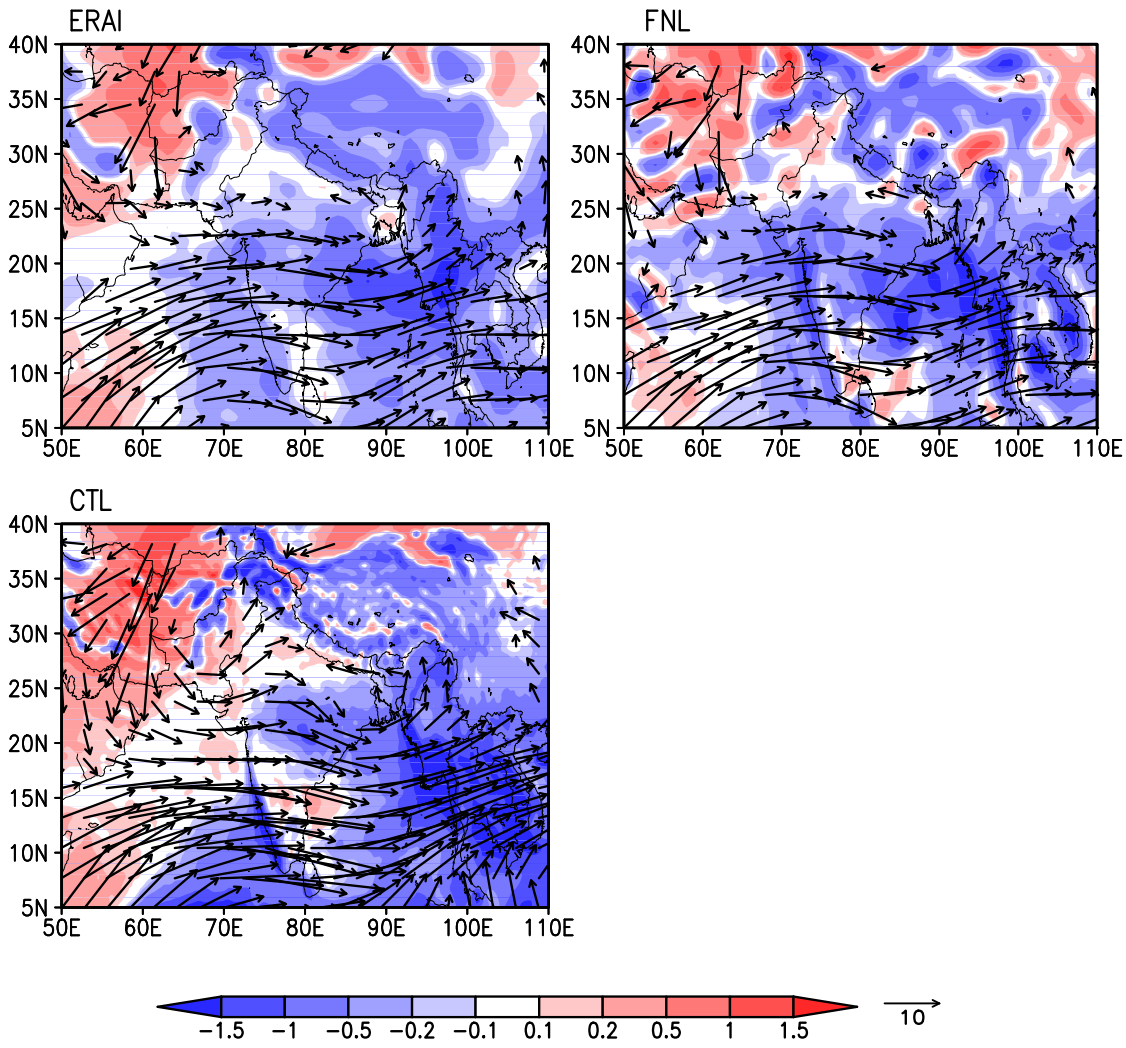

Figure 7.5: June-August 850-hPa wind (m s^{-1}) and 500-hPa vertical velocity (x10 Pa s^{-1}; shaded, positive values representing subsidence).

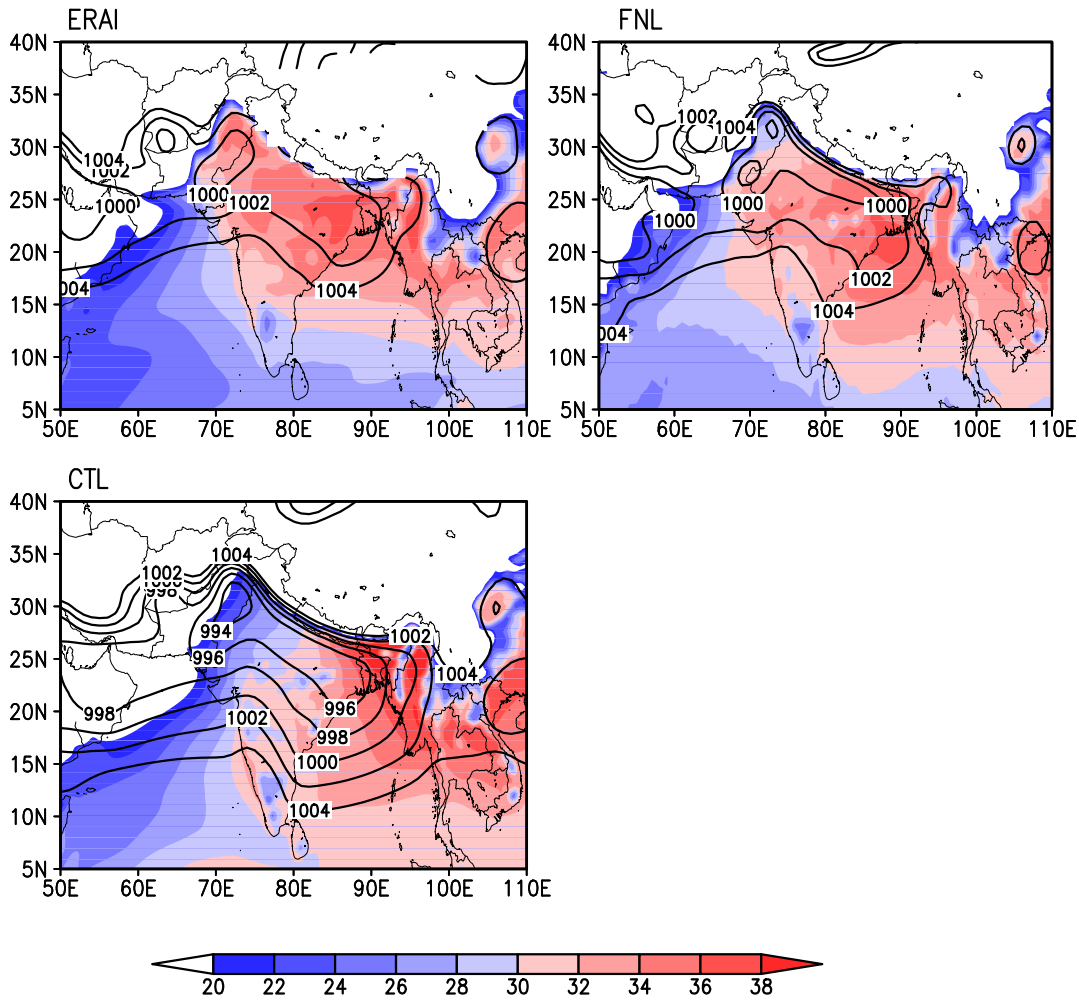

Figure 7.6: June-August sea-level pressure (hPa) and [950-700]-hPa vertical integrated specific humidity (kg m^{-2}, shaded).

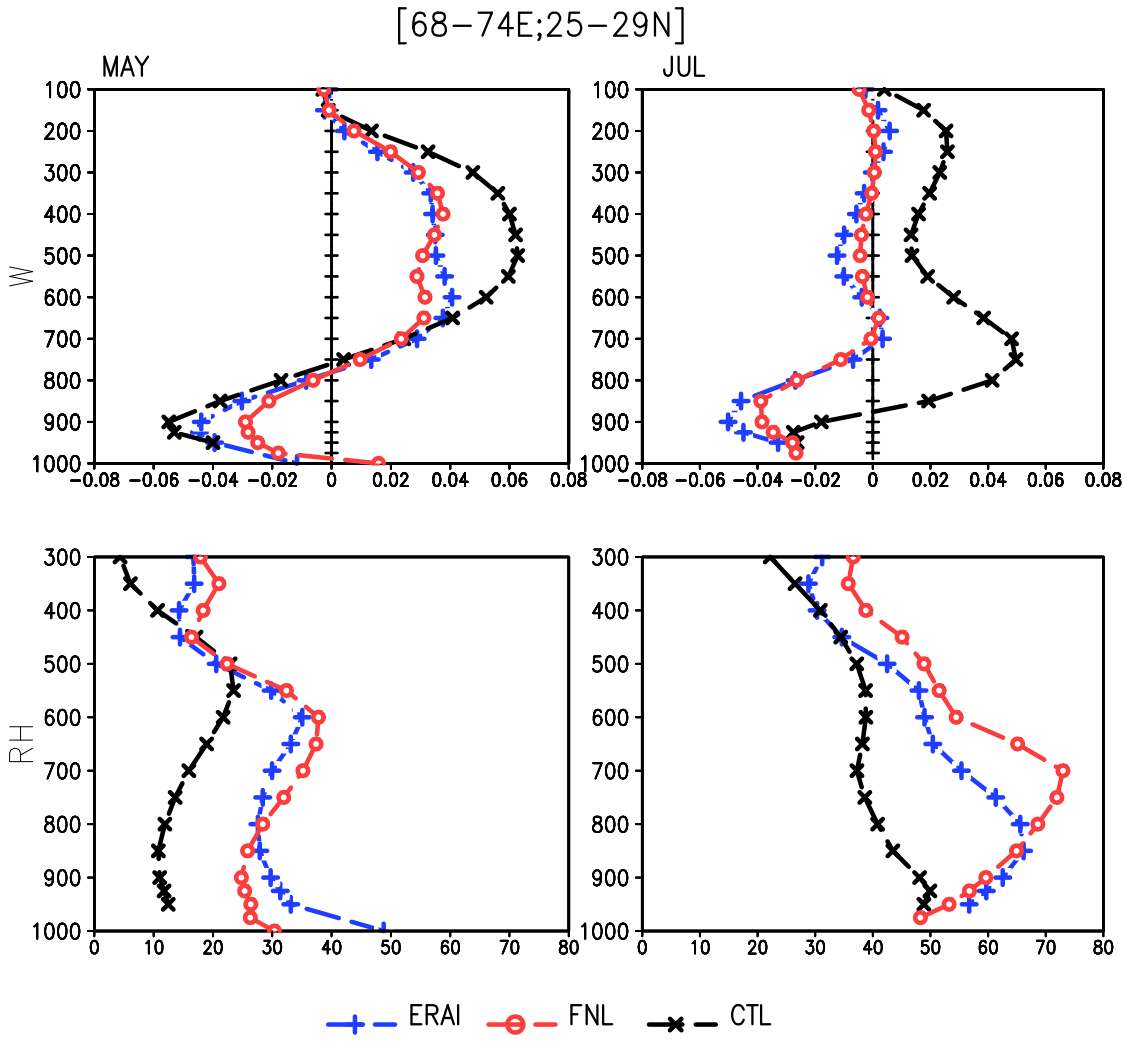

Figure 7.7a: Vertical profile of (top) vertical velocity (Pa s^{-1}) and (bottom) relative humidity (%) for (left) May and (right) July averaged over the area (25°-29°N, 68°-74°E).

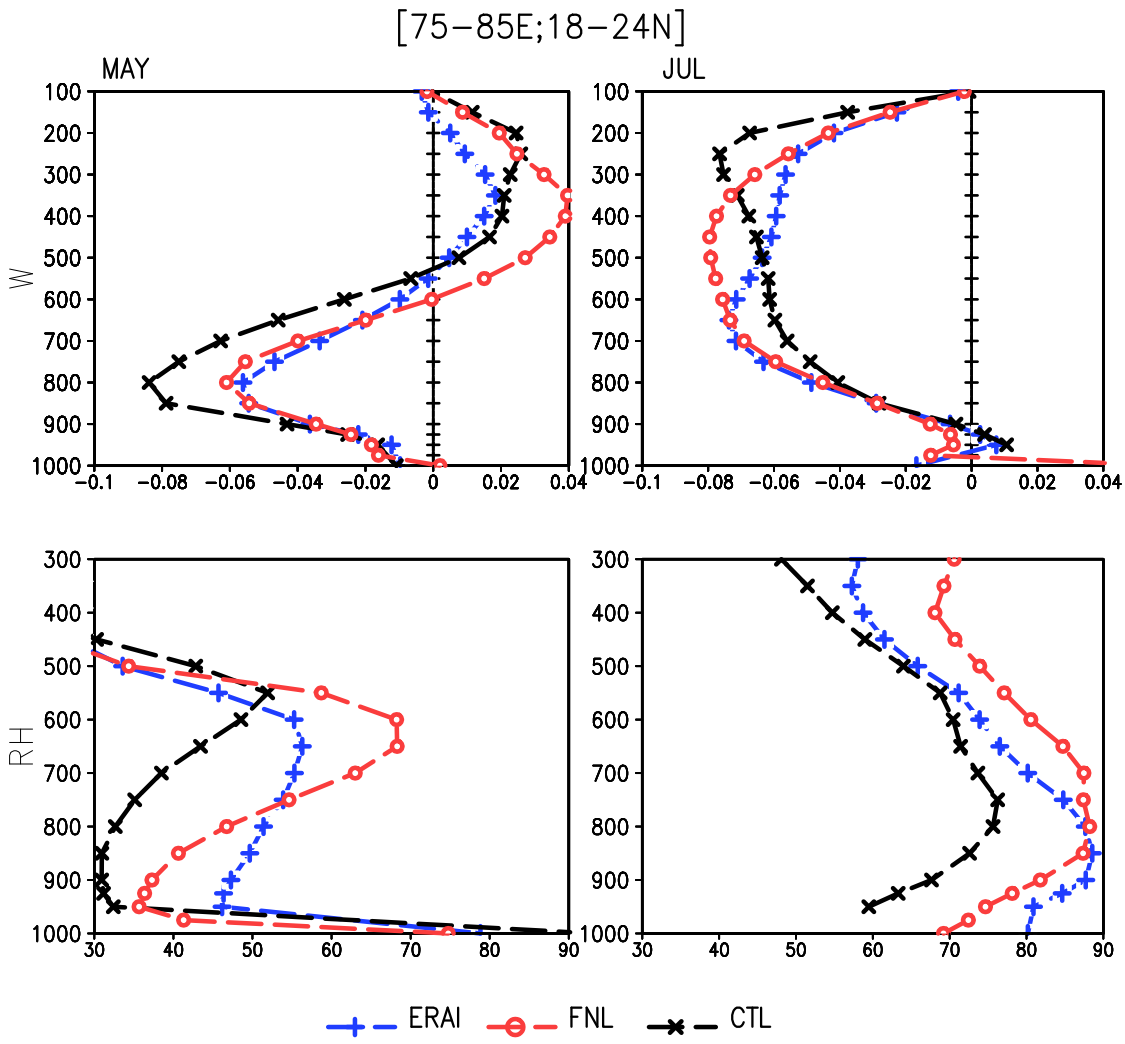

Figure 7.7b: Vertical profile of (top) vertical velocity (Pa s^{-1}) and (bottom) relative humidity (%) for (left) May and (right) July averaged over the area (18°-24°N, 75°-85°E).

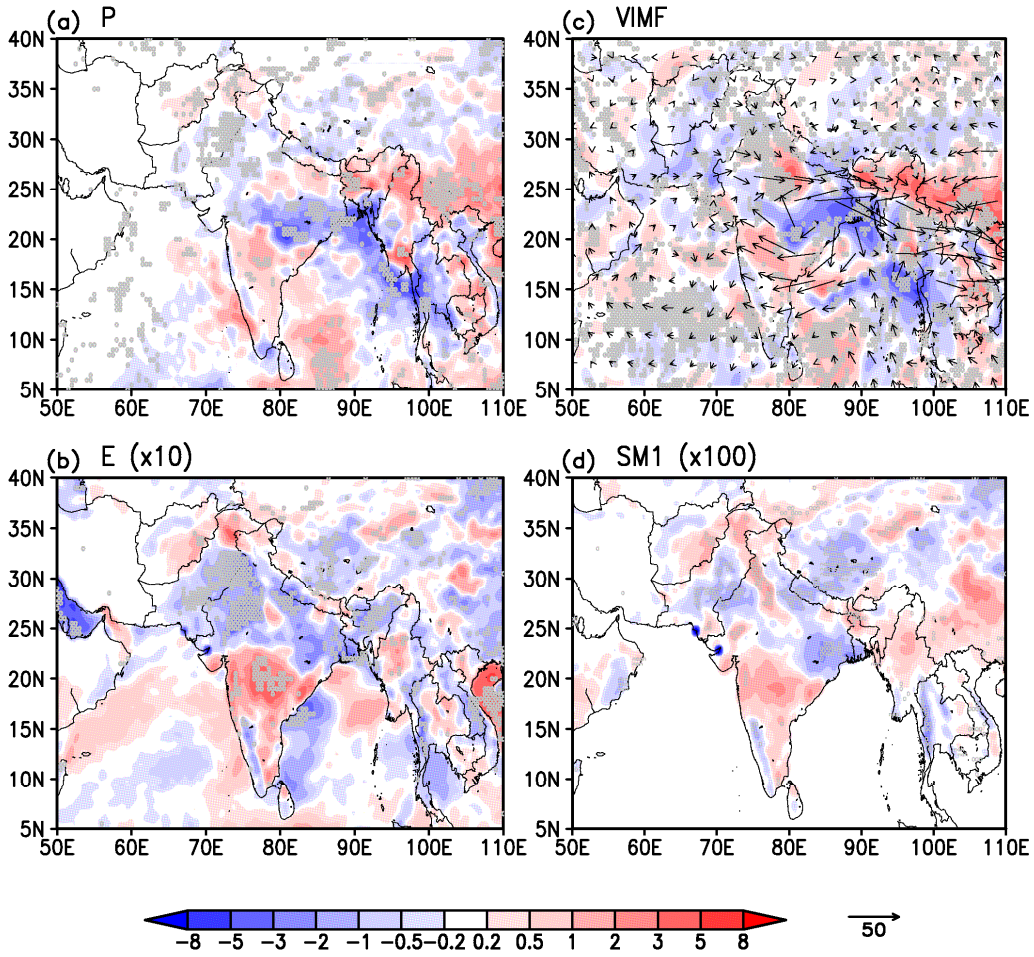

Figure 7.8: JJA average difference DES-CTL for: (a) precipitation (P, mm day^{-1}), (b) evaporation (E, x10 mm day^{-1}), (c) vertically integrated mass-weighted moisture flux (kg m^{-1} s^{-1}) and its convergence (shaded, positive red, mm day^{-1}), and (d) soil moisture in the upper layer (SM1, x100 mm). The light grey hatching is for statistically significant areas at the 80% (a) and 90% (b-d) confidence level.

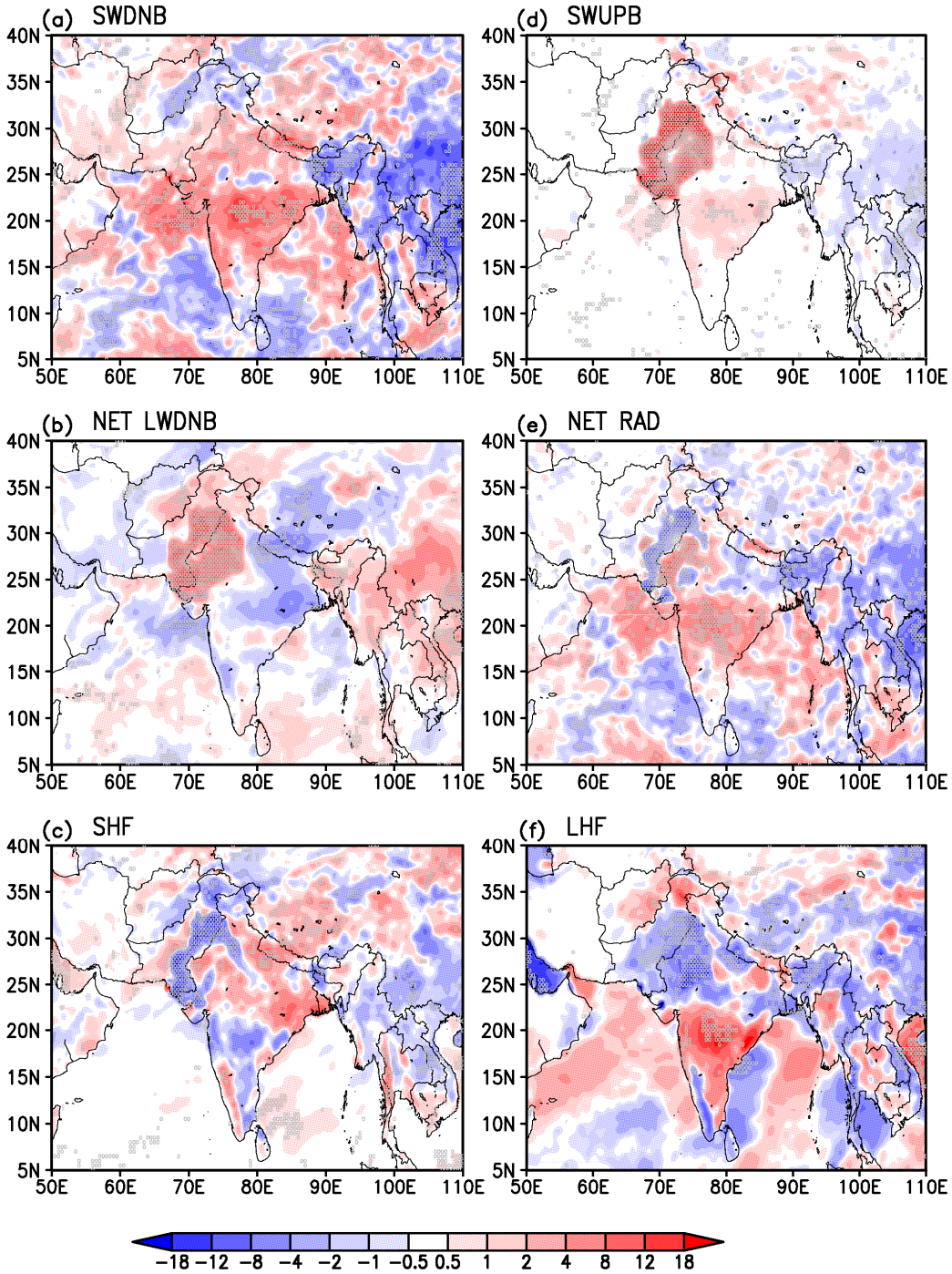

Figure 7.9: JJA average difference DES-CTL for: (a) surface downward shortwave radiation (SWDNB, W m^{-2}), (b) surface net longwave radiation (NET LWDNB, positive downward, W m^{-2}), (c) sensible heat flux (SHF, W m^{-2}), (d) surface upward shortwave radiation (SWUPB, W m^{-2}), (e) surface net radiation (NET RAD, positive downward, W m^{-2}), and (f) latent heat flux (LHF, W m^{-2}). The light grey hatching is for statistically significant areas at the 90% confidence level.

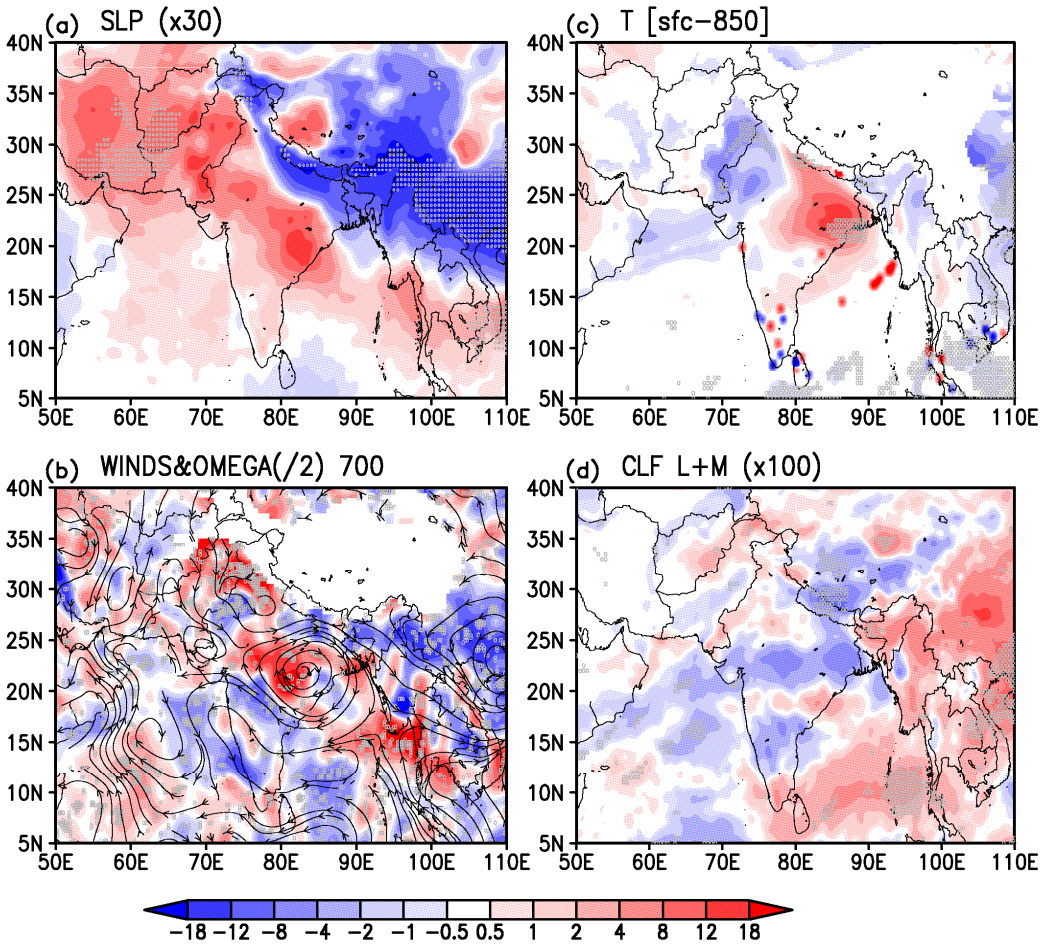

Figure 7.10: JJA average difference DES-CTL for: (a) sea level pressure (SLP, x30 hPa), (b) 700-hPa horizontal wind (streamlines) and *p*-vertical velocity (x0.5 hPa day^{-1}, positive values upward), (c) temperature vertically averaged between the surface and 850 hPa (°C), and (d) average low and middle cloud fraction (%). The light grey hatching is for statistically significant areas at the 90% confidence level.

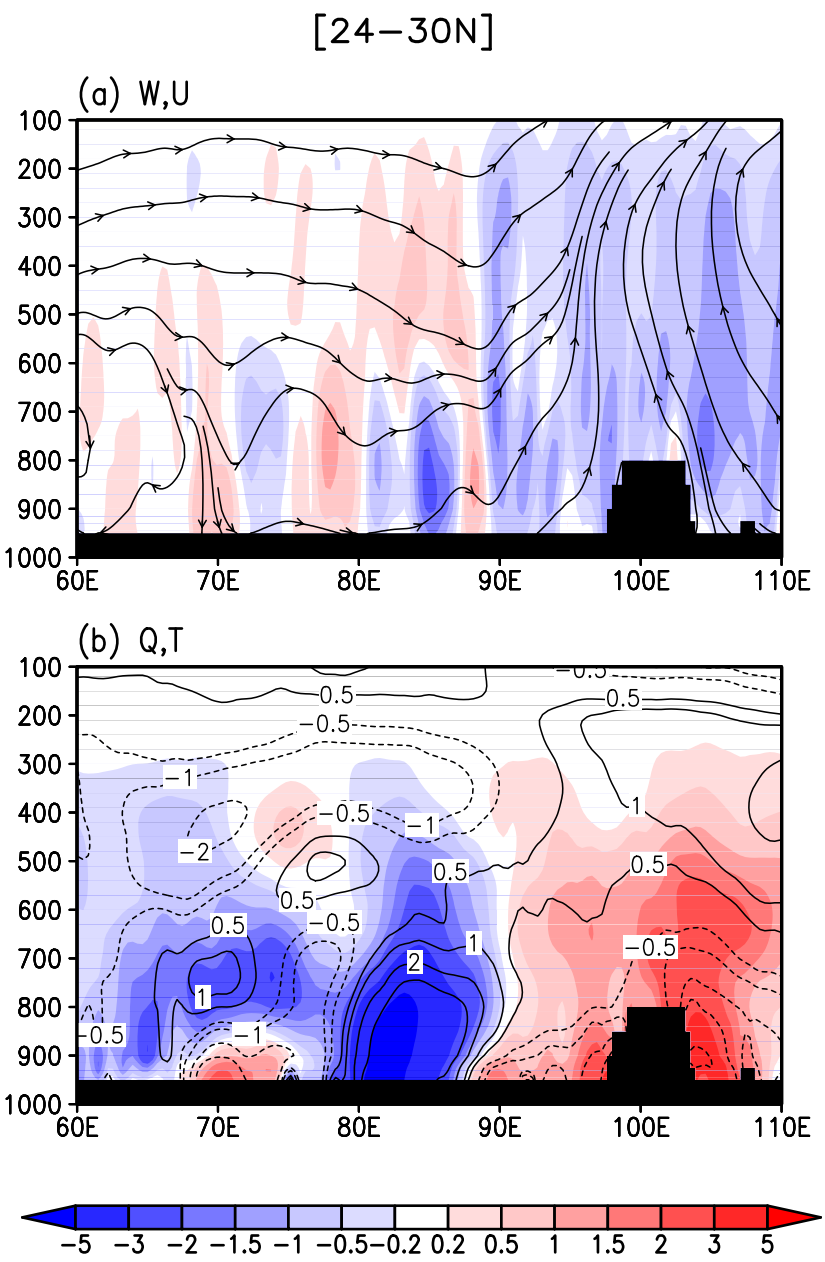

Figure 7.11: JJA average vertical/zonal cross section averaged between 24°-30°N of the difference DES-CTL for: (a) *p*-vertical velocity (shaded, x0.1 hPa day^{-1}, positive values downward) and zonal circulation (streamlines), and (b) specific humidity (shaded, x10 g kg^{-1}) and temperature (contours, x10°C). Values below orography (black area) have been masked out before averaging.

Chapter 8: Conclusions

8.1 Summary and Concluding Remarks

The South Asian monsoon is a coupled land-ocean-atmosphere phenomenon and a major dynamic component of the climate system. Its variability spans a wide range of scales, both in time and space, and is affected by numerous physical processes and feedbacks.

Considering the *mean seasonal cycle* of the monsoon and its *interannual* variations, two areas of research are particularly significant and have received increasing attention within the research community, namely the investigation of the influence of *absorbing aerosols* and of *land-* and *ocean-surface conditions.* More specifically, anomalies in the burden of absorbing aerosols over the IGP, in the heating of the land-surface over India, or a misrepresentation of simulated air-sea interactions in the Indian Ocean play an important role as key forcing factors impacting observed and simulated monsoon hydroclimate.

Given these themes, the motivation of this work was twofold:

(1) To improve the understanding of the role and impact of absorbing aerosols and regional land-ocean-atmosphere interactions on the South Asian monsoon;

(2) To provide insights into how the impact is generated and advance the understanding of the coupled mechanisms and physical processes at play.

A dynamically-oriented strategy was followed, where both structure and mechanisms of variability were targeted, which is an important step in the development of hypotheses on the operative processes. In this framework, several novel elements of discussion were presented in this work.

It was found that:

- Anomalous aerosol loading over the IGP in late spring leads to remarkable and large-scale variations in the monsoon evolution, both using monthly and sub-monthly observational data. Excessive aerosols are associated with reduced cloud amount and precipitation, increased surface shortwave radiation, and land-surface warming. The June-July anomalies associated with excessive springtime aerosols change sign (and pattern) over much of the Subcontinent and the monsoon strengthens. The "semi-direct" effect is suggested to play an important role in setting-up the conditions for a large-scale monsoon response to aerosol anomalies. Anomalous land-surface heating, once triggered by anomalous aerosol loading and induced reduced cloudiness and precipitation, is suggested to mediate the aerosol impact. At the same time, synoptic scale advection (and related vertical motion) plays a significant role in simultaneously shaping the aerosol distribution and associated hydroclimate, precluding further attribution of aerosols' influence. The "Elevated Heat Pump" hypothesis, a mechanism recently proposed for explaining absorbing aerosols' impact on the monsoon, is not viable and lacks of observational support (see Chapters 2-4).

- Coupled models have large systematic and coherent biases in simulating boreal summer precipitation, evaporation, and SST in the Indian Ocean, often exceeding 50% of the climatological values. Many of the biases are pervasive, being common to most simulations. The representation of local and non-local air–sea interactions is also compromised: for example, coupled models tend to overemphasize local forcing in the Indian Ocean, and to unrealistically correlate Indian monsoon rainfall with antecedent Indian Ocean SST (see Chapter 5).
- Both regional and remote forcings modulate the annual cycle of the heat-low over Pakistan and northwestern India. Land-surface heating has a limited role in the development of the low, mainly over its southeastern sector during the nascent phase. Regional orography and monsoon summertime deep-convection over the Bay of Bengal and eastern India, with its associated upstream descent east of the Caspian Sea and related low-level northerlies over the Hindu Kush mountains, contribute to the strengthening of the low from interaction with regional orography (see Chapter 6).
- The expansion of the desert at the expense of cultivated land over northwestern India and Pakistan significantly impacts summer monsoon hydroclimate and circulation both locally and at large scale. Locally, the atmospheric water cycle weakens, air temperature cools and subsidence is generated over the whole area. An anomalous northwesterly flow over the IGP weakens the monsoon circulation over eastern India, causing precipitation to decrease. Orographic-enhanced precipitation occurs over the Eastern Himalayas and southern China (see Chapter 7).

8.2 Future Work

The outcomes of this work, despite several known limitations, contribute to improve the understanding of the impact of aerosols and of land-ocean interactions on the South Asian monsoon. The complexity of the monsoon itself represents a significant challenge and much more has to be done, as new observational data will be available and models will be improved. Specifically, to mention a few possible future research lines:

- Recent aerosol data products, such as those derived from the Multi-angle Imaging SpectroRadiometer (MISR) and the Moderate Resolution Imaging Spectroradiometer (MODIS), as well as from the Cloud-Aerosol Lidar and Infrared Pathfinder Satellite Observations (CALIPSO), could provide more reliable estimates of aerosol composition, optical depth and three-dimensional distribution over northern India, which are expected to help the understanding of the physical processes linking aerosol variations to the monsoon.
- It is expected that aerosols-clouds-precipitation microphysics processes and interactions will be greatly improved in the next generation of climate models (e.g., Ghan and Schwartz 2007), especially with respect to online aerosol transport, gas/aerosol chemistry, and prognostic treatment of aerosol-cloud interactions. Short-term realistic sensitivity experiments might then be run to pinpoint the role of specific variables and associated processes (e.g., suppression of an individual feedback, separate simulations for aerosol direct and indirect effects and aerosol types, aerosol concentration increased/decreased over selected domains). The influence of aerosols on

regional SST and its effect on the monsoon is an issue which needs to be clarified by both observational analysis and modeling. Furthermore, aerosols modify the surface energy budget and the partitioning between sensible and latent heat fluxes, and, as a result, regional circulation dynamics can be significantly affected, as suggested by this analysis. Modeling experiments will clarify the magnitude of the impact of aerosols on land-surface conditions and the pathway by which anomalous land-atmosphere interactions will then feedback on the monsoon dynamics and hydroclimate.

- High-resolution experiments by means of a fully coupled land-atmosphere (and ocean) model represent the next step in the investigation of the forcing factors (e.g., influence of surrounding orography) on the heat-low over Pakistan/northwestern India and the associated desert environment. Furthermore, given that observational analysis and simple linear modeling suggest the monsoon heating in the Bay of Bengal to play an important role in remotely modulating the climate of the Middle East/southwestern Asia, advanced modeling experiments could be run to test this hypothesis.

Although monsoon research is a long walk initiated several centuries ago and far from reaching the conclusion, I believe progress can be made by facing the problem with true criticism and an open-mind, aware of the limitations of available tools, and with a comprehensive and exploratory attitude toward the understanding of the physical processes that determine the occurrence of a specific phenomenon.

Bibliography

AchutaRao, K. M, and K. R. Sperber, 2006: ENSO Simulation in Coupled Ocean-Atmosphere Models: Are the Current Models Better? *Climate Dyn.*, **27**, 1-15.

Ackerman, A. S., O. B. Toon, D. E. Stevens, A. J. Heymsfeld, V. Ramanathan, and E. J. Welton, 2000: Reduction of tropical cloudiness by soot. *Science*, **288**, 1042-1047.

Adler, R. F., G. J. Huffman, A. Chang, R. Ferraro, P. Xie, J. Janowiak, B. Rudolf, U. Schneider, S. Curtis, D. Bolvin, A. Gruber, J. Susskind, P. Arkin, and E. Nelkin, 2003: The Version 2 Global Precipitation Climatology Project (GPCP) Monthly Precipitation Analysis (1979-Present). *J. Hydrometeor.*, **4**, 1147-1167.

Amante, C., and B. W. Eakins, 1998: *ETOPO1 1 Arc-Minute Global Relief Model: Procedures, Data Sources and Analysis*. National Geophysical Data Center, NESDIS, NOAA, U.S. Department of Commerce: Boulder, CO.

Anderson, T. L., R. J. Charlson, S. E. Schwartz, R. Knutti, O. Boucher, H. Rodhe, and J. Heintzenberg, 2003: Climate Forcing by Aerosols - a Hazy Picture. *Science*, **300**, 1103-1004.

Annamalai, H., and R. Murtugudde, 2004: Role of the Indian Ocean in regional climate variability. *Earth's Climate: The Ocean-Atmosphere Interaction*, Geophys. Monograph Series, **147**, 213-246.

Annamalai, H., K. Hamilton, and K. R. Sperber, 2006: South Asian Summer Monsoon and its relationship with ENSO in the IPCC AR4 Simulations. *J. Climate*, **20**, 1071-1092.

Betts A. K., J. H. Ball, A. C. M. Beljaars, M. J. Miller, and P. A. Viterbo, 1996: The land surface–atmosphere interaction: A review based on observational and global modeling perspectives. *J. Geophys. Res*., **101**, 7209–7225.

Bitan, A., and H. Sa'aroni, 1992: The horizontal and vertical extension of the Persian Gulf pressure trough. *Int. J. Climatol.*, **12**, 733–747.

Blake, D. W., T. N. Krishnamurti, S. V. Low-Nam, and J. S. Fein, 1983: Heat low over the Saudi Arabian desert during May 1979 (Summer MONEX). *Mon. Wea. Rev.*, **111**, 1759-1775.

Bollasina, M., and S. Nigam, 2008: Indian Ocean SST, evaporation, and precipitation during the South Asian summer monsoon in IPCC-AR4 coupled simulations. *Climate Dyn.*, **33**, 1017-1033.

Bollasina, M., and S. Nigam, 2009: Absorbing aerosols and pre-summer monsoon hydroclimate variability over the Indian subcontinent: The challenge in investigating links. *Atmos. Res.*, **94**, 338-344.

Bollasina, M., and S. Nigam, 2010: The Summertime "Heat" Low over Pakistan/Northwestern India: Evolution and Origin. Submitted to *Climate Dyn.* on February 17, 2010.

Bollasina, M., S. Nigam, S., and K.-M. Lau, 2008: Absorbing aerosols and summer monsoon evolution over South Asia: An Observational Portrayal. *J. Climate*, **21**, 3221-3239.

Cakmur, R. V., R. L. Miller, and I. Tegen, 2001: A comparison of seasonal and interannual variability of soil dust aerosols over the Atlantic Ocean as inferred by

the TOMS AI and AVHRR AOT retrievals. *J. Geophys. Res.*, **106** (D16), 18287–18304.

Caldwell, P., H.-N. S. Chin, D. C. Bader, and B. Govindasamy, .2009: Evaluation of a WRF dynamical downscaling simulation over California. *Climatic Change*, **95**, 499-521. doi: 10.1007/s10584-009-9583-5.

Cayan, D. R., 1992: Latent and sensible heat flux anomalies over the northern oceans: Driving the sea surface temperature. *J. Phys. Oceanogr.*, **22**, 859–881.

CCSP, 2009: *Atmospheric Aerosol Properties and Climate Impacts*. Report by the U.S. Climate Change Science Program (CCSP) and the Subcommittee on Global Change Research, M. Chin, R. A. Kahn, and S. E. Schwartz (Eds.), NASA, Washington, D.C., USA, 128 pp.

Chan, S. C., and S. Nigam, 2009: Residual diagnosis of diabatic heat from ERA-40 and NCEP reanalyses: Intercomparison with TRMM. *J. Climate*, **22**, 414-428.

Chandrasekar, A., and A. Kitoh, 1998: Impact of localized sea surface temperature anomalies over the equatorial Indian Ocean on the Indian summer monsoon. *J. Meteor. Soc. Japan*, **76**, 841–853.

Chang, J.-H., 1972: *Atmospheric Circulation Systems and Climates*. Oriental Publish Co., Hawaii, 328 pp.

Charney, J. G., 1975: Dynamics of deserts and drought in Sahel. *Q. J. Royal Meteor. Soc.*, **101**, 193-202.

Charney, J., W. J. Quirk, S.-H. Chow, and J. Kornfield, 1977: A comparative study of the effects of albedo change on drought in semi-arid regions. *J. Atmos. Sci.*, **34**, 1366-1385.

Chauhan, S. S., 2003: Desertification Control and Management of Land Degradation in the Thar Desert of India. *The Environmentalist*, **23**, 219–227.

Chen, F., and J. Dudhia, 2001: Coupling an advanced land-surface/ hydrology model with the Penn State/NCAR MM5 modeling system. Part I: Model description and implementation. *Mon. Wea. Rev.*, **129**, 569–585.

Chervin, R. M., 1979: *Response on the NCAR general circulation model to changed land surface albedo*. Report of the JOC study Conference on Climate Models, GARP Pub. Ser. No. 22, WMO, 563-581.

Chiappello, I., J. M. Prospero, J. R. Herman, and N. C. Hsu, 1999: Detection of mineral dust over the North Atlantic Ocean and Africa with the Nimbus 7 TOMS. *J. Geophys. Res.*, **104**, 9277-9291.

Chung, C. E., and S. Nigam, 1999: Asian Summer Monsoon—ENSO Feedback on the Cane–Zebiak Model ENSO. *J. Climate*, **12**, 2787-2807.

Chung, C. E., and V. Ramanathan, 2003: South Asian haze forcing: remote impacts with implications to ENSO and AO. *J. Climate*, **16**, 1791-1806.

Chung, C. E., and V. Ramanathan, 2006: Weakening of North Indian SST gradients and the monsoon rainfall in India and the Sahel. *J. Climate*, **19**, 2036-2045.

Chung, C. E., V. Ramanathan, and J. T. Kiehl, 2002: Effects of the South Asian absorbing haze on the northeast monsoon and surface-air exchange. *J. Climate*, **15**, 2462- 2476.

Chung, C. E., V. Ramanathan, D. Kim, and I. Podgorny, 2005: Global Anthropogenic Aerosol Direct Forcing Derived from Satellite and Ground Based Observations. *J. Geophys. Res.*, **110**, doi:10.1029/2005JD006356.

Clark, C. O., J. E. Cole, and P. J. Webster, 2000: Indian Ocean SST and Indian summer rainfall: predictive relationships and their decadal variability. *J. Climate*, **13**, 2503-2519.

Clark, D. B, Y. Xue, R. J. Harding, and P. J. Valdes, 2001: Modeling the impact of land surface degradation on the climate of tropical North Africa. *J. Climate*, **14**, 1809–1822.

Collier, J. C., and G. J. Zhang, 2009: Aerosol direct forcing of the summer Indian monsoon as simulated by the NCAR CAM3. *Climate Dyn.*, **32**, 313–332, doi:10.1007/s00382-008-0464-9.

Collins, W.D., and Coauthors, 2004: *Description of the NCAR Community Atmosphere Model (CAM 3.0)*. NCAR Technical Note, NCAR/TN-464+STR, 226pp.

Covey, C., K. M. AchutaRao, S. J. Lambert, and K. E. Taylor, 2000: *Intercomparison of Present and Future Climates Simulated by Coupled Ocean-Atmosphere GCMs.* Program for Climate Model Diagnosis and Intercomparison (PCMDI) Report No. 66, Lawrence Livermore National Laboratory, University of California, Livermore, CA.

Covey, C., K. M. AchutaRao, U. Cubasch, P. Jones, S. J. Lambert, M. E. Mann, T. J. Phillips, and K. E. Taylor, 2003: An Overview of Results from the Coupled Model Intercomparison Project (CMIP). *Global Planet. Change*, **37**, 103-133.

Cox., S. J., P. W. Stackhouse, Jr., S. K. Gupta, J. C. Mikovitz, T. Zhang, L. M. Hinkelman, M. Wild, and A. Ohmura, 2006: The NASA/GEWEX Surface

Radiation Budget Project: Overview and Analysis. Proceedings, *12th Conference on Atmospheric Radiation*, Amer. Meteor. Soc., Madison WI, July 10-14.

Csiszar, I., and G. Gutman, 1999: Mapping global land surface albedo from NOAA AVHRR. *J. Geophys. Res.*, **104**, 6215-6228.

Dai, A., 2006. Precipitation characteristics in eighteen coupled climate models. *J. Climate*, **19**, 4605-4630.

Das, P. K., 1962: Mean vertical motion and non-adiabatic heat sources over India during the monsoon. *Tellus*, **14**, 212-220.

Das, S., R. Ashrit, G. R. Iyengar, S. Mohandas, M. D. Gupta, J. P. Geoge, E. N. Rajagopal, and S. K. Dutta, 2008: Skills of different mesoscale models over Indian region during monsoon season: Forecast errors. *J. Earth System Sci.*, **117**, 603-620.

Decharme, B., Ottle', C., S. Saux-Picart, N. Boulain, B. Cappelaere, D. Ramier, and M. Zribi, 2009: A New Land Surface Hydrology within the Noah-WRF Land-Atmosphere Mesoscale Model Applied to Semiarid Environment: Evaluation over the Dantiandou Kori (Niger). *Adv. Meteorol.*, **2009**, doi:10.1155/2009/731874.

Dey, S., and S. N. Tripathi, 2007: Estimation of aerosol optical properties and radiative effects in the Ganga basin, northern India, during the wintertime. *J. Geophys. Res.*, **112**, D03203, doi:10.1029/2006JD007267.

Dey, S., S. N. Tripathi, and R. P. Singh, 2004: Influence of dust storms on the aerosol optical properties over the Indo-Gangetic basin. *J. Geophys. Res.*, **109**, doi: 1029/2004JD004924.

Dickinson, R. E., 1992: Changes in land-use. *Climate System Modeling*, K. E. Trenberth (Ed.), Cambridge University Press: Cambridge, pp. 689-704.

Dirmeyer, P. A., and J. Shukla, 1996: Albedo as a modulator on regional climate response to tropical deforestration. *J. Geophys. Res.*, **99**, 20863-20877.

Dugam, S. S., S. B. Kakade, and R. K. Verma, 1997: Interannual and long-term variability in the North Atlantic Oscillation and Indian summer monsoon rainfall. *Theor. Appl. Climatol.*, **58**, 21–29.

Duncan B. N., R. V. Martin, A. C. Staudt, R. Yevich, and J. A. Logan, 2003: Interannual and seasonal variability of biomass burning emissions constrained by satellite observations. *J. Geophys. Res.*, **108**, 4100, doi:10.1029/2002JD002378.

Eck, T. F., B. N. Holben, O. Dubovik, A. Smirnov, I. Slutsker, J. M. Lobert, and V. Ramanathan, 2001: Column integrated aerosol optical properties over the Maldives during the northeast monsoon for 1998-2000. *J. Geophys. Res.*, **106**, 28555-28566.

Ellsaesser, H. W., M. C. MacCracken, G. L. Potter, and F. M. Luther, 1976: An additional model test of positive feedback from high desert albedo. *Q. J. R. Met. Soc.*, **102**, 655-666.

Gautam, R., N. C. Hsu, M. Kafatos, and S.-C. Tsay, 2007: Influences of winter haze on fog/low cloud over the Indo-Gangetic plains. *J. Geophys. Res.*, **112**, D05207, doi:10.1029/2005JD007036.

Gautam, R., N. C. Hsu, K. ‐ M. Lau, S. ‐ C. Tsay, and M. Kafatos, 2009: Enhanced pre-monsoon warming over the Himalayan-Gangetic region from 1979 to 2007, *Geophys. Res. Lett.*, **36**, L07704, doi:10.1029/2009GL037641.

Gemmill, W., B. Katz, and X. Li, 2007: Daily Real-Time Global Sea Surface Temperature - High Resolution Analysis at NOAA/NCEP. NOAA/NWS/NCEP/MMAB Office Note, **260**, 39 pp.

Ghan, S. J., and S. E. Schwartz, 2007: Aerosol properties and processes: A path from field and laboratory measurements to global climate models. *Bull. Amer. Meteor. Soc.*, **88**, 1059–1083.

Goswami, B. N., 2005: South Asian Summer Monsoon: An Overview. *The Global Monsoon System: Research and Forecast*, C.-P. Chang, B. Wang, and N.-C. G. Lau (Eds.), WMO/TD No. 1266 (TMRP Report No. 70), 47−71.

Goswami, P., and K. V. Ramesh, 2008: The expanding Indian desert: Assessment through weghted epochal trend ensemble. *Curr. Sci.*, **94**, 476-480.

Gupta, S. K., N. A. Ritchey, A. C. Wilber, C. H. Whitlock, G. G. Gibson, and P. W. Stackhouse, 1999: A climatology of surface radiation budget derived from satellite data. *J. Climate*, **12**, 2691-2710.

Gupta, A., P. K. Thapliyal, P. K. Pal, and P. C. Joshi, 2005: Impact of deforestation on Indian monsoon – A GCM sensitivity study. *J. Ind. Geophys. Union*, **9**, 97-104.

Gutman, G. and A. Ignatov, 1997: The derivation of green vegetation fraction from NOAA/AVHRR data for use in numerical weather prediction models. *Int. J. Remote Sensing*, **19**, 1533-1543.

Habib, G., C. Venkataraman, I. Chiapello, S. Ramachandran, O. Boucher, and M. S. Reddy, 2006: Seasonal and interannual variability in absorbing aerosols over

India derived from TOMS: Relationship to regional meteorology and emissions. *Atmos. Envir.*, **40**, 1909-1921.

Hales, K., J. D. Neelin, and N. Zeng, 2004: Sensitivity of tropical land climate to leaf area index: role of surface conductance versus albedo. *J. Climate*, **17**, 1459-1473.

Hansen, J., M. Sato, and R. Ruedy, 1997: Radiative forcing and climate response. *J. Geophys. Res.*, **102**, 6831-6864.

Harzallah R, and R. Sadourny, 1997: Observed lead-lag relationships between Indian summer monsoon and some meteorological variables. *Climate Dyn.*, **13**, 635–648.

Herman, J. R., P. B. Bhartia, O. Torres, N. C. Hsu, C. J. Seftor, and E. Celarier, 1997: Global distribution of UV-absorbing aerosols from Nimbus 7/TOMS data. *J. Geophys. Res.*, **102**, 16911-16921.

Holben, B. N., et al., 2001: An emerging ground-based aerosol climatology: Aerosol optical depth from AERONET. *J. Geophys. Res.*, **106** (D11), 12067–12098.

Hong, S.-Y., and J.-O. J. Lim, 2006: The WRF Single-Moment 6-Class Microphysics Scheme (WSM6). *J. Korean Meteor. Soc.*, **42**, 129–151.

Hong, S.-Y., J. Dudhia, and S.-H. Chen, 2004: A Revised Approach to Ice Microphysical Processes for the Bulk Parameterization of Clouds and Precipitation. *Mon. Wea. Rev.*, **132**, 103–120.

Hong, S.-Y., and Y. Noh, and J. Dudhia, 2006: A new vertical diffusion package with an explicit treatment of entrainment processes. *Mon. Wea. Rev.*, **134**, 2318–2341.

Hsu, N. C., J. R. Herman, O. Torres, B. N. Holben, D. Tanre, T. F. Eck, A. Smirnov, B. Chatenet, and F. Lavenu, 1999: Comparisons of the TOMS aerosol index with

Sun-photometer aerosol optical thickness: Results and applications. *J. Geophys. Res.*, **104** (D6), 6269-6280, 10.1029/1998JD200086.

Hsu, N. C., J. R. Herman, and S. C. Tsay, 2003: Radiative impacts from biomass burning in the presence of clouds during boreal spring in Southeast Asia. *Geophys. Res. Lett.*, **30**, doi: 10.1029/2002GL016485.

Huffman, G. J., R. F. Adler, M. Morrissey, D. T. Bolvin, S. Curtis, R. Joyce, B. McGavock, and J. Susskind, 2001: Global Precipitation at One-Degree Daily Resolution from Multi-Satellite Observations. *J. Hydrometeor.*, **2**, 36-50.

Huffman, G. J., R. F. Adler, D. T. Bolvin, G. Gu, E. J. Nelkin, K. P. Bowman, Y. Hong, E. F. Stocker and D. B. Wolff, 2007: The TRMM Multisatellite Precipitation Analysis (TMPA): quasi-global, multiyear, combined-sensor precipitation estimates at fine scales. *J. Hydrometeor.*, **8**, 38–55.

Intergovernmental Panel on Climate Change (IPCC), 2007: Climate Change 2007: The Physical Science Basis. Summary for Policymakers (available at the web address: http://www.ipcc.ch/SPM2feb07.pdf).

Jayanthi N., M. Rajeevan, A. K. Srivastava, D. Sunitha, S. K. Roy Bhowmik, and H. R. Hatwar, 2006: *Monsoon 2006: A Report*. India Meteorological Department, Pune, 103 pp.

Johnson, R. H., 2003: Thermal low. *Encyclopedia of Atmospheric Science*, J. Holton, J. Pyle, and J. A. Curry (Eds.), Academic Press, London, United Kingdom, pp 2269-2273.

Joseph, R., and S. Nigam, 2006: ENSO evolution and teleconnections in IPCC's Twentieth-Century climate simulations: realistic representation? *J. Climate*, **19**, 4360–4377.

Joshi, P. C., and P. S. Desai, 1985: The satellite-determined thermal structure of heat low during Indian south-west monsoon season. *Adv. Space Res.*, **5**, 57-60.

Kain, J. S., 2004: The Kain-Fritsch convective parameterization: An update. *J. Appl. Meteor.*, **43**, 170–181.

Kang, I.-S., and J. Shukla, 2005: Dynamical Seasonal Prediction and Predictability of Monsoon. *The Global Monsoon System: Research and Forecast*, C.-P. Chang, B. Wang, and N.-C. G. Lau (Eds.), WMO/TD No. 1266 (TMRP Report No. 70), 386-402.

Kang, I.-S., and Coauthors, 2002: Intercomparison of the climatological variations of Asian summer monsoon precipitation simulated by 10 GCMs. *Climate Dyn.*, **19**, 383-395.

Kang, I.-S., J. Y. Lee, and C. K. Park, 2004: Potential predictability of summer mean precipitation in a dynamical seasonal prediction system with systematic error correction. *J. Climate*, **17**, 834-844.

Kaufman, Y. J., and I. Koren, 2006: Some and pollution aerosol effect on cloud cover. *Science*, **313**, 655-658.

Keshavamurty, R. N., and S. T. Awade, 1970: On the maintenance of the mean monsoon trough over North India. *Mon. Wea. Rev.*, **98**, 315-320.

Kiehl, J. T., 2007: Twentieth century climate model response and climate sensitivity. *Geophys. Res. Lett.*, **34**, L22710, doi:10.1029/2007GL031383.

Kinne, S., and Coauthors, 2006: An AeroCom initial assessment optical properties in aerosol component modules of global models. *Atmos. Chem. Phys.*, **6**, 1815-1834.

Kiss, P., I. M. Janosi, and O. Torres, 2007: Early calibration problems detected in TOMS Earth-Probe aerosol signal. *Geophys. Res. Lett.*, **34**, L07803, doi:10.1029/2006GL028108.

Knorr, W., K. Schnitzler, and Y. Govaerts, 2001: The role of Bright Desert Regions in shaping North African climate. *Geophys. Res. Lett.*, **28**, 3489–3492.

Kripalani, R. H., J. H. Oh, A. Kulkarni, S. S. Sabade, and H. S. Chaudhari, 2007: South Asian summer monsoon precipitation variability: Coupled climate model simulations and projections under IPCC AR4. *Theor. Appl. Climatol.*, **90**, 133-159.

Krishnamurti, T. N., and H. N. Bhalme, 1976: Oscillations of a monsoon system. Part I. Observational aspect. *J. Atmos. Sci.*, **33**, 1937-1954.

Krishnamurti, T. N., T. S. V. Vijaya Kumar, and A. K. Mitra, 2006: Seasonal climate prediction of Indian summer monsoon. *The Asian Monsoon*, B. Wang (Ed.), Praxis Pub. Ltd., Chichester, UK, 553-583.

Kulkarni, A., S. S. Sabade, and R. H. Kripalani, 2007: Association between the extreme monsoons and the dipole mode over the Indian subcontinent. *Meteorol. Atmos. Phys.*, **95**, 255-268.

Kwun, J. H., Y.-K. Kim, J.-W. Seo, J. H. Jeong, and S. H. You, 2009: Sensitivity of MM5 and WRF mesoscale model predictions of surface winds in a typhoon to planetary boundary layer parameterizations. *Nat. Hazards*, **51**, 63-77.

Lau K.-M., and H-T. Wu, 2001: Principal modes of rainfall-SST variability of the Asian summer monsoon: a re-assessment of monsoon-ENSO relationship. *J. Climate*, **14**, 2880-2895.

Lau, K.-M., and K.-M. Kim, 2006: Observational relationships between aerosol and Asian monsoon rainfall, and circulation. *Geophys. Res. Lett.*, **33**, L21810, doi:10.1029/2006GL027546.

Lau, K.-M., N.-C. Lau, and S. Yang, 2005: Current Topics on Interannual Variability of the Asian Monsoon. *The Global Monsoon System: Research and Forecast*, C.-P. Chang, B. Wang, and N.-C. G. Lau (Eds.), WMO/TD No. 1266 (TMRP Report No. 70), 440–454.

Lau, K.-M., M. K. Kim, and K.-M. Kim, 2006: Aerosol induced anomalies in the Asian summer monsoon- the role of the Tibetan Plateau. *Climate Dyn.*, **26**, 855-864, doi:10.1007/s00382-006-0114-z.

Lau, K.-M., K. M. Kim, C. Hsu, and B. Holben, 2009: Possible influences of air pollution, dust and sandstorms on the Indian monsoon. *WMO Bulletin*, **58**, 22-30.

Laval, K., and L. Picon, 1986: Effect of a change of the surface albedo of the Sahel on climate. *J. Atmos. Sci.*, **43**, 2418-2429.

Lean, J., and P. R. Rowntree, 1993: A GCM simulation of the impact of Amazonian deforestation on climate using an improved canopy representation. *Q. J. R. Met. Soc.*, **119**, 509–530.

Lelieveld, J., and Coauthors, 2001: The Indian Ocean experiment: widespread air pollution from South and Southeast Asia. *Science*, **291**, 1031-1036.

Leung, L. R., and Y. Qian, 2009: Atmospheric rivers induced heavy precipitation and flooding in the western U.S. simulated by the WRF regional climate model. *Geophys. Res. Lett.*, **36**, L03820, doi:10.1029/2008GL036445.

Li, W., Y. Xue, and I. Poccard, 2007: Numerical investigation of the impact of vegetation indices on the variability of West African summer monsoon. *J. Met. Soc. Japan*, **85A**, 363-383.

Liebmann, B., and C. A. Smith, 1996: Description of a Complete (Interpolated) Outgoing Longwave Radiation Dataset. *Bull. Amer. Meteor. Soc.*, **77**, 1275-1277.

Lin, J. L., 2007: The double-ITCZ problem in IPCC AR4 coupled GCMs: ocean-atmosphere feedback analysis. *J. Climate*, **20**, 4497-4525.

Lohmann, U., and J. Feichter, 2005: Global indirect aerosol effects: a review. *Atmos. Chem. Phys.*, **5**, 715–737.

Massie, S. T., O. Torres, and S. J. Smith, 2004: Total Ozone Mapping Spectrometer (TOMS) observations of increases in Asian aerosol in winter from 1979 to 2000. *J. Geophys. Res.*, **109**, D18211, doi:10.1029/2004JD004620.

Matsuura, K., and C. J. Willmott, 2009a: Terrestrial Precipitation 1900-2008 Gridded Monthly Time series (version 2.01). Center for Climatic Research, Department of Geography, University of Delaware, Newark (available at the web address: http://climate.geog.udel.edu/~climate/html_pages/Global2_Ts_2009/README.global_p_ts_2009.html).

Matsuura, K., and C. J. Willmott, 2009b: Terrestrial Air Temperature 1900-2008 Gridded Monthly Time series (version 2.01). Center for Climatic Research, Department of Geography, University of Delaware, Newark (available at the web

address: http://climate.geog.udel.edu/~climate/html_pages/Global2_Ts_2009/README.global_t_ts_2009.html).

Meehl, G. A., C. Covey, B. McAvaney, M. Latif, and R. J. Stouffer, 2005: Overview of the Coupled Model Intercomparison Project. *Bull. Amer. Met. Soc.*, **86**, 89-93.

Meehl, G. A., J. M. Arblaster, D. M. Lawrence, A. Seth, E. K. Schneider, B. P. Kirtman, and D. Min, 2006: Monsoon Regimes in the CCSM3. *J. Climate*, **19**, 2482-2495.

Meehl G. A., J. M. Arblaster, and W. D. Collins, 2008: Effects of black carbon aerosols on the Indian monsoon. *J. Climate*, **21**, 2869-2882.

Menon, S., 2004: Current uncertainties in assessing aerosol effects on climate. *Annu. Rev. Environ. Resour.*, **29**, 1-30.

Menon, S., J. Hansen, L. Nazarenko, and Y. Luo, 2002: Climate effects of black carbon aerosols in China and India. *Science*, **297**, 2250-2253.

Miao, S., F. Chen, M.A. LeMone, M. Tewari, Q. Li, and Y. Wang, 2009: An Observational and Modeling Study of Characteristics of Urban Heat Island and Boundary Layer Structures in Beijing. *J. Appl. Meteor. Climatol.*, **48**, 484–501.

Mitchell, T. D, and P. D. Jones, 2005: An improved method of constructing a database of monthly climate observations and associated high-resolution grids. *Int. J. Climatol.*, **25**, 693-712.

Mylne, M. F., and P. R. Rowntree, 1991: Modelling the effects of albedo change associated with tropical deforestation. *Climatic Change*, **21**, 317-343.

New, M., M. Hulme, and P. Jones, 2000: Representing twentieth-century space–time climate variability. Part II: Development of 1901–96 monthly grids of terrestrial surface climate. *J. Climate*, **13**, 2217-2238.

Nicholson, S. E., 1988: Land Surface Atmosphere Interaction: Physical processes and Surface Changes and their Impact. *Progress in Physical Geography*, **12**, 36-65.

Nigam, S., 1994: On the dynamical basis for the Asian summer monsoon rainfall-El Niño relationship. *J. Climate*, **7**, 1750-1771.

Nigam S, and A. Ruiz-Barradas, 2006: Seasonal hydroclimate variability over North America in global and regional reanalyses and AMIP simulations: varied representation. *J. Climate*, **19**, 815-837.

Nigam, S., and S. C. Chan, 2009: On the summertime strengthening of the Northern Hemisphere Pacific sea level pressure anticyclone. *J. Climate*, **22**, 1174-1192.

Nigam, S., and M. Bollasina, 2010: Absorbing Aerosols and Pre-Summer Monsoon Hydroclimate Variability over the Indian Subcontinent: The Challenge of Investigating Links. Accepted by *J. Geophys. Res.*

Niyogi, D., H.-I. Chang, F. Chen, L. Gu, A. Kumar, S. Menon, and R. A. Pielke, 2007: Potential impacts of aerosol–land–atmosphere interactions on the Indian monsoonal rainfall characteristic. *Nat. Hazards*, **42**, 345-359.

Oyama, M. D., and C. A. Nobre, 2004: Climatic consequences of a large-scale desertification in Northeast Brazil: A GCM simulation study. *J. Climate*, **17**, 3203-3213.

Parthasarathy, B., K. Rupa Kumar, and A. A. Munot, 1992: Surface pressure and summer monsoon rainfall over India. *Adv. Atmos. Sci.*, **9**, 359-366.

Parthasarathy, B., A. A. Munot, and D. R. Kothawale, 1995: All India monthly and seasonal rainfall series: 1871-1993. *Theor. and Appl. Climatol.*, **49**, 217-224.

Pielke, R.A., R. Avissar, M. Raupach, H. Dolman, X. Zeng, and S. Denning, 1998: Interactions between the atmosphere and terrestrial ecosystems: Influence on weather and climate. *Global Change Biology*, **4**, 461-475.

Pielke, R. A. Sr, G. Marland, R. A. Betts, T. N. Chase, J. L. Eastman, J. O. Niles, D. S. Niyogi, and S. W. Running, 2002: The Influence of Land-Use Change and Landscape Dynamics on the Climate System: Relevance to Climate-Change Policy Beyond the Radiative Effect of Greenhouse Gases. *Phil. Trans. R. Soc. Lond.,* **360**, 1705-1719.

Pielke Sr., R. A., J. O. Adegoke, T. N. Chase, C. H. Marshall, T. Matsui, and D. Niyogi, 2007: A new paradigm for assessing the role of agriculture in the climate system and in climate change. *Agric. Forest Meteor.,* **132***,* 234-254.

Portela, A., and M. Castro, 1996: Summer thermal lows in the Iberian peninsula: A three-dimensional simulation. *Q. J. R. Meteorol. Soc.*, **122**, 1-22.

Prasad, A. K., and R. P. Singh, 2007: Changes in aerosol parameters during major dust storm events (2001–2005) over the Indo-Gangetic Plains using AERONET and MODIS data. *J. Geophys. Res.*, **112**, D09208, doi:10.1029/2006JD007778.

Prospero, J. M., P. Ginoux, O. Torres, S. E. Nicholson, and T. E. Gill, 2002: Environmental characterization of global sources of atmospheric soil dust identified with the Nimbus-7 total ozone mapping spectrometer (TOMS) absorbing aerosol product. *Rev. Geophys.*, **40**, 1002, doi:10.1029/2000RG000095.

Qian, Y., W. I. Gustafson Jr., L. R. Leung, and S. J. Ghan, 2009: Effects of soot-induced snow albedo change on snowpack and hydrological cycle in western United States based on Weather Research and Forecasting chemistry and regional climate simulations. *J. Geophys. Res.*, **114**, D03108, doi:10.1029/2008JD011039.

Rácz, Z., and R. K. Smith, 1999: The dynamics of heat lows. *Q. J. R. Meteorol. Soc.*, **125**, 225-252.

Rahmani, A. R., and R. G. Soni, 1997: Avifaunal changes in the Indian Thar Desert. *J. Arid Environ.*, **36**, 687-703.

Rajeev, K., V. Ramanathan, and J. Meywerk, 2000: Regional aerosol distribution and its long-range transport over the Indian Ocean. *J. Geophys. Res.*, **105** (D2), 2029–2044.

Rajeev, K. and V. Ramanathan, 2002: The Indian Ocean Experiment: aerosol forcing obtained from satellite data. *Adv. Space Res.*, **29**, 1731-1740.

Ramachandran, S., and R. Cherian, 2008: Regional and seasonal variations in aerosol optical characteristics and their frequency distributions over India during 2001–2005. *J. Geophys. Res.*, **113**, D08207, doi:10.1029/2007JD008560.

Ramage, C. S., 1966: The summer atmospheric circulation over the Arabian Sea. *J. Atmos. Sci.*, **23**, 144-150.

Ramana, M. V., V. Ramanathan, I. A Podgorny, B. B. Pradhan, and B. Shrestha, 2004: The direct observations of large aerosol radiative forcing in the Himalayan region. *Geophys. Res. Lett.*, **31**, L05111, doi:10.1029/2003GL018824.

Ramanathan, V. and M. V. Ramana, 2005: Persistent, widespread, and strongly absorbing haze over the Himalayan foothills and the Indo-Ganges Plains. *Pure Appl. Geophys.*, **162**, 1609-1626.

Ramanathan, V., and G. Carmichael, 2008: Global and regional change due to black carbon. *Nature Geosci.*, **1**, 221-227.

Ramanathan, V., and Coauthors, 2001: Indian Ocean experiment: An integrated analysis of the climate forcing and effects of the great Indo-Asian haze. *J. Geophys. Res.*, **106** (D22), 28371–28398.

Ramanathan, V., and Coauthors, 2005: Atmospheric Brown Clouds: Impacts on South Asian Climate and Hydrological Cycle. *PNAS*, **102**, 5326-5333.

Ramanathan, V., and Coauthors, 2008: *Atmospheric Brown Clouds: Regional Assessment Report with Focus on Asia*. United Nations Environment Program, Nairobi, Kenya, pp. 1-360.

Randall, D. A., R. A. Wood, S. Bony, R. Colman, T. Fichefet, J. Fyfe, V. Kattsov, A. Pitman, J. Shukla, J. Srinivasan, R. J. Stouffer, A. Sumi, and K. E. Taylor, 2007: Climate models and their evaluation. *Climate Change 2007: The Physical Science Basis*. Contribution of Working Group I to the Fourth Assessment Report of the Intergovernmental Panel on Climate Change, Solomon, S., D. Qin, M. Manning, Z. Chen, M. C. Marquis, K. B. Averyt, M. Tignor and H. L. Miller (Eds.).

Randles, C. A., and V. Ramaswamy, 2008: Absorbing aerosols over Asia: A Geophysical Fluid Dynamics Laboratory general circulation model sensitivity

study of model response to aerosol optical depth and aerosol absorption. *J. Geophys. Res.*, **113**, D21203, doi:10.1029/2008JD010140.

Rao, K. G., and B. N. Goswami, 1988: Interannual variations in sea surface temperature of the Arabian sea and the Indian monsoon: A new perspective. *Mon. Wea. Rev.*, **116**, 558-568.

Ravi, S., and T. E. Huxman, 2009: Land degradation in the Thar Desert. *Frontiers in Ecology and the Environment*, **7**, 517-518, doi: 10.1890/09.WB.029.

Rodell, M., I. Velicogna, and J. S. Famiglietti, 2009: Satellite-based estimates of groundwater depletion in India. *Nature*, **460**, 999-1002.

Rodwell, M. J., and B. J. Hoskins, 1996: Monsoons and the dynamics of deserts. *Q. J. R. Meteorol. Soc.*, **122**, 1385-1404.

Rodwell, M. J., and B. J. Hoskins, 2001: Subtropical anticyclones and summer monsoons. *J. Climate*, **14**, 3192-3211.

Rosenfeld, D., Y. Rudich, and R. Lahav, 2001: Desert dust suppressing precipitation: A possible desertification feedback loop. *PNAS*, **98**, 5975-5980.

Rossow, W. B., A. W. Walker, D. E. Beuschel, and M. D. Roiter, 1996: *International Satellite Cloud Climatology Project (ISCCP) Documentation of New Cloud Datasets*. WMO/TD-No. 737, World Meteorological Organization, 115 pp.

Routray, A., U. C. Mohanty, D. Niyogi, S. R. H. Rizvi, and K. K. Osur, 2010: Simulation of heavy rainfall events over Indian monsoon region using WRF-3DVAR data assimilation system. *Meteor. Atmos. Phys.*, **106**, 107-125.

Sarkar, S., R. Chokngamwong, G. Cervone, R. P. Singh, and M. Kafatos, 2006: Variability of aerosol optical depth and aerosol forcing over India. *Adv. Space Res.*, **37**, 2153-2159.

Sen, O. L., Y. Wang, and B. Wang, 2004: Impact of Indochina deforestation on the East Asian summer monsoon. *J. Climate*, **17**, 1366-1380.

Shukla, J., and Y. Mintz, 1982: Influence of land-surface evapotranspiration on the earth's climate. *Science*, **215**, 1498-1501.

Sikka, D. R., 1997: Desert climate and its dynamics. *Curr. Sci.*, **72**, 35-46.

Simmons, A., S. Uppala, D. Dee, and S. Kobayashi, 2006: ERA-Interim: New ECMWF reanalysis products from 1989 onwards. *ECMWF Newsletter*, **110**, 25–35, ECMWF, Reading, UK (Available at web address: http://www.ecmwf.int/publications/newsletters).

Singh D., C. V. V. Bhadram, and G. S. Mandal, 1995: New regression model for Indian summer monsoon rainfall. *Meteorol. Atmos. Phys.*, **55**, 77-86.

Singh N., N. A. Sontakke, and H. N. Singh, 2005: *Atlas of spatial features of rainfall of India: 1871-2003, Part I.* Department of Science and Technology project "Atlas of spatial features of moisture regions and rainfall of India during 19th and 20th, centuries", Indian Institute of Tropical Meteorology, Pune, 334 pp.

Skamarock W. C., J. B. Klemp, J. Dudhia, D. O. Gill, D. M. Barker, M. G. Dudhia, X.-Y. Huang, W. Wang, and J. G. Powers, 2008: *A description of the Advanced Research WRF Version 3*. NCAR Tech. Note NCAR/TN-475+STR, 125 pp.

Smith, E. A., 1986: The structure of the Arabian heat low. Part II: bulk tropospheric heat budget and implications. *Mon. Wea. Rev.*, **114**, 1084-1102.

Spengler, T., and R. K. Smith, 2008: The dynamics of heat lows over flat terrain. *Q. J. R. Meteorol. Soc.*, **134**, 2157-2172.

Sperber, K. R., and T. Yasunari, 2006: The 1st Pan-WCRP workshop on monsoon climate systems: Toward better prediction of monsoons. *Bull. Amer. Meteor. Soc.*, **87**, 1399–1403, doi: 10.1175/BAMS-87-10-1399.

Sud, Y. C., and M. Fennessy, 1982: A study of the influence of the surface albedo on July circulation in semiarid regions using the GLAS GCM. *J. Climate*, **2**, 105-125.

Sud, Y. C., and M. Fennessy, 1984: Influence of evaporation in semi-arid regions on the July circulation: A numerical study. *J. Climatol.*, **4**, 383-398.

Sud, Y. C., and A. Molod, 1988: A GCM simulation study of the influence of Saharan evapotranspiration and surface-albedo anomalies on July circulation and rainfall. *Mon. Wea. Rev.*, **116**, 2388-2408.

Sud, Y. C., J. Shukla, and Y. Mintz, 1988: Influence of land surface roughness on atmospheric circulation and precipitation: A sensitivity study with a general circulation model. *J. Appl. Meteorol.*, **27**, 1036-1054.

Sud, Y. C., and Coauthors, 2009: Sensitivity of boreal-summer circulation and precipitation to atmospheric aerosols in selected regions – Part 1: Africa and India. *Ann. Geophys.*, **27**, 3989-4007.

Sumi, A., N.-C. Lau, and W.-C. Wang, 2005: Present Status of Asian Monsoon Simulation. *The Global Monsoon System: Research and Forecast*, C.-P. Chang, B. Wang, and N.-C. G. Lau (Eds.), WMO/TD No. 1266 (TMRP Report No. 70), 376–385.

Torres, O., P. K. Bhartia, J. R. Herman, Z. Ahmad, and J. Gleason, 1998: Derivation of aerosol properties from satellite measurements of backscattered ultraviolet radiation: Theoretical basis. *J. Geophys. Res.*, **103**, 17099–17110.

Torres, O., P. K. Bhartia, J. R. Herman, A. Sinyuk, P. Ginoux, and B. Holben, 2002: A long-term record of aerosol optical depth from TOMS observations and comparison to AERONET measurements. *J. Atmos. Sci.*, **59**, 398-413.

Trenberth, K. E., J. W. Hurrell, and D. P. Stepaniak, 2006: The Asian monsoon: Global perspectives. *The Asian Monsoon*, B. Wang (Ed.), Praxis Pub. Ltd., Chichester, UK, 67-87.

United Nations Environment Programme (UNEP), 1998: *Land cover assessment and monitoring: Pakistan*. Environmental Assessment Technical Reports, 10-A, 50 pp, UNEP/EAP.TR/95-06 (available at the web address: http://www.rrcap.unep.org/lc/cd/html/country_reports.html).

United States Department of Agriculture (USDA), 1994: *Major World Crop Areas and Climatic Maps*. Agricultural Handbook No. 664, Washington DC, 293pp (available at the web address: http://www.usda.gov/oce/weather/pubs/Other/MWCACP/world_crop_country.htm).

Uppala, S. M., and Coauthors, 2005: The ERA40 reanalysis. *Q. J. Royal Met. Soc.*, **131**, 2961-3012.

Yanai, M., C. Li, and Z. Song, 1992: Seasonal heating of the Tibetan Plateau and its effects on the evolution of the Asian summer monsoon. *J. Meteor. Soc. Japan*, **70**, 319-351.

Yasunari, T., 2007: Role of Land Atmosphere Interaction on Asian Monsoon Climate. *J. Met. Soc. Japan*, **85**, 55-75.

Waliser, D., K. W. Seo, S. Schubert, and E. Njoku, 2007: Global water cycle agreement in the climate models assessed in the IPCC AR4. *Geophys. Res. Lett.*, **34**, L16705, doi: 10.1029/2007GL030675.

Wang, B., 2006: *Monsoons - Current Status, Science directions and Needs: An AAMP perspective*. Report of the CLIVAR SSG- 14 (available at the web address: http://www.clivar.org/organization/ssg/ssg15/docs/Monsoon_Status_issues.pdf).

Wang, B., I.-S. Kang, and J. Y. Li, 2004: Ensemble simulation of Asian-Australian monsoon variability by 11 AGCMs. *J. Climate*, **17**, 803-818.

Warner, T. T., 2004: *Desert meteorology*. Cambridge University Press, United Kingdom, 612 pp.

Washington, R., M. Todd, N. J. Middleton, and S. Goudie, 2003: Dust storm source areas determined by the Total Ozone Mapping Spectrometer and surface observations. *Ann. Assoc. Am. Geogr.*, **93**, 297-313.

Webster, P. J., 2006: The coupled monsoon system. *The Asian Monsoon,* B. Wang (Ed.), Praxis Pub. Ltd., Chichester, UK, 3-66.

Webster, P. J., V. O. Magana, T. N. Palmer, J. Shukla, R. A. Tomas, M. Yanai, and T. Yasunari, 1998: Monsoons: Processes, predictability, and the prospects for prediction *J. Geophys. Res.*, **103**, 14451-14510.

Webster, P. J., C. Clark, G. Cherikova, J. Fasullo, W. Han, J. Loschnigg and K. Sahami, 2002: The Monsoon as a self-regulating coupled ocean-atmosphere

system. In *Meteorology at the Millennium*, International Geophysical Series, **83**, Academic press, pp. 198-219.

Wong, C. M., C. E. Williams, J. Pittock, U. Collier, and P. Schelle, 2007: *World's top 10 rivers at risk*. WWF International. Gland, Switzerland (available at the web address: http://assets.panda.org/downloads/worldstop10riversatriskfinalmarch13.pdf).

World Resource Institute (WRI), 2003: *Watersheds of the World*. The World Conservation Union (IUCN), the International Water Management Institute (IWMI), the Ramsar Convention Bureau, and the World Resources Institute (WRI): Washington, DC, (available at the web address: http://multimedia.wri.org/watersheds_2003/index.html).

Wu, J., A. D. Del Genio, M.-S. Yao, and A. B. Wolf, 2009: WRF and GISS SCM simulations of convective updraft properties during TWP-ICE. *J. Geophys. Res.*, **114**, D04206, doi:10.1029/2008JD010851.

Wu, R., and B. P. Kirtman, 2005: Roles of Indian and Pacific Ocean air-sea coupling in tropical atmospheric variability. *Climate Dyn.*, **25**, 155-170.

Wu, R., and B. P. Kirtman, 2007: Regimes of seasonal air-sea interaction and implications for performance of forced simulations. *Climate Dyn.*, **29**, 393-410.

Wu, R., B. P. Kirtman, and K. Pegion, 2006: Local air-sea relationship in observations and model simulations. *J. Climate*, **19**, 4914-4932.

Wu, R, B. P. Kirtman, and K. Pegion, 2007: Surface latent heat flux and its relationship with sea surface temperature in the National Centers for

Environmental Prediction Climate Forecast System simulations and retrospective forecasts. *Geophys. Res. Lett.*, **34**, L17712, doi:10.1029/2007GL030751 .

Xie, P., and P. A. Arkin, 1997: Global precipitation: A 17-year monthly analysis based on gauge observations, satellite estimates, and numerical model outputs. *Bull. Amer. Meteor. Soc.*, **78**, 2539-2558.

Xue, Y., 1996: The impact of desertification in the Mongolian and the Inner Mongolian grassland on the regional climate. *J. Climate*, **9**, 2173–2189.

Xue, Y., and J. Shukla, 1993: The influence of land surface properties on Sahel climate: Part I: Desertification. *J. Climate*, **6**, 2232-2245.

Xue, Y., and J. Shukla, 1996: he influence of land surface properties on Sahel climate. Part II: Afforestation. *J. Climate*, **9**, 3260–3275.

Xue, Y., and M. D. Fennessy, 2002: Under what conditions does land cover change impact regional climate? *Global Desertification: Do Humans Cause Deserts?*, J. F. Reynolds and D.M. Stafford Smith (Eds.), Dahlem University Press, Berlin, 59–74.

Yoshioka, M., N. M. Mahowald, A. J. Conley, W. D. Collins, D. W. Fillmore, C. S. Zender, and D. B. Coleman, 2007: Impact of desert dust radiative forcing on Sahel precipitation: relative importance of dust compared to sea surface temperature variations, vegetation changes, and greenhouse gas warming. *J. Climate*, **20**, 1445-1467.

Yu, L., X. Jin, and R. A. Weller, 2008: *Multidecade Global Flux Datasets from the Objectively Analyzed Air-sea Fluxes (OAFlux) Project: Latent and sensible heat fluxes, ocean evaporation, and related surface meteorological variables*. Woods

Hole Oceanographic Institution, OAFlux Project Technical Report. OA-2008-01, 64pp., Woods Hole, Massachusetts.

Zeng, N., and J. D. Neelin, 1999: A land–atmosphere interaction theory for the tropical deforestation problem. *J. Climate*, **12**, 857-872.

Zeng N., R. E. Dickinson, and X. Zeng, 1996: Climatic impact of Amazon deforestation - A mechanistic model study. *J. Climate*, **9**, 859–883.

Zhang, J., W.-C. Wang, and L. R. Leung, 2008: Contribution of land-atmosphere coupling to summer climate variability over the contiguous United States. *J. Geophys. Res.*, **113**, D22109, doi:10.1029/2008JD010136.

Zhang, Y., W. B. Rossow, A. A. Lacis, V. Oinas, and M. I. Mishchenko, 2004: Calculation of radiative fluxes from the surface to top of atmosphere based on ISCCP and other global data sets: Refinements of the radiative transfer model and the input data. *J. Geophys. Res.*, **109**, D19105, doi:10.1029/2003JD004457.

Zhu, Y., and D. D. Houghton, 1996: The impact of Indian Ocean SST on the large-scale Asian summer monsoon and the hydrological cycle. *Int. J. Climatol.*, **16**, 617-632.